2009

The Multi-Input Multi-Output (MIMO) Channel Modeling, Simulation and Applications

Harsharan Singh Hujan
Western University

The Multi-Input Multi-Output (MIMO) Channel Modeling, Simulation and Applications

(Spine title: The Multi-Input Multi-Output (MIMO) Channel Modeling)

(Thesis format: Monograph)

by

Harsharan Singh Hujan

Graduate Program
in
Engineering Science
Electrical and Computer Engineering

2

A thesis submitted in partial fulfillment
of the requirements for the degree of
Master of Engineering Science

School of Graduate and Postdoctoral Studies
The University of Western Ontario
London, Ontario, Canada

Abstract

This thesis mainly focus on the Multi-Input Multi-Output (MIMO) channel modeling, simulation and applications. There are several ways to design a MIMO channel. Most of the examples are given in Chapter 2, where we can design channels based on the environments and also based on other conditions. One of the new MIMO channel designs based on physical and virtual channel design is discussed in Unitary-Independent-Unitary (UIU) channel modeling. For completeness, the different types of capacity are discussed in details. The capacity is very important in wireless communication. By understanding the details behind different capacity, we can improve our transmission efficiently and effectively. The level crossing rate and average duration are discussed.One of the most important topics in MIMO wireless communication is estimation. Without having the right estimation in channel prediction, the performance will not be correct. The channel estimation error on the performance of the Alamouti code was discussed. The design of the transmitter, the channel and the receiver for this system model is shown. The two different types of decoding scheme were shown - the linear combining scheme and the Maximum likelihood (ML) decoder. Once the reader understands the estimation of the MIMO channel, the estimation based on different antenna correlation is discussed. Next, the model for Mobile-to-Mobile (M2M) MIMO communication link is proposed. The old M2M Sum-of-Sinusoids simulation model and the new two ring models are discussed. As the last step, the fading channel modeling using AR model is derived and the effect of ill-conditioning of the Yule-Walker equation is also shown. A number of applications is presented to show how the performance can be evaluated using the proposed model and techniques.

Key words: MIMO, Channel Modeling, Channel Prediction and Estimation, Alamouti, Pairwise error, Mobile-to-Mobile Communication,ML decoder,ill-conditioning of the Yule-Walker equation, Sum-of-Sinusoids,Capacity.

Acknowledgements

Completing a thesis is a challenge, thanking all those who contributed to it is an even greater one. Due to the nature of my study, many people were involved in one or the other way in it. I want to thank all of them, including those not mentioned here by name.

My utmost gratitude goes to my thesis advisor, Dr. Serguei Primak, for his expertise, kindness and most of all his patience and for allowing me to join his team. I believe that one of the main gains of this 2 year program was working with Dr. Primak and gaining his trust and friendship. He led me to achieve the basic skills in academic research with care through his mentorship. He always reminded me that it is a good thing to have new problems to solve. I thank him again for sharing his knowledge with me, and not only when it comes to research but many other aspects as well.

I would also like to thank Dr. Khaled Almustafa, who has suggested me to work under Dr. Primak's supervision, and who has shared his knowledge and concern throughout both my undergraduate and Master's degree programs. I would also like to thank my colleagues from the Bell Research Lab who have finished their Master's degrees, Marco Luccini and Dan Dechene, for their unlimited support throughout my research life. They were my role-models when I was just considering graduate school. They seemed to assume that I would do fine and this helped me more than they know. I want to thank my best friends who are currently finishing their Master's and Ph.D. programs in Engineering, Adam K. and Jordan DeMello, for their patience and support. The road to my graduate degree has been a long and winding one and for that I would also like to thank some people from early days: Anna Sauer, Mina, Andrew Roberts, Crystal and the Soccer Team form the summer (I am not so good with remembering names). I would also like to thank the Department of Electrical and Computer Engineering where I met many special people. I would also like to thank the special ladies - Sandra, Rachel and Jacquie.

Table of Contents

Appendices

List of Tables

List of Figures

Acronyms

AR	*Autoregressive Model*
ACK	*Acknowledgment*
ACF	*Autocorrelation Function*
AoA	*Angle of Arrival*
AoD	*Angle of Departure*
AOD	*Average Outage Duration*
AWGN	*Additive White Gaussian Noise*
BER	*Bit Error Rate*
BPSK	*Binary Phase Shift Keying*
BS	*Base Station*
BW	*Bandwidth*
CCF	*Cross-Correlation function*
CSI	*Channel State Information*
dB	*Decibel*
DFT	*Discrete Fourier Transform*
Hz	*Hertz*
i.i.d	*Independent and Identically Distributed*
I/Q	*In-phase or Quadrature*
ISI	*Inter Symbol Interference*
IDFT	*Inverse Discrete Fourier Transform*
LCR	*Level Corssing Rate*
LC-STD	*Linear Combination Space-Time Decoder*
LOS	*Line of Sight*
M2M	*Mobile-to-Mobile*
MIMO	*Multi-Input Multi-Output*
MISO	*Multi-Input Single-Output*
ML	*Maximum Likelihood*
ML-STD	*Maximum Likelihood Space-Time Decoder*

MMSE	*Minimum Mean Square Error*
MS	*Mobile Station*
MSE	*Mean Square Error*
NLOS	*Non Line of Sight*
OSTBC	*Orthogonal Space-Time Coding*
PDF	*Probablity Density Function*
PSAM	*Pilot symbol assisted modulation*
PSD	*Power Spectrum Density*
PEP	*Pairwise probability of error*
QAM	*Quadrature Amplitude Modulation*
QPSK	*Quadrature phase shift keying*
RTV	*Road-to-Vehicle*
R2M	*Road-to-Mobile*
SISO	*Single-Input Single-Output*
SIMO	*Single-Input Multi-Output*
SNR	*Signal to Noise Ratio*
SoS	*Sum of Sinusoids*
STC	*Space Time Coding*
ToA	*Time of Arrival*
UIU	*Unitary-Independent-Unitary*
VCR	*Virtual Channel Representation*
V2V	*Vehicle-to-Vehicle*
WCDMA	*Wideband Code Division Multiple Access*
WSS	*Wide Sense Stationary*

Notation

μ	mean
ε	constant bias used in AR model
ρ_{kl}	cross-correlation coefficient between channel k and l
σ_n^2	variance of the AWGN
$\leq$	Less than Equal To
$Im\{x\}$	the imaginary part of x
κ	parameter for the bandwidth of the won Mises AoA PDF
λ	wavelength
$\bar{\gamma}_p$	average pilot SNR
$\bar{\gamma}_s$	average data SNR
$\sigma_p^2(\tau)$	variance of the pilot
τ_i	time delay of the i^{th} scatterer
$a_{ij}[k]$	multichannel AR model coefficients
$a[k]$	coefficient of AR model
$\mathbf{A}[k]$	matrix of multichannel AR model coefficients
$E[x]$	expectations of a random variable x
E_s	Energy of data symbol
E_p	Energy
f_c	carrier frequency
f_D	maximum Doppler frequency
f_m	normalized maximum Doppler frequency
$\mathbf{H}$	channel matrix with actual channel coefficients
h	filter coefficients
$I_n(.)$	modified Bessel function of first kind and n^{th} order
$\Im(u)$	Imaginary part of the complex vector u
$\mathbf{I}_n$	n x n identity matrix
$J_0()$	Bessel function of the first kind and zeroth order
K	Rice factor

K_i	Rice factor of i^{th} channel
$L(\rho)$	level crossing rate
$min...$	minimum of arguments
$max...$	maximum of arguments
$AR(p)$	AR model order of p
$p(\theta)$	PDF of AoA of scattering components
$p_{x,y}(x,y)$	joint distribution of random variables x and y
$r(\tau)$	temporal fading autocorrelation function
$R_{II}[n]$	In-phase components of the sampled autocorrelation function
$R_{QQ}[n]$	Quadrature components of the sampled autocorrelation function
$R_{IQ}[n]$	Cross correlation components between in-phase and quadrature components
$\Re(u)$	Real part of complex vector u
$\mathbf{R}$	autocorrelation matrix
$\mathbf{R_H}$	correlation matrix for channel matrix $\mathbf{H}$
N_R	Number of receiver
$s(t)$	Complex baseband transmitted signal
T	channel sampling period
T_s	symbol period
N_T	number of transmitter
$w(t)$	Complex zero mean AWGN
$w[n]$	vector of driving noise process for multichannel AR fading generator
W	Bandwidth
$x(t)$	Complex Gaussian flat fading channel process
$y[n]$	noisy samples of complex fading channel
y	vector of noisy fading samples
v	velocity of mobile
$\hat{\mathbf{H}}$	channel matrix with estimated channel coefficients

Chapter 1
Introduction

1.1 Introduction to Wireless Communication

We have seen over the past two decades or so a huge growth in the demand for providing reliable high speed wireless communication links in order to support a wide range of applications such as voice, video, email and web. To provide such a link to perform all these tasks are very challenging because in wireless communication the channel is time varying. The transmitted signals are received through multiple paths which usually add destructive value resulting in serious performance degradations. This type of phenomenon is known as *fading*. Since we have a lot of sharing between users and applications there can also be significant interference. There are other challenges for high-speed wireless applications including the ability of bandwidth, high power constrain and complexity in hardware.

Since we only have a limited frequency spectrum and the steady increase in the number of new wireless applications or redesigning the existing ones, we can see that there will be a problem in being able to accommodate all of them. One of the simple approaches that is suggested in the literature is to resort to higher order modulation schemes to improve the bandwidth efficiency. There is one drawback to this idea, which is the poor reliability associated with it. The problem is, for the same level of transmit power, higher order modulation yields performance that is inferior to that of the lower order modulation schemes.

The most effective technique to improve the performance many previous researchers suggest is *"diversity"*. It attempts to provide the receiver with independently faded copies of the transmitted signal with the hope that at least one of these replicas will be received correctly. There are different types of diversity: frequency diversity, time diversity, antenna diversity and modulation diversity. One of the examples that we encounter in everyday life which uses this method is handsets in mobile communications which are capable of polarization diversity. Another simple way of diversity that we have learnt through out our career is channel coding, which is also used to provide diversity for immunization against the impairment of the wireless channel. The few examples of channel coding are convolutional and block codes, trellis-coded modulation, multi-level coding, bit-interleaving coded modulation and capacity approaching coding schemes such as turbo and low density parity check codes.

Another diversity method is also known as transmit and/or receive antenna diversity, or spatial diversity. Systems with multiple antennas are also known as multiple-input multiple-output (MIMO) systems. Future sections will explain more on how the MIMO wireless communication works. One of the major advantages of MIMO system is the substantial increase in the channel capacity, which immediately translates into higher data throughput. Another advantage of MIMO systems is the significant improvement in data transmission reliability. These advantages can be achieved without any expansion in the required bandwidth or increase in the transmit power. We can combine other various diversity techniques to improve the system performance in the wireless environment. We can combine the spatial diversity obtain by transmit and receive antennas with the idea of channel coding. This scheme is also known as space time coding and the system is know as a coded MIMO system. Recent studies have shown that combining the coding with spatial diversity opens up new dimensions in wireless communications and it can offer solutions to the challenges faced in high speed wireless links [1].

1.2 MIMO Wireless Communication

Due to its powerful performance capabilities, the use of MIMO technology has rapidly gained popularity over the past decade. The MIMO systems can be simply defined as any communication link with multiple antenna elements at the transmitting and the receiving ends. The concept behind MIMO system is that the signals transmitted over the channels would have a combined effect between the transmit and receive antennas which leads to lower BER and also improved data rate. As we have mentioned, these features help us to design and improve our old design in terms of speed reliability. The cost of improvement is the complexity of systems and signal processing. A MIMO system transmits two or more unique copies of data streams in the same radio channel at the same time, therefore technically it should deliver two or more times of the SISO data rate. MIMO system takes the advantage of multipath reflections of the signals. Therefore the received signal can be seen as a liner combination of the multiple transmitted data streams at the receiver. We will explain more details on how the wireless channels works. The data streams are separated at the receiver using MIMO algorithms that rely on estimates of all links between each transmitter and receiver. In a MIMO channel, each multipath route can be treated as a separate channel assuming that there is no correlation between each antennas. We can imagine them as "wires" that is used to transmit signals. Then the system employs multiple, spatially separated antennas to take advantage of these "imaginary wires" created by multipath to transfer more data. The range of transmission is also increased due to antenna diversity advantage.

1.2.1 Wireless Channels

There are fundamental difference between wireless channels and the conventional wire line channels. In wireless channel, there are multi path effects [2] and also we have significant time variation caused by the relative motion of the transmitter and the receiver as well as the changes in the environment. Therefore, different signals transmitted at different environment will interact with different interference.

Electromagnetic waves travel through three different mechanisms: reflection, refraction, and diffraction. We know that when the waves impinge upon the surface with surface variations significantly larger than their wavelength, part of the signal reflects as shown in Figure 1.1. The second mechanism, i.e. refraction, is basically the process of secondary wave production by "knife edge" effect. Scattering usually arises due to surface variations of nearby objects that are smaller than the signal wavelength, (e.g trees, roughness of surfaces, buildings, cars). As results of these

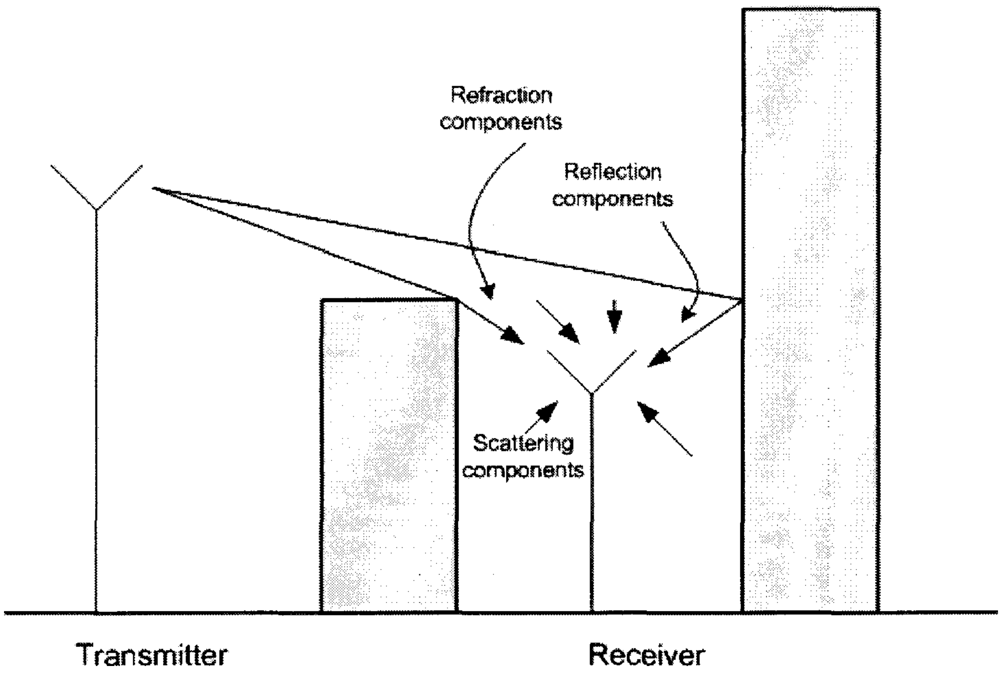

Figure 1.1: Illustration of the wireless propagation

effects, the electromagnetic wave propagation, the signals transmitted over a wireless channel are received via multiple secondary paths, in addition to the possible line-of-sight (LoS). In different multipath propagation, due to the materials involved and the frequency of the operation, penetration of electromagnetic waves through walls, allow the reception of signals even when there is no direct line of sight between the transmitter and the receiver. One example that we encounter every day is using wireless internet at home where the router is not in line-of-sight with the user.

The effects of multipath propagation are usually deleterious. This is due to the fact that different paths have different length, resulting in different attenuation factors and the phase differences for replicas of the transmitted signals [3]. We all know that the frequencies that we use in wireless communications are usually very high, therefore, the corresponding wavelengths are very small. For example, for cell phones, the transmission bands are usually in the range of 800 $MHz - 2\ GHz$, thus the wavelengths of the transmitted signals are in the range of $15 - 37.5\ cm$. In this case, the path length difference can be in the order of tens of meters. Therefore, the phase differences between the different replicas of the received signals will be significant often exceeding duration T_s of a symbol. The amplitude variations will also be significant, since there are scattering , reflection and refraction effects.

1.2.2 MIMO System Functionality

MIMO can be subdivided into three main categories. They are precoding, spatial multiplexing and diversity coding.

1.2.2.1 Precoding

Precoding is generalized beamforming to support multi-layer transmission in MIMO radio systems. Old beamforming considers linear single layer precoding so that the same signal is emitted from each of the transmit antennas with appropriate weighting such that the signal power is maximized at the receiver output. In precoding, the multiple streams of the signals are emitted from the transmit antennas with independent and appropriate weighting per each antenna such that the link throughput is maximized at the receiver output.

1.2.2.2 Spatial Multiplexing

It is a transmission technique in MIMO communications to transmit independent and separately encoded data signals so called streams, from each of the multiple transmitters. Therefore, the space dimension is reused, or also known as multiplexed, more than one time. If the transmitter is equipped with N_t antennas and the receiver has N_r antennas, the maximum spatial multiplexing order or the number of streams is

$$N_s = min(N_t, N_r) \tag{1.1}$$

if a linear receiver is used. This means that N_s streams can be transmitted in parallel, leading to a N_s times increase in the spectral efficiency.

1.2.2.3 Antenna Diversity

Antenna diversity also known as space diversity is one in a superset of wireless diversity schemes that utilizes two or more antennas to improve the quality and reliability of a wireless link. When there is NLoS, in urban and indoor environments, between the transmitter and receiver, instead the signal is reflected along multiple paths before finally reaching to the receiver. Antenna diversity is effective at mitigating this condition. This is because multiple antennas afford to receive several observations of the same signal. Each antenna will experience a different interference environment. The idea is that if one of the antenna is experiencing a deep fade, it is likely that another one receives a sufficiently strong signal. An antenna diversity scheme requires additional hardware and integration versus a single antenna system. However, due to the commonality of the signal paths, a fair amount of circuitry can be shared coefficients to increase [4][5].

1.3 MIMO Channel Estimation

High quality channel estimation is essential for reliable performance of any MIMO channel model considered. Channel estimation is required when the change of the phase and amplitude of the channel are not compensated at the receiver [6]. The reliability of such estimation will be based on the performance of the considered model in the presence of the channel estimation will react to its performance in the perfectly known channel. Channel estimation causes some channel capacity due to using some of the channel bandwidth for estimation. One approach for channel estimation is to transmit a pilot tone alongside the data signals, under the assumption that they are equally affected by the fading channel [7]. Another approach is to use a pilot-symbol-aided technique, which involves inserting known training symbols, into the data stream [8]. The received training symbols will be used at the receiver for channel estimation. Pilot symbo is a preferred choice of channel estimation, because it gives a better BER performance, needs smaller spectral occupancies and lower implementation complexity when compared to pilot tone techniques [6]. Pilot symbol channel estimation can be classified into two types. The training based estimators, which perform channel estimation based on the observation of pilot symbols, are used for fast fading channels [9]. The other class is semiblind estimators, which use the observation of both pilot and data symbols for channel estimation. They are commonly used for slow fading channels [10].

One of the best well known estimation schemes is the pilot symbol assisted modulation (PSAM). This approach involves inserting a single pilot symbol in a fixed and known interval into the transmitted stream to sound the channel at the pilot locations. The received pilot signals can be grouped and used to estimate the complex channel fading at the data symbol locations [9]. This is the first method that was introduced for Rayleigh environment and shown to provide high quality channel estimation with a fractional trade off of channel capacity. It was also shown in [9], that for a time selective Gaussian fading channels, the Wiener channel interpolator provides optimum minimum mean square error estimation for fading and demodulation of the data sequence.

1.4 Capacity of MIMO System

We all know that the wireless systems continue to strive for ever higher data rates. There are two different challenges we face along with this problem: (1) systems that are limited in terms of power, bandwidth, complexity and (2) significant increase in channel capacity. Since we are using multiple transmit and receive antennas, there should be a higher increase in capacity. Pioneering work by Foschini and Telatar ignited much interest in this ara by predicting remarkable spectral efficiencies for wireless systems with multiple antennas when the channel exhibits rich scattering and its variation can be accurately tracked.

Most of the large spectral efficiencies associated with MIMO channels are based on the premise that a rich scattering environment exists, which provides independent transmission paths from each transmit antenna to each receive antenna. For a single user MIMO system, the structure achieves capacity on approximately $\min(N, M)$ where N is the number of transmit antennas and M is the number of receive antennas.

MIMO channel capacity depends heavily on the statistical properties and antenna element correlations of the channel. Recent work has developed both analytical and measurement based MIMO channel models along with the corresponding capacity calculations for typical indoor and outdoor environments. Antenna correlation varies drastically relative to the scattering environment, the distance between transmitter and receiver, the antenna configurations, and the Doppler spread. The effect of channel correlation on capacity depends on what is known about the channel at the transmitter and receiver, which means correlations sometimes increase capacity and sometimes reduce it [11]- [14]. Channels with very low correlations between antennas can still exhibit a "keyhole" effect where the rank of the channel gain matrix is very small and leads to a limited capacity.

First, we can focus on the MIMO channel capacity in the Shannon theoretic sense. The Shannon capacity, also known as the maximum mutual information, of a single user time invariant channel corresponds to the maximum data rate that can be transmitted over the channel with an arbitrarily small probability of error. Here we will explain some detail on the Shannon theory.

Shannon theory was created by Claude Shannon, the eminent engineer and mathematician and the founder of information theory. Consider the most common example of a channel for which Shannon found the capacity explicitly. This is the additive white Gaussian noise or AWGN channel where the input signals to be transmitted are encoded as continues, Gaussian appearing waveforms with average power S, and the channel bandwidth of W in Hertz. The noise introduce the power of N during the signal transmission. The capacity of this channel of bandwidth W in Hertz is then shown to be

$$C = W\ log_2 \det\left(I + \frac{\gamma}{N_T}\mathbf{H}\mathbf{H}^H\right) \tag{1.2}$$

We should note that Shannon formula of (1.2) does not give us any information on the type of coding or transmission we should use. Many researchers have been engaged over the years in finding coders and codes for them that approach channel capacity as closely as possible. However, the capacity is found to be approached by so call

M-array orthogonal signaling but only for $M \to \infty$.

When the channel is time varying channel capacity has multiple definitions depending on what is known about the instantaneous channel state information at the transmitter or/and receiver. It also depends on if the capacity is based on averaging the rate over all channel states or maintaining a fixed rate for most channel states. If the channel state information is known at both ends, the transmitter can adjust the transmission scheme relative to the channel, therefore the channel capacity is characterized by the ergodic, outage or minimum rate capacity. Ergodic capacity is defined as the maximum average rate under an adaptive transmission strategy averaged over all channel states. Outage capacity is defined as the maximum rate that can be maintained in all channel states with some probability of outage which mean no data transmission at times. Minimum rate capacity is defined as the maximum average rate under an adaptive transmission strategy that maintains a given minimum rate in every channel states and then averages the total rate in excess of this minimum over all channel states.

When the channel state information (CSI) is only known to the receiver, then the transmitter should maintain a fixed-rate transmission strategy based on knowledge of the channel statistics. In this case, the ergodic capacity can be explain as the rate that can be achieved via this fixed rate strategy based on receiver averaging over all channel states. On the other hand, the transmitter can send at a rate that cannot be supported by all channel states: in these poor channel states the receiver declares an outage and the transmitted data is lost. In this case, the transmission rate has an outage probability associated with it and capacity is measured relative to outage probability.

1.5 Contribution of the Thesis

The main contribution of this thesis is the investigation of MIMO techniques and the performance of those techniques. There are many MIMO designs used in this thesis to simulate real life wireless channel and then used them in many ways to test the performance. They are listed as follows:

In Chapter 3, UIU channel model design will be presented. This model is a much better fit compare to other models when it comes to real life cases. After re-simulation of this model, we set up some conditions to create a channel that would be a better match to the design. Once this has been completed, we perform the performance analysis using Alamouti and Pairwise Probability of Error (PPE). There have been several papers that used Alamouti and PPE on other channel models but not on Unitary-Independent-Unitary (UIU) channel Model. As the final step in this chapter, we also discus channel capacity and its effects based on different scattering environment. We also discus the performance of time evolution of capacity and its results.

In Chapter 4, we explain in detail a new methodology for Mobile-to-Mobile (M2M) channel design. This chapter explains the difference in the old SoS model and the new channel model and all the auto-correlation and cross-correlation, derived and simulated. Once we have a good match between the simulation and the theoretical results, we described the Alamouti scheme and the pairwise probability of errors in grate details. Then, we compare the results between i.i.d Gaussian channel results and the M2M channel results for both Alamouti and PPE case.

In Chapter 5, we use the AR fading channel model with the desired AoA correlations for system analysis. We presented our finding in the performance and the evaluation of this model. We also analyze performance using Alamouti and PPE schemes for this channel model.

In Chapter 6, the study of capacity on different MIMO channels will be discuss. In this chapter, the main goal is to understand how different capacity is produce and how different performance test give different knowledge on how a MIMO channel behave. This chapter is also to give an idea on how a joint PSD is used in a MIMO channel design and its effect on time evolving capacity and its properties.

In Chapter 7, the effect of channel estimation error on performance of Alamouti will be discuss in details. Different types of encoding and decoding schemes will be also discussed in this chapter. This chapter will give the better understanding on how a block fading is performed. The Winer filter is used to produce the channel coefficient to compete the task of channel estimation. This chapter will explain how the spacing in antenna effects the estimation results and how the bit SNR effects the performance.

In Chapter 8, the effect of channel estimation error on the performance of Alamouti code will be presented. There have been several papers that did similar simulations but, in our case we have done the block fading estimation. Our main goal in this chapter has been to find out how the estimation changes, based on the correlation of the antennas. All the simulation results were presented based on the spacing of the antennas and shows the changes in the probability of errors based on the antenna spacing.

1.6 Thesis organization

An overlap may exist between the introductory and the body sections of each chapter, based on the development of the thesis. Some of the references might appear in more than one chapter, based on their relevance to the work done in the chapter and to help the reader follow the development of each chapter individually.

The remainder of the thesis is organized as follows. Chapter 1 and 2 introduce the reader to the communication and the background of the mobile communication of the MIMO channel. The UIU channel modeling was discussed in detail in Chapter 3. Chapter 4 and 5 includes M2M channel modeling and the AR channel modeling respectively. Then the three different types of capacity and the most importantly, the time evolution of capacity on UIU channel model is also discussed in Chapter 6. We have shown the simulation using the Alamouti scheme and the pair wise probability of error to test the performance of the channel. Chapter 7 covers the effects of channel estimation error on the performance of the Alamouti code. The chapter also discusses the effect of antenna spacing on the channel estimation error. Then we discussed the performance of the OSTBC using both M2M and AR models. Chapter 9 covers the conclusion and suggestions for the future research work.

Chapter 2
Models of MIMO Wireless Channels

2.1 Mobile Radio Communication

Mobile radio communication in cellular radio takes place among a fixed BS and a number of roaming MSs. The propagation area where the communication occurs is known as a cell. The cell is the maximum distance that the MS can roam from the BS before the quality of communications becomes unacceptably poor. The presence of LOS has a profound effect on radio propagation [2], and this means that the characteristics of radio propagation are highly dependent on the cell size and shape. As the distance between the BS and the MS increases, the received signal level tends to decreases due to path losses [2, 15] and scattering.

Let us consider a BS transmitting an unmodulated harmonic carrier which provides the coverage area in which a MS is traveling. The MS does not receive one version of the transmitted carrier, instead it receives a number of reflected and diffracted waves by buildings and other urban obstacles. In real life, each copy of transmitted signals received by the MS is subjected to a specific time delay, amplitude, phase and Doppler shift, depending on its path from the BS to the MS and propagation conditions. A constant amplitude carrier signal transmitted may be substantially different from the signal the MS receives. When the signals from the various paths sum constructively at the MS antenna, the received signal level is enhanced.It can also sum to decrease the signal amplitude. This is known as multipath fading [16]. As the MS travels it passes though an electromagnetic field that results in the received signal level experiencing fades approximately every half wavelength along its route. When a very deep fade occurs the received signal is zero and the receiver output is dependent on the channel noise.

The above idea applies to the transmission of an unmodulated carrier, that does not really occur in practice. Since it does not carry any information by itself, the carrier is modulated to represent symbols to familiar denotation T_S. As the result, in digital mobile communications, the propagation phenomena are highly dependent on the ratio of the symbol duration to the delay spread of the time variant radio channel. The delay spread may be considered as the length of the received pulse when the impulse is transmitted. If we transmit data at a slow rate the data can easily be resolved at the receiver. This is because the extension of a data pulse due to the multi-paths is completed before the next impulse is transmitted. However, if we increased the transmitted data rate a point would be reached where each data symbol significantly spreads into adjacent symbols, a phenomenon known as inter symbol interference (ISI). Without the use of channel equalizers to remove the ISI, the BER may become unacceptably high. Suppose that we continue to transmit at the higher data rate which caused ISI, but move the MS closer to the BS while decreasing the radiated distance. If this distance is sufficiently small the delay spread will have decreased as delays of the multi paths components are smaller. The fading is said to be flat as it occurs uniformly across the frequency band of the channel. The frequency selective fading occurs because some frequencies fade relative to others over the channel Bandwidth.

2.1.1 Gaussian Channel

The Gaussian channel is the simplest type of channel. It is also known as the additive white Gaussian noise (AWGN) channel.

$$r = h\,s + n \tag{2.1}$$

$$h = \text{const} \tag{2.2}$$

The noise n is assumed to have a constant power spectral density over the channel bandwidth and a Gaussian amplitude probability density function (PDF). This type of channel is considered to be unrealistic in digital mobile radio. In micro-cells it is possible to have a LOS with essentially no multipath, giving almost a Gaussian channel. Even when there is multipath fading, but the mobile stationary and there are no other moving objects, such as vehicles in its vicinity, the mobile channel may be though of as Gaussian with the effects of fading represented by a local path loss. This channel is important since it provides an upper bound on system performance. For a given modulation system, we may calculate the BER performance in the presence of a Gaussian Channel. When multipath fading occurs the BER will increase for a given channel SNR.There are other types of channel and we shall discuss them in detail further on in this section.

2.1.2 Rayleigh Fading Channel

Rayleigh fading is a statistical model for a propagation environment in wireless communication when the phase of the received signal is sufficiently randomized [2]. This fading model assumes that the magnitude of the signal that has passed thought the medium will vary randomly which is also know as fading according to Rayleigh distribution which is defined as the radial component of the sum of two uncorrelated Gaussian random variables. This fading model is a very reasonable model for tropospheric and ionospheric signal propagation as well as in heavily built up urban environments. Rayleigh fading is most applicable when there is no dominant propagation along a line of sight between the transmitter and receiver. If there is a dominant line of sight then Rician fading may be more applicable. There will be an explanation on Rician fading in section 2.1.3.

Rayleigh fading is a reasonable model when there are many objects in environment that scatter the radio signal before it arrives at the receiver. The central limit theorem holds that, if there are sufficiently many scatter, the channel impulse response will be well modeled as a Gaussian process regardless of the distribution of the individual components. If there is no dominant component to the scatter, then such a process will have zero mean and phase evenly distributed between 0 and 2π radians. The envelope of the channel response will therefore be Rayleigh distributed.

The probability density function of this model is

$$P_R(r) = \frac{2r}{\Omega} e^{-\frac{r^2}{\Omega}}, \quad r \geq 0 \tag{2.3}$$

where $\Omega = E(R^2)$. The gain (magnitude) and the phase elements of the channel's distortion are represented in complex form. Note that the parameters discussed here are for a non-static channel. If a channel is not changing with time, clearly it does not fade and instead remains at some level. At two separate time intervals the channel are uncorrelated with one another because we have assumed that each of the scattered components fades independently. Once relative motion is introduced among any of the transmitter, receiver and scatterers, the fading becomes correlated and varying in time. In this case, we will have more properties such as Correlation, Level crossing rate, average fade duration and doppler power spectral density.

2.1.3 Rician Channel

In mobile radio, a dominant path that is LOS, often occurs at the receiver, in addition to the many scattered paths. This dominant part will decrease the depth of the fading. The Rician parameter is also defined as

$$K = \frac{\textit{power in the LoS}}{\textit{power in the scattered paths}} = \frac{P_{LoS}}{\Omega} \tag{2.4}$$

We can say that, when K is zero the channel is Rayleigh, when K is infinite the channel is Gaussian. The PDF can be written as

$$P_R(A) = \frac{2(k+1)}{\Omega} A \exp\left[-k - \frac{(k+1)A^2}{\Omega}\right] I_0\left(2A\sqrt{\frac{k(k+1)}{\Omega}}\right) \tag{2.5}$$

2.2 Non-Physical MIMO channel Models

The non physical models are based on the channel's statistical characteristics using non-physical parameters. These models provide accurate channel characteristics under the conditions in which the model is defined. Such models give limited insight, since the MIMO channel propagation depends on the non-physical parameters identifying the system, as well as the measurement equipment, e.g. bandwidth, configuration of the arrays and the heights and response of antenna in both sides of the MIMO system. Another approach is physical models, where these models choose actual physical parameters to describe the MIMO propagation channels. Some typical parameters include AoA, AoD and ToA. One of the drawbacks is that we cannot fully describe a MIMO propagation channel by a small number of physical parameters, which makes it difficult to validate the model and puts a limitation on such approaches. In later sections, we will discuss the last classification in more detail and classify the MIMO channel models into non-physical and physical models.

Non-physical channel models characterize the impulse response of the channel $\mathbf{H}$ between the individual transmit N_T and receive N_R antennas in a mathematical way by capturing the physical wave propagation and antenna configuration simultaneously. These models can be further subdivided into propagation-motivated and correlation base models.

2.2.1 Propagation Motivated Methods

These models represent the channel matrix via propagation parameters. We will only discuss those of them that are relevant to our future investigation - the finite scatter [17], maximum entropy [18] and the virtual channel [19] models.

2.2.1.1 Finite Scatterer Model

The concept of the finite scatterers model is illustrated in Fig 2.1. Its fundamental assumption is that the signal travels from transmitter to receiver via a number of discrete paths, referred to as multipath components, or simply multi-paths. These are treated according to the concepts of ray optics, although diffraction can also be treated using concepts from the geometrical theory of diffraction. The fundamental setup in Fig 2.1 showing the scattering from a single scatterer (path(a)) and multiple reflections (path(b)). We can also have both single and double scatterer (path(c)).

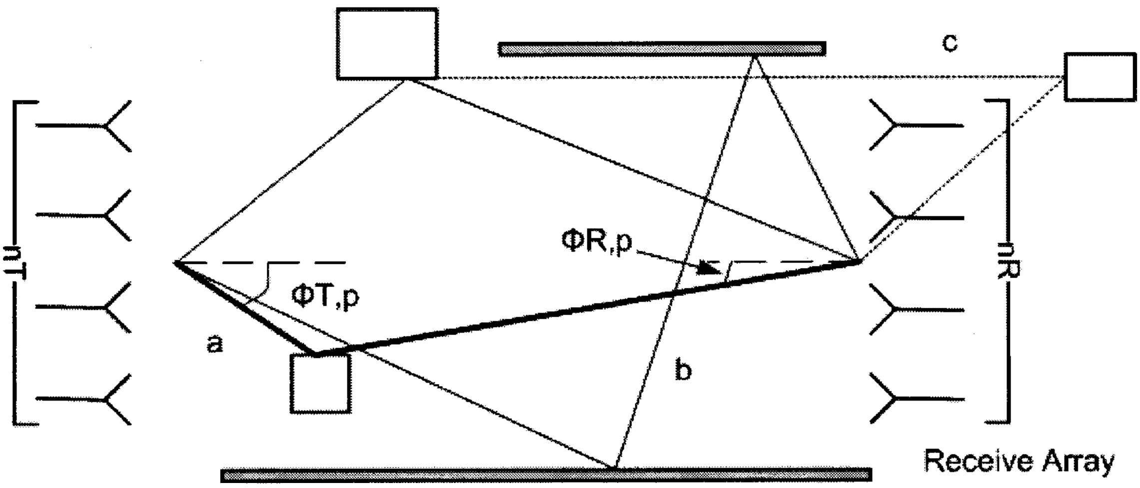

Figure 2.1: Concept of the finite scatterers channel model.

For each of the components (indexed by an integer (p)), angle of departure (AoD), the angle of arrival (AoA) and path gain ξ_p , and delay τ_p are specified, and the resulting channel matrix $\mathbf{H}$ for the narrow band case, neglecting the time delay τ_p, is given by [17]

$$\mathbf{H} = \sum_{p=1}^{P} \xi_p \Psi(\psi_p) \Phi^T(\phi_p) \tag{2.6}$$

where $\Phi^T(\phi_p)$ and $\Psi(\psi_p)$ are the transmitter and the receiver steering vectors [20] corresponding to the p^{th} multipath component. These vectors incorporate the geometry, direction, and coupling of the antenna array elements and ξ_p is the multipath amplitude [17], i.e. connect the environment (channel) to the received signal. In [20] has expressions for circular, square and other arrays.

2.2.1.2 Maximum Entropy Model

The maximum entropy principle was proposed [21],[22]and [23] to determine the distribution of the MIMO channel matrix based on an available *a priori* information. This information might include properties of the propagation environment and system parameters (e.g., bandwidth DoA, AoA, etc). The maximum entropy principle was justified by the objective to avoid any model assumptions not supported by the prior information.

If the prior information I_1, which is the basis for channel model H_1, is equivalent to the prior information I_2 of channel model H_2 then both models must be assigned the same probability distribution, $f(H_1) = f(H_2)$. To give an example of the maximum entropy model, assume the following *a priori* information is available:

1. The numbers s_{Tx} and s_{Rx} of scatterers at the Tx and Rx side, respectively;
2. The steering vectors for all Tx and Rx scatterers, contained in the m x s_{Tx} and n x s_{Rx} matrices Φ and Ψ respectively
3. The corresponding scatterer powers P_{Tx} and P_{Rx}; and
4. The path gains between Tx and Rx scatterers, characterized by s_{Rx} x s_{Tx} pattern mask (coupling matrix) Ω.

Then, the maximum entropy channel model was shown to equal

$$H = \Psi P_{Rx}^{1/2}(\Omega \odot G)P_{Tx}^{1/2}\Phi^T \tag{2.7}$$

where G is an s_{Rx} x s_{Tx} Gaussian matrix with i.i.d elements and $\odot$ is known as Kronecker product.

2.2.1.3 Virtual Channel Representation

Suppose there are K scatterers, within one cluster, between the transmitter and the receiver, one physical MIMO channel model for this cluster is

$$\mathbf{H} = \sum_{k=1}^{K} \beta_k \mathbf{a}_R(\phi_{R,k})\mathbf{a}_T^H(\phi_{T,k}) \tag{2.8}$$

where β_k is the path gain for the k^{th} scatterer; $\phi_{T,k}$ and $\phi_{R,k}$ are the AoD and AoA, respectively. We can assume that both the antennas arrays are uniform and only plane

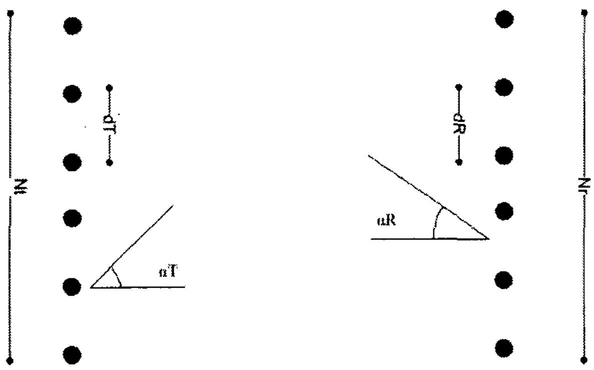

Figure 2.2: Unitary Linear Array for both Transmitter and Receiver.

waves impinge the array due to large distance to the scatterers. Then we can say that the array response vectors at both sides are given by [24],

$$a_T(\phi_{T,k}) = [1, e^{-j2\pi\theta_{T,k}}, \ldots, e^{-j2\pi(M-1)\theta_{T,k}}]^T \tag{2.9}$$

$$a_T(\phi_{R,k}) = [1, e^{-j2\pi\theta_{R,k}}, \ldots, e^{-j2\pi(N-1)\theta_{R,k}}]^T \tag{2.10}$$

where $\theta_{T,K} = d_t \sin(\phi_{T,k})/\lambda$ and $\theta_{R,K} = d_t \sin(\phi_{R,k})/\lambda$; λ is the wavelength and d_t and d_r are the element spacing of the transmitter and the receiver respectively. We can also write this in matrix form

$$\mathbf{H} = \mathbf{A}_R \mathbf{H}_P \mathbf{A}_T^H \tag{2.11}$$

where $A_T = [a_T(\phi_{T,1}), \ldots, a_T(\phi_{T,K})]$ M x K matrix, $A_R = [a_R(\phi_{R,1}), \ldots, a_R(\phi_{R,K})]$, N x K matrix and $\mathbf{H}_p = diag(\beta_1, \ldots, \beta_K)$ (KxK) diagonal matrix. In the model, the virtual AoD $\psi_{T,p}$ and virtual AoA, $\psi_{R,q}$ from different scatterers are fixed according to the number of elements at both sides, i.e.

$$\psi_{T,p} = \arcsin \frac{a_p \lambda}{M d_t} \tag{2.12}$$

$$\psi_{R,p} = \arcsin \frac{b_q \lambda}{N d_r} \tag{2.13}$$

where $a_i = -(M-1)/2, \ldots, (M-1)/2$ when M is odd and $a_i = -M/2, \ldots, M/2$ where M is even.$b_i = -(N-1)/2, \ldots, (N-1)/2$ when N is odd and $b_i = -N/2, \ldots, N/2$ where N is even.

The MIMO channel can be modeled as

$$\begin{aligned} \mathbf{H} &= \sum_{q=1}^{N} \sum_{p=1}^{M} \mathbf{H}_v(p,q) \mathbf{a}_R(\psi_{R,q}) \mathbf{a}_T^H(\psi_{T,p}) \\ &= \tilde{\mathbf{A}}_R \mathbf{H}_V \tilde{\mathbf{A}}_T^H \end{aligned} \tag{2.14}$$

where $\mathbf{H}_V$ is the virtual channel representation, $\mathbf{A}_T$ and $\mathbf{A}_R$ are defined similarly as in equation 2.11. Note that both A_T and A_R are unitary matrices and $\mathbf{H}_v$ is no longer a diagonal matrix in general.

2.2.2 Correlation-Based Models

Many narrow band non-physical MIMO channel models are based on the multivariate complex Gaussian distribution [25] of the MIMO channel coefficients (i.e., Rayleigh or Rician fading). The channel matrix $\mathbf{H}$ can be written in the following way:

$$\mathbf{H} = \sqrt{\frac{1}{1+K}} \mathbf{H}_s + \sqrt{\frac{K}{1+K}} \mathbf{H}_d \tag{2.15}$$

where $K \geq 0$ denotes the Rice factor, $\mathbf{H}_s$ is a zero-mean Gaussian random matrix that characterizes the NLoS components and $\mathbf{H}_d$ is a deterministic matrix which accounts for the LOS components of the channel's parameters. In the following, as in [26], we focus on the NLoS components given by the Gaussian matrix $\mathbf{H}_s$. We also assume $K = 0$ for simplicity, i.e. $\mathbf{H} = \mathbf{H}_s$. The zero-mean multivariate complex Gaussian distribution of $h = vec(\mathbf{H})$, where $vec\{.\}$ is a vectorization operation [20], is given by

$$f(\mathbf{h}) = \frac{1}{\pi^{nm} \det\{\mathbf{R_H}\}} \exp(-\mathbf{h}^H \mathbf{R_H}^{-1} \mathbf{h}) \tag{2.16}$$

where $(.)^H$ is the Hermitian transpose and $\mathbf{R_H}$ is the $nm \times nm$ full correlation matrix [[27],[28]] of size $nm \times nm$. $\mathbf{R_H}$ describes the spatial MIMO channel statistics and contain the correlations of all channel matrix elements and is given by

$$\mathbf{R_H} = E(\mathbf{hh}^H) \tag{2.17}$$

where $E(.)$ denotes the expected values. By using the distribution in equation(2.16), the realizations of the MIMO channel can be obtained by

$$\mathbf{H} = unvec(\mathbf{h}) \tag{2.18}$$

which is the inverse operation of $vec(.)$ with

$$\mathbf{h} = \mathbf{R_H}^{1/2} g \tag{2.19}$$

Here, $\mathbf{R_H}^{1/2}$ denotes an arbitrary matrix square root and $\mathbf{g}$ is an nm x 1 vector with i.i.d. Gaussian elements with zero mean and unit variance.

In order words, correlation-based models characterize the MIMO channel matrix statistically in terms of the correlations between the matrix entries. Popular correlation-based non physical channel models are the i.i.d Gaussian, Kronecker and the Weichselberger models.

2.2.3 The i.i.d Model

The i.i.d model is the simplest non-physical MIMO model, consisting of only one parameter ρ^2, the channel power. The correlation matrix $\mathbf{R_H}$ is given by

$$\mathbf{R_H} = \rho^2 \mathbf{I} \tag{2.20}$$

where I is the $nm \times nm$ identity matrix. In this model, all the elements of the channel matrix $\mathbf{H}$ are uncorrelated, statistically independent and have equal variance ρ^2 [29].

2.2.4 The Kronecker Model

This model assumes that spatial N_T and N_R correlation are separable, and the correlation matrix will be given in the following Kronecker product

$$\mathbf{R}_H = \mathbf{R}_{N_T} \otimes \mathbf{R}_{N_R} \tag{2.21}$$

with the N_T and N_R correlation matrix given by $R_{N_T} = E(\mathbf{H}^H\mathbf{H})$ and $R_{N_R} = E(\mathbf{H}\mathbf{H}^H)$ respectively. It can be shown that under the above assumption [26], the equation (2.19) simplifies to the Kronecker model

$$\mathbf{h} = (\mathbf{R}_{T_x} \otimes \mathbf{R}_{R_x})^{1/2}\mathbf{g} \tag{2.22}$$

$$\mathbf{H} = \mathbf{R}_{R_x}^{1/2}\mathbf{G}\mathbf{R}_{T_x}^{1/2} \tag{2.23}$$

with $G = \text{unvec}(g)$ an i.i.d unit variance MIMO channel matrix.

The enforcement of a separable AoD - AoA in this model will have a limitation on the Kronecker model. The model will not be able to reproduce the coupling of a single AoD with single AoA, which is an elementary feature of MIMO channels with single bounce scattering.

2.2.5 The Weichselberger Model

This model [30] aims to remove the restriction of the Kronecker model to separable that neglects significant parts of the spatial structure of MIMO channels. Its definition is based on the eigen value decomposition of the N_T and N_R correlation matrices

$$\mathbf{R}_{N_T} = \mathbf{U}_{N_T}\Lambda_{N_T}\mathbf{U}_{N_T}^H \tag{2.24}$$

$$\mathbf{R}_{N_R} = \mathbf{U}_{N_R}\Lambda_{N_R}\mathbf{U}_{N_R}^H \tag{2.25}$$

where, $\mathbf{U}_{N_T}$ and $\mathbf{U}_{N_R}$ are unitary matrices whose columns are the eigen vectors of R_{NT} and R_{N_R}, respectively, and Λ_{N_T}, Λ_{N_R} are diagonal matrices with corresponding eigen values. The model itself is given by

$$H = \mathbf{U}_{N_R} \left(\tilde{\Omega} \bullet \mathbf{G} \right) \mathbf{U}_{N_T}^T \tag{2.26}$$

where $\mathbf{G}$ is again an nxm i.i.d MIMO matrix, and $\tilde{\Omega}$ is the element-wise square root of an nxm coupling matrix Ω, whose elements determine the average power coupling between the N_T and N_R eigen modes. This coupling matrix allows for joint modeling of the N_T and N_R channel correlations. We note that the Kronecker model is a special case of the Weichselberger model obtained with the rank one coupling matrix $\Omega = \lambda_{R_x} \lambda_{T_x}^T$, where λ_{T_x} and λ_{R_x} are vectors containing the eigenvalues of the T_x and R_x correlation matrix, respectively.

2.3 Physical MIMO Models

Physical channel models characterizes the MIMO system by describing the double directional multipath wave propagation [31], between the location of the transmit N_T arrays and the location of the receiver N_R array without taking the antenna configurations and system bandwidth into account. Physical model give an accurate simulation of the wave propagation parameters. Physical MIMO channel model can be divided into - deterministic, geometry based, and non-geometric physical models.

2.3.1 Deterministic Models

These models reproduce the actual physical radio propagation parameters for a given environment. In urban environments, the geometric and electromagnetic characteristics of the environment and of the radio link can be easily restored in the files and the corresponding propagation process can be simulated through computer programs. These models are physically meaningful, and potentially accurate even though they can only represent certain type of environment. Due to the high accuracy and adherence to the actual propagation process, deterministic models may be used to replace measurements when time is not sufficient to set up a measurement campaign or when particular cases, which are difficult to measure in the real world, would be studied.

The most appropriate physical deterministic model for radio propagation in an urban area are Ray Tracing (RT) models [32]. RT models use the theory of geometrical optics to represent the MIMO channel propagation scenario.

2.3.2 Geometry-based Physical Models

With geometry based channel models, the impulse response of the channel H is characterized by the laws of wave propagation applied to specific N_T, N_R and scatterer geometry, which are chosen in a random manner. The most common geometry based MIMO channel models are the one-ring model and two-ring model [33].

2.3.2.1 One-Ring Model

In the one-ring model, the base station (BS) is assumed to be elevated and therefore not obstructed by local scattering while the mobile station (MS) is surrounded by scatterers. In this case, no line-of-sight (LOS) is assumed between the BS and MS and each ray is reflected only once. Actual power is accumulated by proper angular distribution.

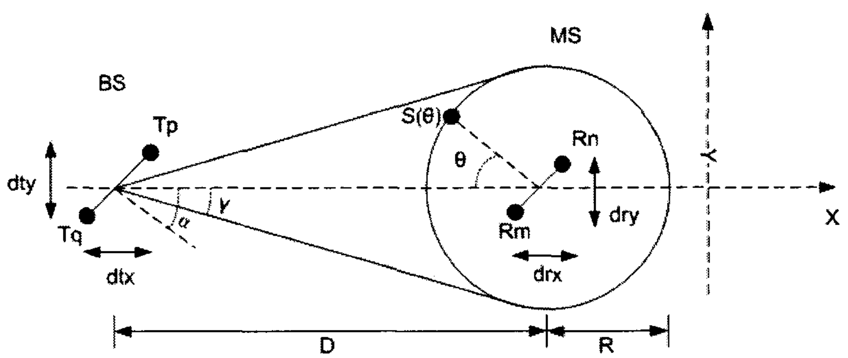

Figure 2.3: The one-ring model.

Figure 2.3 illustrates the one ring model. In the figure, T_p is the p^{th} antenna element at the BS, R_n is the n^{th} antenna element at the MS, D is the distance between the BS and MS, R is the radius of the ring of scatterers, α is the AOA at the BS, and γ (in the diagram Y) is the angle spread. Since D and R are much larger than the spacing between antenna elements, $\gamma = \arctan(R/D)$.

Taking these assumptions into consideration, an analytical expression for the channel matrix **H** was derived. Each complex element of the channel matrix is given in terms of specified channel parameters (number of antenna element at both BS and MS, AoA, radius of scattering ring, angle spread, and distance between the receiver and the transmitter).In the model, it is assumed that $S(\theta)$ is uniformly distributed in θ and the phase shift, $\phi(\theta)$, associated with each scatterer, $S(\theta)$,is distributed uniformly over $[-\pi, \pi)$ and i.i.d in θ.

Suppose that there are K effective scatterers $S(\theta_k)$,$k = 1, 2, \ldots, K$ distributed on the ring. The complex channel coefficient between the p^{th} elements at the BS and n^{th} element at the MS can be expressed as

$$H_{p,n} = \frac{1}{\sqrt{K}} \sum_{k=1}^{K} \exp\left(-j\frac{2\pi}{\lambda}(D_{T_p \to S(\theta_k)} + D_{S(\theta_k) \to R_n}) + j\phi(\theta_k)\right) \tag{2.27}$$

where $D_{X \to Y}$ denotes the distance between X and Y and λ is the wavelength. Due to the central limit theorem, when the number of scatterers becomes large, the channel coefficient is Gaussian distributed [24].

2.3.2.2 Two-ring Model

In the narrow band two-ring model presented in [27], both the BS and MS are surrounded by scatterers as shown in Figure 2.4. This can be not only outdoor wireless communications but also the case for indoor wireless communication. In this model, each ray is reflected twice and the complex channel matrix coefficients are given in terms of specified channel parameters (number of antenna elements at the BS and MS, AoA, AoD, radius of scatter rings, angle spread, and distance between BS and MS, very similar to one-ring model) and the channel coefficients are given by [24].

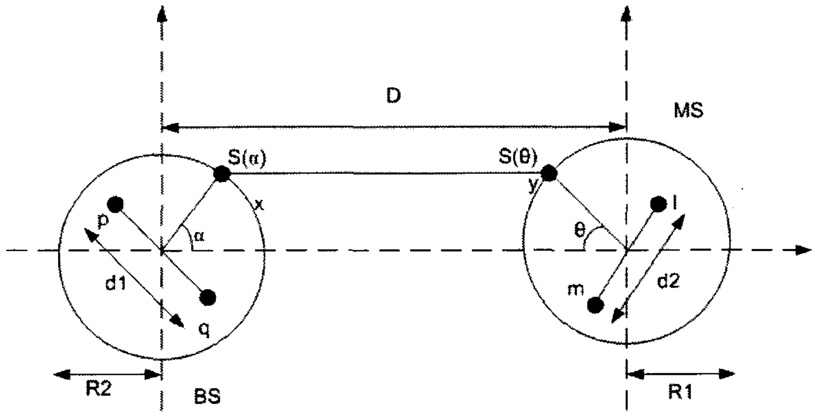

Figure 2.4: The two-ring model.

$$H_{p,n} = \frac{1}{\sqrt{K_1 K_2}} \sum_{k=1}^{K_1} \sum_{l=1}^{K_2} \exp\Big(-j\frac{2\pi}{\lambda}[D_{T_p \to S_1(\alpha_k)} + D_{S_1(\alpha_k)\to S_2(\beta_l)} + D_{S_2(\beta_l)\to R_n}] + j\phi_1(\alpha_k) + j\phi_2(\beta_l)\Big) \tag{2.28}$$

The difficulty in this model is that the signals reflected by the scatterers at the receive side are possibly not independent. Even if the number of scatterers, K_1 and K_2 go to infinity,the channel coefficient is still not zero-mean complex Gaussian. Therefore, the channel covariance matrix can not completely describe the MIMO channel [24].

2.3.3 Ring Models with von Mises Angular Distribution of AoA & AoD

Models that were proposed in [34], [35] that uses the von Mises angular probability density function as the angular PDF at he mobile side and takes the Doppler spread into account. We know that the angular spread of the BS, γ is small and $D \gg R \gg max(d_{pq}, d_{mn})$ where $d_{p,q}$ and $d_{n,m}$ are the element spacing at the BS and MS respectively, the cross covariance between two normalized channel coefficients can be approximated as follows

$$
\begin{aligned}
E[H_{p,n}(t)H_{q,m}^{H}(t+\tau)] &= \Bigg(\int_{0}^{2\pi} \exp(\frac{j2\pi}{\lambda}[d_{pq}\gamma\sin(\alpha)])\sin(\theta) \\
&\quad + d_{n,m}\cos(\theta-\beta) - j2\pi f_D[\cos(\theta-\phi)]\times \\
&\quad \tau p(\theta)d\theta \exp\left(\frac{j2\pi d_{pq}\cos(\alpha)}{\lambda}\right)\Bigg)
\end{aligned} \tag{2.29}
$$

where $f_D = v/\lambda$ is the Doppler shift, v is the speed of the MS and ϕ is the moving direction of the MS, and τ us the relative time difference between the two links. It been well known and proven that the von Mises angular PDF is a good model for the angular PDF, $p(\theta)$. The von Mises PDF is given as

$$
p(\theta) = \frac{\exp(k\cos(\theta-\mu))}{2\pi I_0(k)}, \quad \theta \in [-\pi, \pi) \tag{2.30}
$$

where $I_0(.)$ is the zero order modified Bessel function and μ is the mean AoA at the MS. After we insert the equation 2.30 into the equation 2.29, we will get the following equation:

$$
\begin{aligned}
E[H_{p,n}(t)H_{q,m}^{H}(t+\tau)] &= \Bigg(\frac{\exp[jc_{pq}\cos(\alpha)]}{I_0(k)}\times \\
&\quad I_0(k^2 - a^2 - b_{nm}^2 - c_{pq}^2\gamma^2\sin^2(\alpha) + 2ab_{nm}\cos(\beta-\phi)) \\
&\quad +2c_{pq}\gamma\sin(\alpha)[a\sin(\phi)b_[nm]\sin(\beta)] - j2ka\cos(\mu-\phi) \\
&\quad -b_{nm}\cos(\mu-\beta) - c_{pq}\gamma\sin(\alpha)\sin(\mu)^{1/2}\Bigg)
\end{aligned}
$$

where $a = 2\pi f_D\tau$,$b_{nm} = 2\pi d_{nm}/\lambda$ and $c_{pq} = 2\pi d_{pq}/\lambda$. The distribution gives a closed-form expression and therefore, it can be used to study the channel covariance analytically.

2.3.4 Distributed Scattering Model

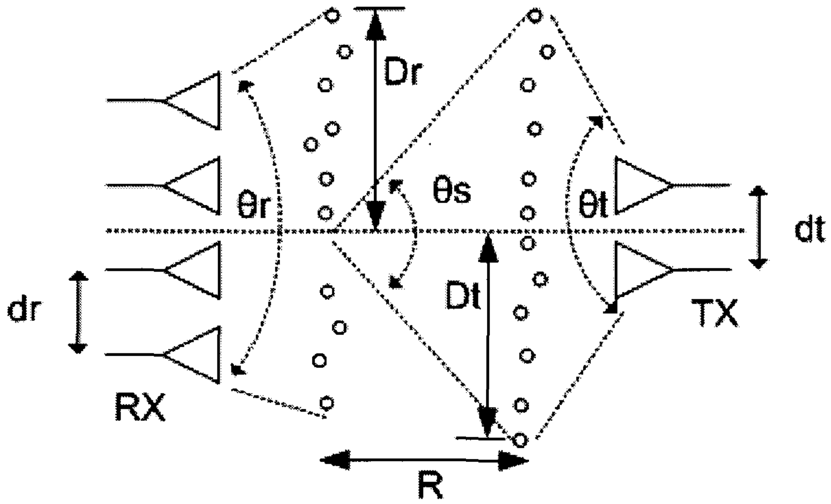

Figure 2.5: The distributed scattering model.

Assume there are N_T transmit elements and N_R receive elements. We also assume that there is a plane wave because both the transmitter and receiver are obstructed by the surrounding scatterers where the distance between them is large enough. We also assume that there are S scatterers on both sides where it is large enough to have random fading. The scatterers at the receive side can be seen as a virtual array between the transmitter and receiver. Therefore the channel function can be shown as

$$\mathbf{H} = \frac{1}{\sqrt{S}}\mathbf{R}^{1/2}_{\theta_r,d_r}\mathbf{G}_r\mathbf{R}^{1/2}_{\theta_s,2D_r/S}\mathbf{G}_t\mathbf{R}^{T/2}_{\theta_t,d_t} \tag{2.31}$$

where $\frac{1}{\sqrt{S}}$ is a normalization factor, $\mathbf{G}_t$ and $\mathbf{G}_r$ are random matrices with i.i.d zero mean complex Gaussian elements. R_{θ_t,d_t},$R_{\theta_s,2D_r/S}$ and R_{θ_r,d_r} are the correlation matrices seen from the transmitter, virtual array, and receiver respectively. For uniformly distributed AoA, the (m,k), the element of the correlation matrix can be expressed as

$$[R_{\theta,d}]_{m,k} = \frac{1}{S}\sum_{i=-\frac{S-1}{2}}^{\frac{S-1}{2}} e^{-2j\pi(k-m)d\cos(\pi/2+\theta_i)} \tag{2.32}$$

where S should be odd, d is the array element distance and θ_i is the AoA of the i^{th} scatterer. We should note that when the angle spread of the AoA is small or the array inter-element distance is small, the correlation matrix lose rank, otherwise it will converge to the identity matrix, i.e. a full rank matrix. When the distance R is large compared with the product of D_t, D_r the virtual array correlation matrix will be low rank and the MIMO channel will be low rank.

2.4 Standardized models

These models are an important tool for the development of new systems. They allow different parties to work and improve a specific design using different techniques such as signal processing, multiple assets,etc. in an unified manner. There are several MIMO models - COST 259 [36], COST 273 [37], 3GPP [38], SCM, WINNER, IEEE and SUI Models. We will only discuss a few models in this section.

2.4.1 Cost 259/275

"COST" is an abbreviation for European Cooperation in the field of Scientific and Technical research. Several COST initiatives were dedicated to wireless communications, in particular COST 259 "Flexible personalized wireless communications" which is a physical model that gives a model for a delay and angular dispersion at BS and MS, for different environments. It was the first model that explicitly took the rather complex relationship between BS-MS-distance, delay dispersion, angular spread, and other parameters into account.

Each environment is described by external parameters (e.g.,BS position, radio frequency, average BS and MS height) and by global parameters,which are sets of probability density function and/or statistical moments characterizing a specific environment.Each environment contains a number of propagation environments,(which are defined as realizations of the global parameters), are approximately constant; they are typically several meters in diameter. These parameters are randomly generated realizations of the global parameters and describe the instantaneous channel behavior. We should note that the COST 259 model can handle the continuous movement of the MS over several propagation environments, and even across different radio environments. Details can be found in [39],[40]. There are two major restrictions in this model. Scatterers are assumed stationary so that channel time variations are solely due to MS movements; this obviously excludes certain environments (e.g., indoor scenarios with person moving around). Delay attenuations are modeled as complex Gaussian random variables. This requires a sufficiently large number of multi path components within each delay bin, a condition that is not met in some situations. The latter assumption is also made in all other standardized channel models.

The COST 273 is "Towards mobile broad-band multimedia networks". The COST 273 channel models are different in several key respects,to the COST 259:

1. To reflect new applications of MIMO systems, new radio environments are defined (e.q., peer-to-peer and fixed-wireless-access scenarios).

2. All parameters are updated based on new measurement.

3. Same modeling is approach is used for all types of cells as COST 259.

4. The model for AoA and AoD is different then the COST 259.

One cluster is split up into two representations of itself: one that represents the cluster as seen by the BS and one as it is seen by the mobile terminal. Both realizations look identical, like twins. Each ray propagated at the transmitter is bounced at each scatterer in the corresponding cluster and reradiated at the same scatterer of the twin cluster towards the receiver. The two cluster representations are linked via a stochastic cluster link delay,which is the same for all the scatterers inside the cluster. The cluster link delay ensures realistic path delays as, for example, derived from measurement campaigns, whereas the placement of the cluster is driven by the angular statistics of the cluster as observed from BS/MT, respectively.

2.4.2 The WINNER Channel Models

The channel model developed in the Information Society Technologies (IST)-WINNER [41] project are related to both the COST 295 model and the 3GPP SCM model. The spatial channel model (SCM) was developed by 3GPP/3GPP2 to be a common reference for evaluating different MIMO concepts in outdoor environments at the center frequency of 2GHz and a system bandwidth of 5MHz. The WINNER models adopted the SCM principle to model all channel scenarios with the same generic structure [26]. Generic models are intended for system-level simulations, while clustered delay line (CDL) models, with fixed small scale parameters, are used for calibration simulations [26].

In the first stage of the WINNER modeling work, the 3GPP SCM model was selected for immediate simulation needs, due to the narrow bandwidth and the limited frequency applicability range, the SCM model was extended to the SCM-Extended (SCME). Then the model was extended to have a bigger bandwidth and also have new definition of path loss functions. Further upgrades to the original model include the LOS option, the consideration of elevation in indoor scenarios, auto-correlation function modeling of large scales and dependent polarization modeling. The model is scalable from single SISO or MIMO link to a multi-link [26][41].

2.4.3 SUI Models and IEEE 802.16a

The Stanford University Interim (SUI) channel models were developed for macro-cellular fixed wireless networks and were further enhanced in the framework of IEEE 802.16a for fixed broad band wireless access [26].The targeted scenario for these models is as follows:

- cell size is less than 10km in radius
- user's antenna is fixed and installed on rooftop (Nlos is required)
- the base station height is 15 to 40 m, above the rooftop
- bandwidth is from 2 to 2 MHz.

The MIMO direction components of the SUI/802.16a models is not highly developed within the standard itself, but the extensions of the standards were investigated and are described here as well.

SUI Channel Models: For each tap-delay line, the SUI channel is characterized by a single antenna correlation coefficient at the user's terminal, without giving any consideration to the user's terminal array configuration, while the antenna correlation at the BS is taken as equal to zero, assuming a large BS antenna spacing. This is the only characteristic that is included in this model. We should note that in the original models, antennas were assumed to be omnidirectional at both sides. Another specific aspect of SUI models is that the Doppler spectrum of each tap is not given by the classical Jakes spectrum, but by a rounded shape centered around 0 Hz [26].

IEEE 802.16a Models: These models are based on the modified version of the SUI channel models. They are valid for both omnidirectional and directional antennas. In the standard, the use of directional antennas naturally causes the K-factor of the Rician taps to increase and the global delay-spread to decrease. However, the model does not modify the correlations at the user's terminal when reducing the bandwidth, we might have expected the correlation.

2.5 MIMO Channel Modeling and Simulation

We all know that the increasing demand for high data rates and the limited available bandwidth motivates the investigation of wireless systems that efficiently exploit the spatial domain. We use antenna arrays only at the base stations due to the cost size and its complexity but using it on both transmitter and receiver will improve not only coverage and throughput but also allow a higher degree of spectral reuse and increase the system capacity. Channel capacity can be increased by using antenna array at both transmit and receiver side, as long as the environment provides sufficient scattering. Some field measurements investigating MIMO channel capacity have recently been reported in [42],[43]. Most of these reports have presented that the scattering has been sufficiently rich to provide capacities close to the ideal situation. It is every one interest to characterize and model the MIMO channel for different conditions in order to predict, simulate and design high performance communication systems. One of the advantages is that the simulation of MIMO propagation channel can assist in the choice of efficient modulation schemes under different scenarios and system performance can be accurately predicted. There have been reports regarding SISO channel modeling, indoor radio channels [44]- [49] and outdoor radio channels [50],[51]. A great effort was also explained recently to conduct measurements for MIMO channel. However they are very expensive and not open to public use.

We review some of the published research on MIMO channel modeling and we focus on the non-physical and physical models. The non-physical models are derived from the statistical characteristics of the MIMO channel,whereas the physical models use channel parameters to clearly describe the characteristics of the MIMO channel as well as the surrounding scattering environment.

2.5.1 AR Model

If a model can be successfully fitted to a data stream, it can be transformed into the frequency domain instead of the data upon which it is based, producing a continuous and smooth spectrum. This is the basic premise of the spectra produced using autoregressive (AR) modeling. In an AR model, a value at time t is based upon a linear combination of prior value (forward prediction), upon a combination of subsequent values (backward prediction) or both (forward-backward prediction. The linear models give rise to rapid and robust computations. To preserve the degrees of freedom for statistical tests and to furnish a common reference for all AR algorithms, AR model can be define as follows:

$$\begin{aligned} y_k &= \sum_{j=1}^{p} a_j x_{k+j} \quad k = p, \dots, 1 \\ y_k &= \sum_{j=1}^{p} a_j x_{k-j} \quad k = p+1, \dots, N \end{aligned}$$

In these equations, x is the data series of length N and a is the autoregressive parameters array of order p. The first equation uses a positive sign, which defined as reverse prediction of the first p values, and forward prediction for the remaining $N-p$ values.

The AR coefficients can be computed in a variety of ways. The coefficients can be computed from autocorrelation estimates, from partial autocorrelation coefficients, and from lease squares matrix procedures. An AR model using the autocorrelation method will depend on the truncation threshold (maximum lag) used to compute the correlations. The partial autocorrelation method will depend on the specific definition for the reflection coefficient. The least-squares methods will also yield results that are a function of how data are treated at the bounds as well as whether the data matrix or normal equations are fitted.We will explain more about this in the later sections. The details for this chapter are explained in AR chapter.

2.5.2 Cluster Models

Statistical cluster models directly specify distributions on the multipath AoA/AoD, Time of Arrival (ToA), and complex amplitude. Most current models are based on initial work by Turin u,et al. who observed that multipath components can be grouped into clusters that decay exponentially with increasing delay time. Intuitively, a single cluster of arrivals might corresponds to a single scattering object and the arrivals within the cluster arise because of smaller objects features. Statistical descriptions of the multipath arrival parameters can be obtained from measurements or from ray tracing simulations [52]. Provided that the underlying statistical distributions are properly specified, these models can offer highly accurate channel representations. One of the well known model that fits into this category is Saleh-Valenzuela model which include AoA/AoD in addition to ToA and multipath amplitude. The Saleh-Valenzuela Model with Angle (SVA model) is based on the experimentally observed phenomenon that multipath arrivals appear at the receiver in clusters in both space and time. We will refer to arrivals within a cluster as rays and will restrict our discussion to the horizontal plane for simplicity ($\theta_T = \theta_R = \pi/2$). If we assume we have L clusters will K rays per cluster, then the directional channel impulse response can be written as

$$
\begin{aligned}
h_p(\tau, \theta_R, \theta_T) &= \frac{1}{\sqrt{LK}} \sum_{l=0}^{L-1} \sum_{k=0}^{K-1} \beta_{kl} \delta(\tau - T_l - \tau_{kl}) \\
&= \delta(\phi_T - \Phi_{T,l} - \phi_{T,kl}) \delta(\phi_R - \Phi_{R,l} - \phi_{R,kl})
\end{aligned}
$$

where we have removed the time dependence, and the summation now explicitly reveals the concepts of clusters and rays within the clusters. The parameters T_l, $\Phi_{T,l}$ and $\Phi_{R,l}$ represent the initial arrival time, mean departure angle, and mean arrival angle respectively, of the l^{th} cluster. Also, in this context, the k^{th}, ray arrival time τ_{kl}, departure angle $\phi_{T,kl}$ and arrival angle $\phi_{R,kl}$ are taken with respect to the mean time/angle values for the l^{th} cluster.

2.5.3 Data Model

The baseband relationship for Multi-Input Multi-Output system with N_T transmitting and N_R receiving antennas can be expressed as

$$
\mathbf{y}(t) = \mathbf{H}(t) * \mathbf{s}(t) + \mathbf{n}(t) \tag{2.33}
$$

where $\mathbf{s}(t)$ is the transmitted signal, $\mathbf{y}(t)$ is the received signal, $\mathbf{n}(t)$ is additive white Gaussian noise (AWGN) and " $*$ " denotes convolution. $\mathbf{H}(t)$ is an N_T x N_R channel impulse response matrix.

If $\mathbf{H}$ is a narrow band MIMO channel matrix, where the signal bandwidth is narrow, comparing to the coherence bandwidth of the channel [2], $\mathbf{H}$ can be treated as approximately constant over frequency (frequency flat channel). Then the input and out put relationship simplifies to

$$
y = \mathbf{H}s + n \tag{2.34}
$$

where $\mathbf{H}$ is the narrow band MIMO channel matrix. In many cases, the elements of narrow band MIMO channel matrix are assumed to be i.i.d to study the MIMO channel capacity. We will discuss about different type of channel capacity in later sections. We will also explain how this i.i.d changes in reality due to insufficient spacing between antenna elements and limited scattering in the environment, and how this effect our MIMO channel capacity.

2.5.4 Model Classification

Recently, much interest has been based on modeling channel of the channel impulse response $\mathbf{H}(t)$ for wideband system or the narrowband system, because it is very critical for the simulation of MIMO communication systems. Several research and measurement works have been reported in this area and the proposed models can be classified in several different ways.

2.5.5 Wideband vs. Narrowband Models

The MIMO channel can be divided into two models - wideband and narrowband model. The wideband scenario considered the propagation channel as frequency selective, which means that different frequency will have different channel coefficient. The narrowband assume that the channel has frequency nonselective fading also known as flat fading therefore the channel has the same response over the entire system BW. The time varying wide band models treat the MIMO channel as the sum of a line-of-sight (LoS) component and fading components

$$\mathbf{H}(\tau) = \sum_{i=1}^{L} \mathbf{H}_i \delta(\tau - \tau_i) \tag{2.35}$$

where only $\mathbf{H}_1 = \mathbf{H}_{LOS} + \mathbf{H}_{random}$ contains a LOS component and a random fading component [53]. $\mathbf{H}(\tau)$ is a complex matrix and the H_i is the linear transformation between the two antenna arrays at delay τ_i. We can use any of the flat fading models to design $\mathbf{H}_i$ in this case. Now for narrow band models, the channel is modeled as a sum of the LOS and the NLOS component of the channel matrix H as follows:

$$\mathbf{H} = \mathbf{H}_{LOS} + \mathbf{H}_{NLOS} \tag{2.36}$$

These could be correlated or not based on the specification of the given model. The model of the channel matrix $\mathbf{H}$ is related to so called the Rican factor K, which is the ratio between the power of the LOS component and the mean power of the NLOS component. We can find wide band MIMO channel models in [54],[55]and[56].

2.5.6 Field Measurement vs. Scatter Models

One of the approaches to model a MIMO channel is to measure the MIMO channel response through field measure, where some characteristics of the MIMO channel can be obtained by investigating the recorded data, then the channel can be modeled to have similar characteristics. Models based on MIMO channel measurements are reported in [54] - [59]. An alternate approach is to assume a model which captures the channel's characteristics by using distributed scatterers. If the scattering environment is reasonable enough, the model represents the fundamental characteristics of the MIMO channel. Examples of scatterer models can be found in [27] and [60].

We can categorize the scattering around the antennas at the both ends as strong or weak scattering. Strong scattering is formed from large spatial separations of reflectors and/or fast moving antenna. Therefore, there will be a large phase variations θ from the antennas and the scatterers. The probability density function of the phase variation is uniform in this case and given by

$$P_\theta(\theta) = \frac{1}{2\pi} \tag{2.37}$$

Weak scattering is formed from closely spaced reflectors and a relatively small variation in the phase of different rays. In this case, the probability density function (PDF) of the phase variation can be conveniently descried by the von Mises PDF [24].

$$\rho_\theta(\theta) = \frac{\exp\left[k\cos(\theta-\mu)\right]}{2\pi I_0(k)}, \quad \theta \in [-\pi, \pi), \tag{2.38}$$

where $I_0(.)$ is the zero order modified Bessel function and μ is the mean of angle of arrival (AoA) at the mobile station (MS) or angle of departure (AoD) at the BS. The following figure illustrates slopes of $\rho_\theta(\theta)$ for different values of k more about

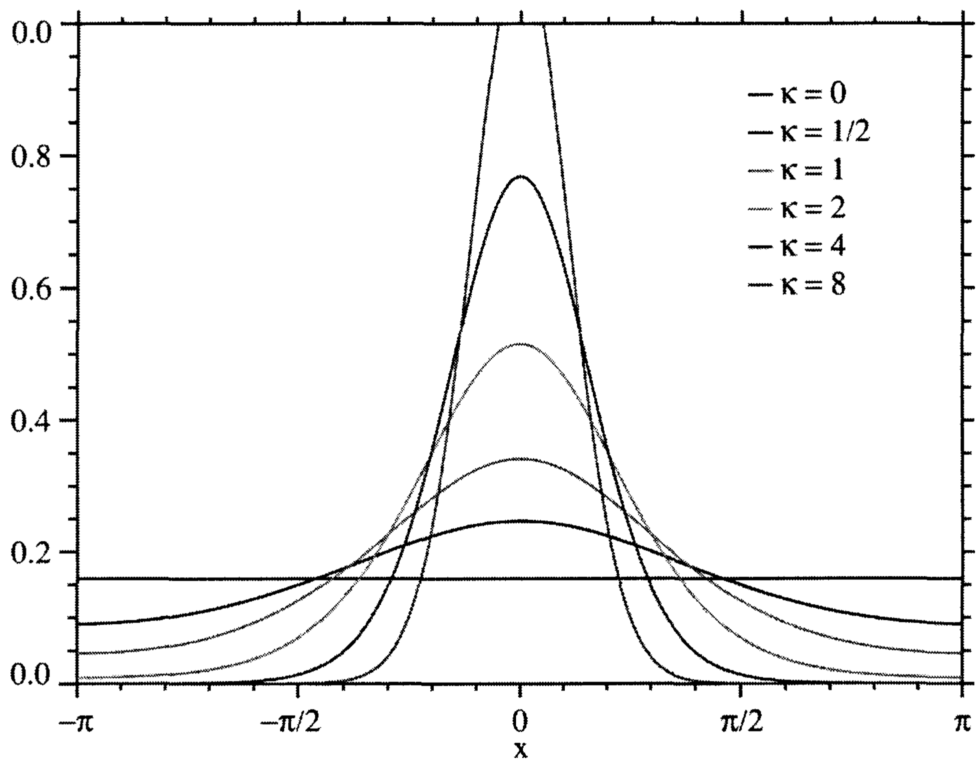

Figure 2.6: The phase PDF based on different k values.

Equation (2.37) and Equation (2.38).

For example, the parameter k can be chosen between $k = 0$ for isotropic scattering, which results in a uniform phase distribution or $k = \infty$ for extreme non isotropic scattering. This model is widely used by researchers due to its convenient analytical properties [33].

2.6 Conclusion

This chapter should give the reader better understanding of how the models of MIMO wireless channels work. We explained from very simple basic design up to more complex and mathematical designs of the channels in this chapter. The reader should note that some of the sections are repeated in the latter chapters to be explained in more depth. The following table summarizes the list of models that was discussed in this chapter:

Physics Based(Propagation Based)	**Other Models**
Gaussian Channel	Autoregressive Model
Rayleigh Fading Channel	Unitary-Independent-Unitary(UIU) Model
Rician Channel	Wide band & Narrow band Model
Deterministic/Geometry Base	Non-Physical Channel
Propagation Motivated Channels	
Physical MIMO Models	
Mobile-to-Mobile Model	

Table 2.1: Standards of MIMO channel models.

Chapter 3
Unitary-Independent-Unitary (UIU) Channel Modeling

3.1 Introduction

Recent research results have shown tremendous potential capacity improvement achieved by Multiple-Input Multiple Output (MIMO)systems [61] [62] which employ antenna arrays at both sides to create multiple parallel channels between transmitter and receiver and increase data rates without additional power or bandwidth consumption. While initial studies were based on an idealized i.i.d channel model, recent analytical and experimental results show that the statistics of MIMO channels, especially the correlation between antennas, have a significant impact on channel capacity [63] [67]. Moreover, MIMO systems are expected to support high-data-rate communications, which inherently requires large bandwidths and inevitably leads to frequency-selective channels. Therefore, a better understanding of wideband MIMO channels is critical for the design and performance prediction of MIMO systems. Many channel models have been proposed to study the MIMO system performance and can be basically classified as propagation-inspired and analytic models. Performance inspired models are aimed at describing the channel via individual physical paths. Each path is associated with distinct transmit/receive angles, delay, Doppler shift and complex path amplitude. It is very accurate but the large number of nonlinear physical parameters make the propagation models difficult to analyze theoretically.

Instead of modeling each individual path, analytical models are aimed at modeling the joint statistics of channel coefficients. Initial studies assumed that the channel coefficients associated with different transmit and receive antenna pairs are uncorrelated Gaussian random variables. This assumption corresponds to rich scattering environment and promises a linear capacity growth with the minimum of the number of transmiter and receiver antennas. Recent experimental and analytical investigations have reveled that the realistic MIMO channels show significantly lower capacity due to the correlation of channel coefficients [43][64][66]. To incorporate correlation, the Kronecker model has been proposed, which assumes that the channel correlation is a product of the correlations at the transmitter and receiver sides. Based on this assumption, it models the channel matrix as a product of receive and transmit correlation matrices and an i.i.d Gaussian random matrix. The product correlation assumption implies a product structure on the 2D angular power spectrum, which is usually not the case in realistic channel.

The recently proposed Virtual Channel Representation (VCR)[19] for Uniform Linear Arrays (ULA) provides an intuitive and tractable representation of MIMO channel and yields many insights into channel statistics and capacity behavior. Virtual representation is essentially 2D Fourier transform of the actual channel matrix, and the transformed matrix can be modeled as element wise product of a virtual channel power matrix and an i.i.d Gaussian random matrix. Therefore, unlike the Kronecker model, the non separable channel statistics are preserved. Virtual channel representation can be easily extended to the time varying frequency selective scenario. For our research, we will show how to design the virtual representation model,its estimation and channel responses.

3.2 Channel Modeling

We investigate narrow band channel here. Consider a transmitter array with P elements and a receiver array with Q elements. In the absence of noise, the transmitted and received signals are related as

$$\mathbf{x} = \mathbf{H}\mathbf{s} \tag{3.1}$$

where $\boldsymbol{s}$ (P-dimensional transmitted signal),$\boldsymbol{x}$ (Q-dimensional received signal) and H (channel matrix coupling the transmitter and receiver elements). We can define the index entries of $\mathbf{H}$ as $H(m,n) : m = 0,1,\ldots,Q-1,\ n = 0,1,\ldots,P-1$.

For simplicity of presentation we focus on one dimensional (1-D) uniform linear arrays (ULAs) of antennas at both the transmitter and the receiver and consider far field scattering characteristics. Far field scattering is defined as taking place with the scatterers sufficiently distant from both the transmitter and receiver. The array steering and response vectors are given by [20]

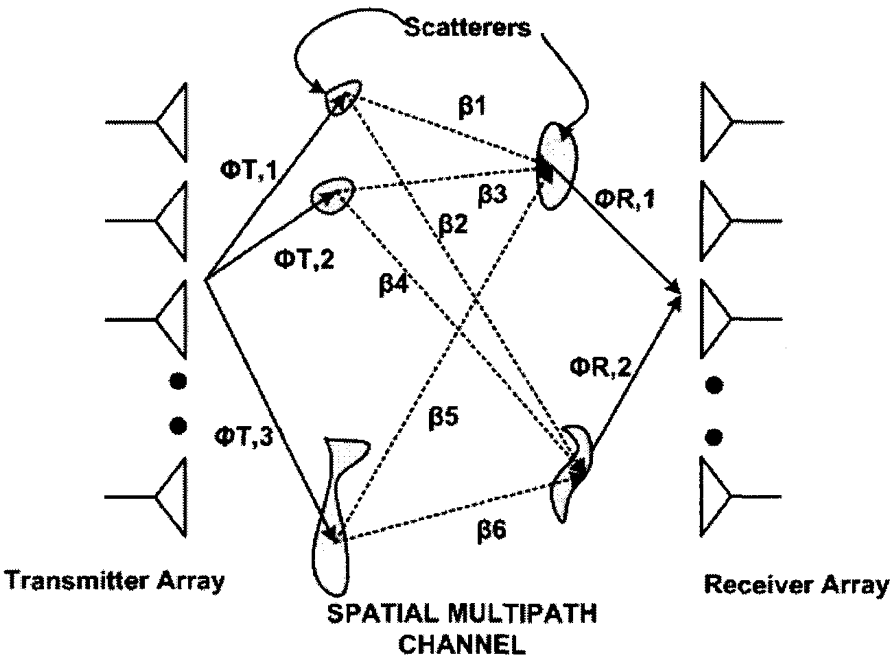

Figure 3.1: Schematic illustrating physical channel modeling

$$a_T(\theta_T) = \frac{1}{\sqrt{P}}\left[1, e^{-j2\pi\theta_T,\ldots,e^{-j2\pi(P-1)\theta_T}}\right]^T \tag{3.2}$$

$$a_R(\theta_R) = \frac{1}{\sqrt{Q}}\left[1, e^{-j2\pi\theta_R,\ldots,e^{-j2\pi(Q-1)\theta_R}}\right]^T \tag{3.3}$$

where θ and ϕ are related as

$$\theta = \frac{d\sin(\phi)}{\lambda} = \alpha\sin(\phi) \tag{3.4}$$

$$\phi = \arcsin\left(\frac{\theta}{\alpha}\right) \tag{3.5}$$

λ is the wavelength of propagation, and $\alpha = d/\lambda$ is the normalized antenna spacing. The angle ϕ is measured relative to the horizontal axis (see in Figure 3.1 and 3.2). The vector $a_R(\theta_R)$ represents the signal response at the receiver array due to a point source in the direction θ_R. Similarly, $a_T(\theta_T)$ represents the array weights needed to transmit a beam focussed in the direction θ_T. We notes that due to the finite array aperture, the receiver array collects some signals from directions in the neighborhood of θ_R, and the transmit array couples energy at angles in the neighborhood of θ_R as well. We should note that equation (3.4) defines a one-to-one map between $-\pi/2 \leq \phi < \pi/2$ and $\alpha \leq \theta < \alpha$. In case of $\alpha = 0.5$, there is a one-to-one mapping between$\theta \in [-0.5, 0.5]$ and $\phi \in [-\pi/2, \pi/2]$.

3.2.1 Physical Modeling of Scattering Environment

The channel matrix $\mathbf{H}$ can be modeled as [19]

$$\mathbf{H} = \int_{-\alpha_R}^{\alpha_R}\int_{-\alpha_T}^{\alpha_T} G(\theta_R, \theta_T)\ x\ a_R(\theta_R)a_T^H(\theta_T)d\theta_R d\theta_T \tag{3.6}$$

$$H(m,n) = \frac{1}{\sqrt{PQ}}\int_{-\alpha_R}^{\alpha_R}\int_{-\alpha_T}^{\alpha_T} G(\theta_R, \theta_T)\ x\ e^{-j2\pi\theta_R m}e^{j2\pi\theta_T n}d\theta_R d\theta_T \tag{3.7}$$

where $G(\theta_R, \theta_T)$ represents the physical scattering and we can call is as the spatial spreading function. We will explain more in details how we create this in our simulation. When $G(\theta_R, \theta_T)) = 0$ for $|\theta_R| > \alpha_R$,$|\theta_T| > \alpha_T$, we can rewrite the above equation as

$$H = \int_{-1/2}^{1/2}\int_{-1/2}^{1/2} \hat{G}(\theta_R, \theta_T) a_R(\theta_R) a_T^H(\theta_T)\, d\theta_R\, d\theta_T \tag{3.8}$$

$$G(\theta_R, \theta_T) = G(\theta_R\ mod1, \theta_T\ mod1) \tag{3.9}$$

where θ mod 1 denotes the value of θ in the principal period $[-0.5, 0.5)$. We can note here that, in many realistic environments, $G(\theta_R, \theta_T)$ is nonvanishing in smaller regions corresponding to scattering clusters with limited angular spreads, as illustrated in Figure 3.1. Each cluster is represented by a non-vanishing sub-kernel of $G(\theta_R, \theta_T)$ with support $[-\alpha_T, \alpha_T] \times [-\alpha_R, \alpha_R]$. We have designed out matrix G for both Uniform and Gaussian distribution.

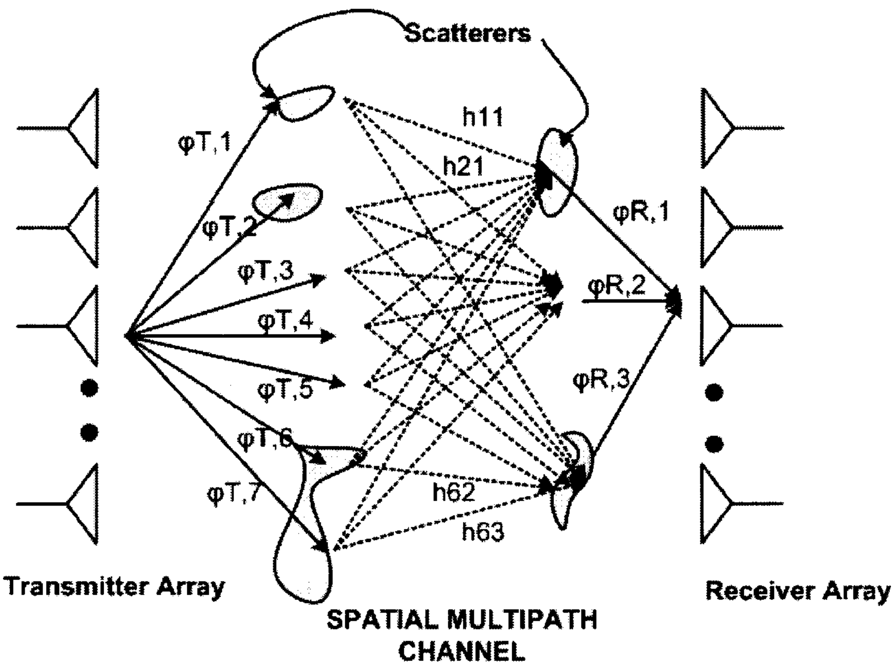

Figure 3.2: Schematic illustrating virtual channel modeling

A widely used discrete physical model which is given in figure 3.1 and is given by

$$H = \sum_{l=1}^{L} \beta_l \, a_R(\theta_{R,l}) a_T^H(\theta_{T,l}) = \mathbf{A}_R(\theta_R) \; \mathbf{H}_P \; \mathbf{A}_T^H(\theta_T) \tag{3.10}$$

with corresponding G matrix as

$$G(\theta_R, \theta_T) = \sum_{l=1}^{L} \beta_l \; \delta(\theta_R - \theta_{R,l}) \; \delta(\theta_R - \theta_{T,l})$$

In the above model, the transmitter and the receiver are coupled via propagation along L paths with $\theta_{T,l}$ and $\theta_{R,l}$ as the spatial angles seen by the transmitter and receiver, respectively, and the β_l as the corresponding independent path gains. We can write $\mathbf{A}_R(\theta_R)$ and $\mathbf{A}_T(\theta_T)$ in the following form as well:

$$\begin{aligned}
\mathbf{A}_R(\theta_R) &= [a_R(\theta_{R,1}, \ldots, \theta_R(\theta_{R,l}))] \; (Q \; \times \; L) \\
\mathbf{A}_T(\theta_T) &= [a_T(\theta_{T,1}, \ldots, \theta_T(\theta_{T,l}))] \; (P \; \times \; L) \\
\mathbf{H}_P &= \mathrm{diag}(\beta_1, \ldots, \beta_L) \; (L \; \times \; L)
\end{aligned}$$

One important thing we should note here is that, it is linear in the path gains β_l but nonlinear in the spatial angles $\{\theta_{R,l}, \theta_{T,l}\}$.

3.2.2 Virtual Channel Representation

The finite dimensionality of the spatial signal space can be exploited to develop a linear virtual channel representation that uses spatial beams in fixed virtual direction. This is similar to beam space and wave number domain in array processing literature. We will assume that both P and Q are odd and define:

$$\begin{aligned}
\tilde{Q} &= (Q-1)/2 \\
\tilde{P} &= (P-1)/2
\end{aligned}$$

The virtual channel can be represented as shown in Figure 3.2 and the channel matrix can be written as

$$H = \sum_{q=-\tilde{Q}}^{\tilde{Q}} \sum_{p=-\tilde{P}}^{\tilde{P}} H_V(q,p)\mathbf{a}_R(\tilde{\theta}_{R,q})\mathbf{a}_T^H(\tilde{\theta}_{T,p}) = \tilde{\mathbf{A}}_R \, \mathbf{H}_V \, \tilde{\mathbf{A}}_T^H \tag{3.11}$$

where the matrices

$$\begin{aligned} \tilde{\mathbf{A}}_R &= [\mathbf{a}_R(\tilde{\theta}_{R,-\tilde{Q}}), \ldots, \mathbf{a}_R(\tilde{\theta}_{R,\tilde{Q}})] \\ \tilde{\mathbf{A}}_T &= [\mathbf{a}_T(\tilde{\theta}_{T,-\tilde{P}}), \ldots, \mathbf{a}_T(\tilde{\theta}_{T,\tilde{P}})] \end{aligned}$$

are defined by the fixed virtual angels $\{\theta_{R,q}\}$ and $\{\theta_{T,p}\}$ and are full rank. The $\mathbf{H}_V$ is the virtual channel representation. Following [66], we decided to use virtual spatial angles to be uniformly sampled and get

$$\begin{aligned} \tilde{\theta}_{R,q} &= \frac{q}{Q}, \quad -\tilde{Q} \leq q \leq \tilde{Q} \\ \tilde{\theta}_{T,p} &= \frac{p}{P}, \quad -\tilde{P} \leq p \leq \tilde{P} \end{aligned} \tag{3.12}$$

which results in the steering/response vectors in equation 3.2 being sinusoids with frequencies $\tilde{\theta}_{T,p}/\tilde{\theta}_{R,q}$ and the $\tilde{\mathbf{A}}_R$ and $\tilde{\mathbf{A}}_T$ matrices becomes unitary matrices. Now we will explain how we will chose the ϕs that is given in the figure 3.2. These corresponding fixed angles in the ϕ domains are shown in the figure 3.3 for different values of α.

$$\begin{aligned} \phi_{T,p} &= \arcsin\left(\frac{\tilde{\theta}_{T,p}}{\alpha_T}\right) = \arcsin\left(\frac{p}{P\alpha_T}\right) \\ \phi_{R,q} &= \arcsin\left(\frac{\tilde{\theta}_{R,q}}{\alpha_R}\right) = \arcsin\left(\frac{q}{Q\alpha_R}\right) \end{aligned} \tag{3.13}$$

The virtual channel coefficients $\mathbf{H}_V(q,p)$ represents the coupling between the

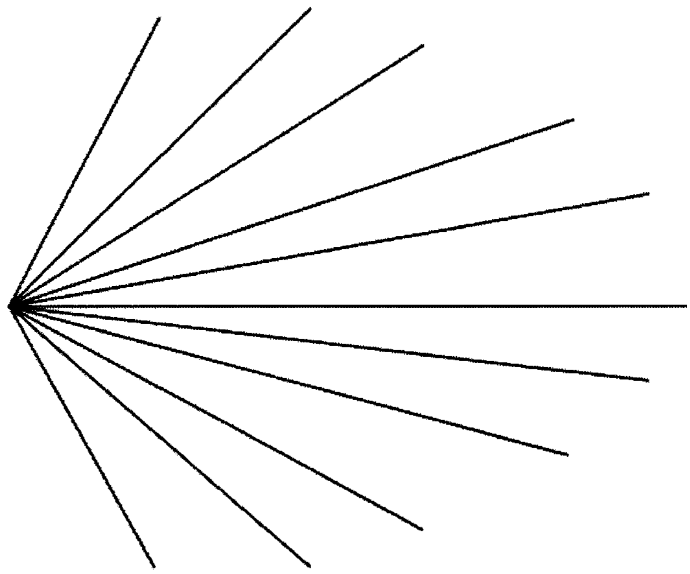

(a)

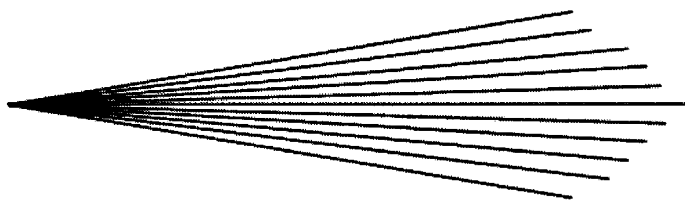

(b)

Figure 3.3: Beams in the ϕ domain corresponding to the fixed virtual angles for different values of α. The above plots correspond to an 11-element ULA (a) $\alpha = 0.5$ (b) $\alpha = 1.5$ $N = 11$

P virtual transmit angles $\{\phi_{T,p}\}$ and the Q virtual receive angles $\{\phi_{R,q}\}$.

3.2.3 Formulation of Channel Model

We can express H_V in matrix form for the continuous physical model as

$$\mathbf{H}_{model} = \mathbf{A}_R \left(\tilde{\Omega} \odot G \right) \mathbf{A}_T^H \tag{3.14}$$

where $\mathbf{G}$ is the random matrix with i.i.d zero-mean complex-normal entries with unit variance, and $\tilde{\Omega}$ is full rank and consists of real valued non negative elements. In our case, we have generated the channel from using the joint AoA/AoD PDF as the input function for $\tilde{\Omega}$ (e.g, Gaussian PDF as an input function or uniform, etc). Now, we will explain how each of the simulation is performed for our case and how the results are evaluated.

3.3 Simulation and Evaluation

In this section, we will explain sequence of steps that it takes to create the channel realization based on the theory mentioned above. The following are conditions taken as input parameters:

1. Joint AoA/AoD PDF $p(\theta_T, \theta_R)$ and the net power P_0. The corresponding PAS is then just $P_0 p(\theta_T, \theta_R)$
2. Number of Transmit N_T and receive, N_R antennas as well a s the separation between antennas d_T and d_R in λ (in wavelengths). We will assume Uniform Linear Array(Explained in the above sections).
3. Maximum Doppler frequency f_D and the sampling frequency F_s.
4. Number of required samples L.

As the first step, we have started creating an uncorrelated channel matrix H_w which is generated by individual SISO channel designed in Mobile-to-Mobile communication channel for SISO.In this case, we assumed that there is no line-of-sight (Rayleigh Fading Model) with $f_d T_s = 0.025$. Once we achieved this step, we generate Unitary matrices(A_T and A_R using the equations given above). We used $\alpha_T = 0.5 = \alpha_R$ and found out ϕ_T and ϕ_R using equation (3.13).

For the joint probability function at the input, we decided to use Gaussian PDF with mean at π (assuming it is from 0 to 2π), with some variance and with very fine resolution to get better calculation results for each end. The output of our Gaussian joint PDF is as shown in figure 3.4.

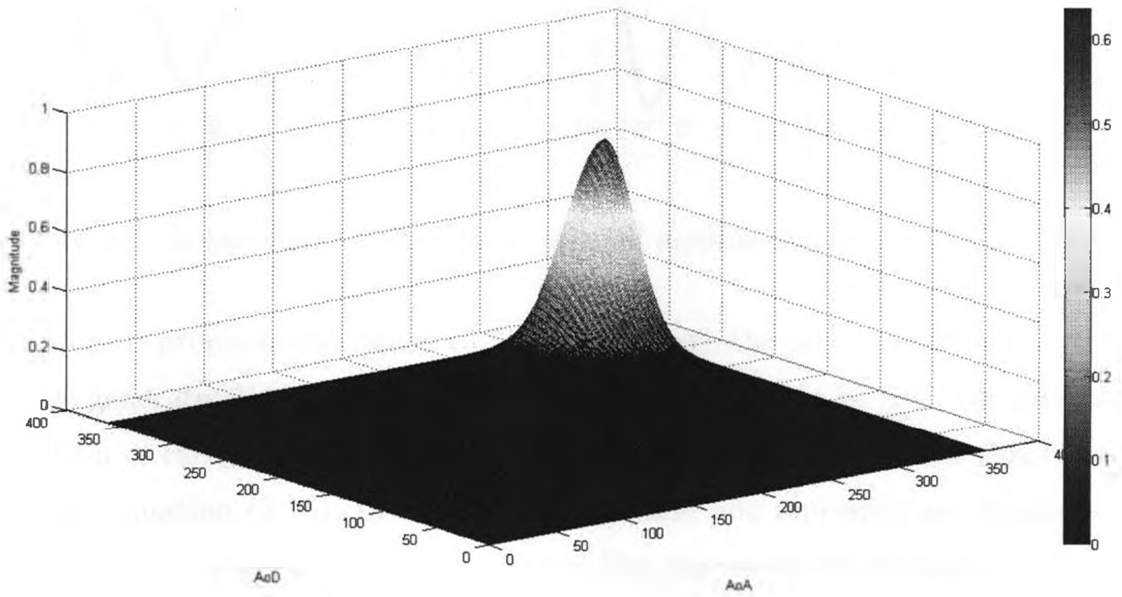

Figure 3.4: Gaussian Joint Probability Density Function

As we can see, the shape will depend based on our input such as the mean, variance and resolution. We can also create uniform joint PDF in this case. We should note here that, the ϕ is between the limited range ($-\pi/2$ to $\pi/2$). We found $\tilde{\Omega}$,given in equation (3.14), using the above joint PDF. Then we can find out H_{model} using equation (3.14). Now that we have created a UIU Channel Model we need to test against some theoretical result for comfirmation. For our theoretical simulation we used Jake's model:

$$R_{xx} = J_0(2\pi f_d \tau) \tag{3.15}$$

The result of each channel's autocorrelation to theoretical results are given below.

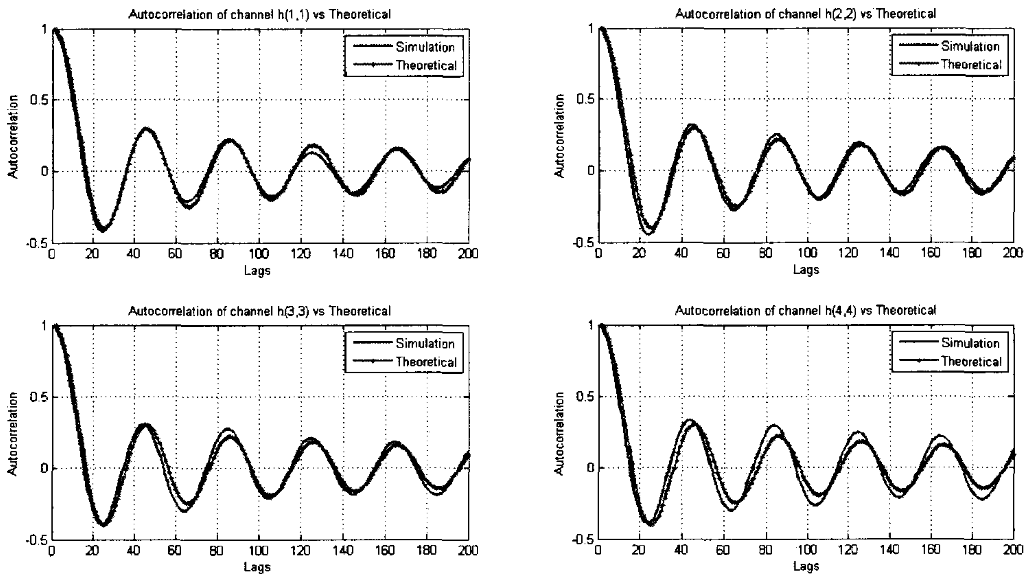

Figure 3.5: Autocorrelations of each channel against theoretical model

In order to produce the figure (3.5), we followed the steps described further on. First, we generate the UIU model following similar steps as in [19]. We generate autocorrelation of each channel coefficient over time and plot against the theoretical equation from equation (3.15). In our results, the blue line represent our simulation of autocorrelation for each channel and the red line represent the theoretical result. We can see that our results in every single graph matches the theoretical results, as predicted.

3.4 Communication System Performance over Correlated Channels

Now that we have created a UIU MIMO channel we will investigate the performance of the channel. We all know that, there are several ways to do channel performance simulations. We decided to do this using Alamouti scheme and pairwise scheme. Both of these scheme were explained in previous chapter.

3.4.1 Alamouti Scheme

Alamouti scheme is the easiest process to perform in our channel design. The exact detail regarding this scheme is given in the M2M channel communication in Chapter 4. For this simulation, we have used the UIU channel designed for the previous sections. All the theoretical and simulation schemes are given in M-to-M channel design and performance chapter in this thesis. Figure 3.6, shows that the simulation results match

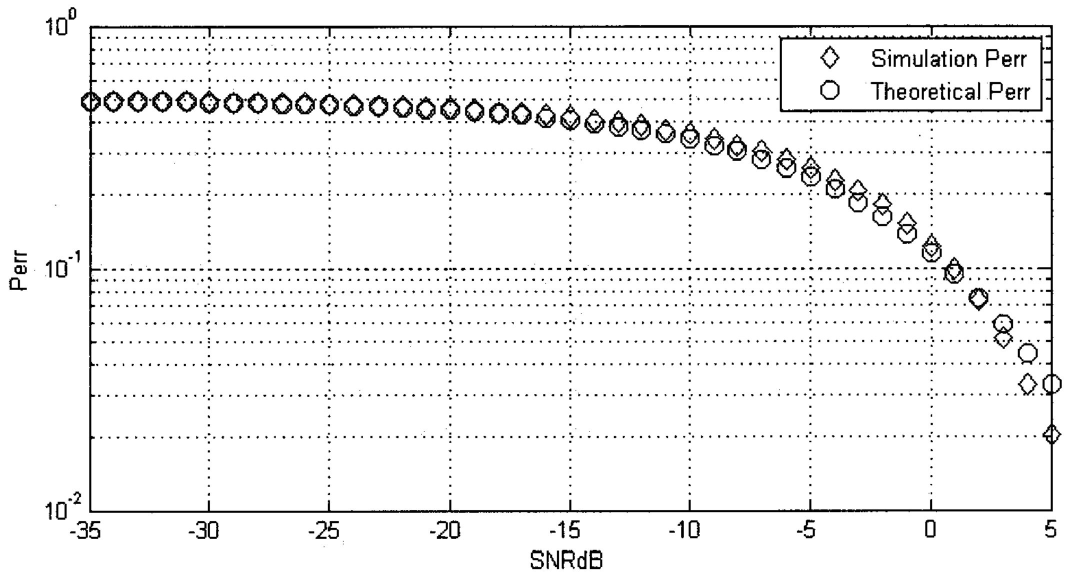

Figure 3.6: Alamouti probability of error on UIU MIMO channel Model

the theoretical results from from -35dB SNR to 5dB SNR. The probability of error is not so high as in the i.i.d Gaussian case because in this case,the Doppler effect and diversity are included.

3.4.2 Pairwise Probability Error

For pairwise probability of error, we have given all the details of the steps, and have shown the equation that are needed to produce the result listed bellow in M2M channel modeling chapter. Figure 3.7, shows that the simulation results outperformed the theoretical results from -20 dB SNR to 7 dB SNR. The method how to produce this result will be explained in detail in M2M channel model and performance.

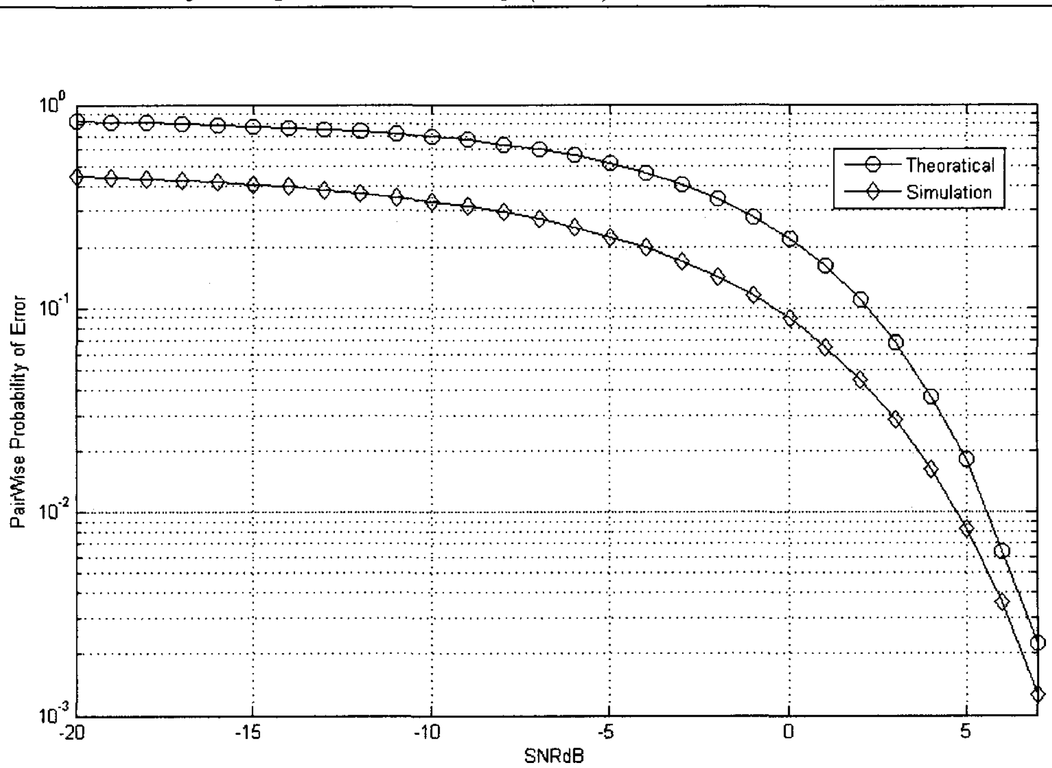

Figure 3.7: pairwise probability of error on UIU MIMO channel Model

3.5 Conclusion

As in conclusion, the design of modeling a MIMO channel using Unitary-Independent-Unitary (UIU) model is discussed in this chapter. The design is based on virtual and physical channel modeling. This chapter should explain how a MIMO channel is design based on input of a joint PDF between AoA/AoD. By using this input the channel is generated and the performance test is done based on the MIMO channel. All the simulation results matches with the theoretical results as we have predicted.

Chapter 4
M2M Channel Modeling

4.1 Introduction

Mobile-to-Mobile (M2M) communications are expected to play an important role in *adhoc* networks and intelligent transportation systems, where the communication links must be extremely reliable. While both terminals are mobile, for example, one main vehicle in a given location of a city or a suburb might communicate with one or more moving vehicles in other locations. This situation might arise between rescue squads, emergency vehicles, military or security squad vehicles in cases of emergency or disastrous events. In such channels, the line of sight is more likely to be obstructed by buildings and obstacles between the transmitter and the receiver. The signal components will arrive at the receiver by means of scattering, diffraction, and reflection mechanisms.

To cope with problems presented by the development and performance investigation of future M2M radio transmission systems, a detailed knowledge of the multipath fading channel and its statistical properties is essential. Several papers dealing with the modeling of M2M propagation channels have been appeared in the literature for single-input single-output (SISO) systems [68] [69]. Early studies were reported in [70] [71], where the statistics of a narrowband mobile to mobile fading channel has been investigated by focusing on the characterization of the time varying channel transfer function. In the later days, the temporal correlation properties and the Doppler power spectral density were studied for the case of 3-D scattering environments. In another approach, [72], ray optical techniques were used to model the wave propagation. The resulting impulse responses incorporate the complete channel information in the form of time series, which can be used directly for system simulations.

There have been experimental and measured results suggesting that the statistics of certain M2M fading channels can appropriately be described by a multiple Rayleigh channel model [73]. Experimental results of the propagation characteristics of radio waves at 60 kHz between running vehicles were reported in [74], in which the feasibility of data transmission was demonstrated. The designing of simulation models for SISO M2M channel was addressed in [75]. It is well known from several studies [29][62], that MIMO channels offer large gains in capacity over SISO channels. We believe that especially this fact, combined with the enhancement offered by large vehicle surfaces on which multi element antenna can be placed, makes MIMO techniques very attractive for M2M communication system.

For M2M communication channels, where both the transmitter and receiver are in motion and equipped with low elevation antennas, find application in mobile ad-hoc wireless networks, intelligent transportation systems and relay based cellular networks. M2M channels differ from conventional fixed to mobile cellular radio channels, where the base station is stationary, elevated and relatively free of local scattering. Akki and Haber showed that the received signal envelope of M2M channels is Rayleigh faded under non-line of sight conditions, but the statistical properties differ from F2M channels. They were the first to proposed a mathematical reference model for M2M Rayleigh fading channels. Then, Vatalaro and Forcella extended their models to account for scattering in three dimensions. More recently, measurements for wide-band mobile-to-mobile communications have been reported [76]. There has been several method of proposal for simulating M-to-M channels in literature. Wang and Cox [77] described a model that approximates the continuous Doppler spectrum by a discrete line spectrum.The correlation functions are periodic functions of the time delay, and method requires numerical integration of the Doppler spectrum. Patel et al. [75] proposed two sum-of-sinusoids models for M-to-M channels. The SOS models approximate the underlying random processes by the superposition of a finite number of properly selected sinusoids. Deterministic SOS models have sinusoids with fixed phases, amplitudes and Doppler frequencies for all simulation trials. Statistical SOS models leave at least one of the parameter sets as random variables that vary with each simulation trial. The statistical properties of the statistical SOS models vary for each simulation trial, but coverage to the desired properties when averaged over a large number of simulation trials. An ergodic statistical model is one that converges to the desired properties in a single simulation trial. The paper that we based on [78] this simulation proposed a new statistical SOS model for M-to-M Rayleigh fading channels. They used double ring model, which will be explained in detail in the latter section, where orthogonal functions are chosen as the in-phase and quadrature components of the complex faded envelope. This new model is designed to directly generate multiple un-correlated complex faded envelopes, a lacking feature in the existing models reports in [77] and [75].

4.2 Existing M2M Scenarios

One of the first reference on M2M channel was [79], where the authors assumed that small scale fading has Rayleigh statistics. They generalized the work of Jakes and derived new envelope auto correlation function and Doppler spectra. As expected, in the case when both transmitter and receiver are mobile, channel time variation can be more rapid than in the case when one or the other is motionless. Kato et al. [75], described effective means of simulating such a channel, using the SoS approach. In these models, they have assumed that there is isotropic scattering about both vehicles, applicable mostly in urban environments. In real M2M scenarios, isotropic scattering will be rare and WSS condition will pertain for a generally shorter time period than in single mobile platform cases. There have been several articles using 5 GHz band that developed several models with different M2M settings [80]. An alternate where it is shown method for M2M communication is presented in [81] , shown that there can be at least 6 different types of scenarios we can have in M2M design and they are explain briefly below.

For VTV Expressway Oncoming, each of the vehicles entered the highway at the same from facing to one another. Both cars were accelerated up to 65 mph and recordings were produced of the appropriate speed and distance. In VTV urban canyon oncoming case, the measurements were done at about 20-30 mph speed. Problem with this test is that, both cars has to be at the same speed, but they also have to work with traffic lights. For the next case, RTV suburban street, the transmitter was mounted on a pole near the intersection of a street corner. According to the article, the antenna was 6.1 m high and the receiver was moving from all 4 different directions. The speed was also 20-30 mph in this case. RTV expressway was done by mounting the antenna on a pole of the side of the highway. The measurements were done from both directions on the highway. The speed was also set to be 65 mph. The second last case, VTV expressway same direction with wall, in this case there was a dividing wall between the roads. They assumed that there will be some degradation in the signal due to the wall. The last case was, RTV urban canyon, where the transmitter was mounted on a pole near the urban intersection. The receiver was moving at 20-30 mph with the desired range. All these scenarios cover any possible communication between two moving mobiles.

4.3 Modeling of M2M channel

4.3.1 Reference Model

M-to-M reference model that was designed by Akki and Haber [78] defines the complex faded envelope as

$$g(t) = \sqrt{\frac{2}{N}} \sum_{n=1}^{N} \exp[j[\omega_1 t \cos(\alpha_n) + \omega_2 t \cos(\beta_n) + \phi_n]] \tag{4.1}$$

$$\omega_{1,2} = 2\pi f_{D_{1,2}} = 2\pi v_{1,2}/c$$

where N is the number of propagation paths, ω_1 and ω_2 are the maximum Doppler frequencies, α_n and β_n are the angle of departure and the angle of arrival of the n^{th} propagation path measured with respect to the Tx and Rx velocity vectors,respectively, and ϕ_n is the phase associated with the n^{th} propagation path. It is assumed that α_n,β_n and ϕ_n are mutually independent random variables and that ϕ_n is uniformly distributed on the interval $[-\pi, \pi)$. By using the central limit theorem [82], the real part $g_i(t) = \Re\{g(t)\}$ and the imaginary part $g_q(t) = \Im\{g(t)\}$ of the complex faded envelope are Gaussian random process as $N \to \infty$. Therefore, the envelope $|g(t)|$ is

Rayleigh distributed and the phase $\Theta_g(t)$ is uniformly distributed. The auto and cross correlation functions of the reference model, assuming omni-directional antennas and a 2-D scattering environment, are in the limit $N \rightarrow \infty$

$$R_{g_i g_I}(\tau) = E[g_i(t+\tau)g_i(t)] = J_0(\omega_1\tau)J_0(\omega_2\tau) \tag{4.2}$$

$$R_{g_q g_q}(\tau) = E[g_q(t+\tau)g_q(t)] = J_0(\omega_1\tau)J_0(\omega_2\tau) \tag{4.3}$$

$$R_{g_i g_q}(\tau) = E[g_i(t+\tau)g_q(t)] = 0 \tag{4.4}$$

$$R_{gg}(\tau) = \frac{1}{2}e[g(t+\tau)g(t)^*] = J_0(\omega_1\tau)J_0(\omega_2\tau) \tag{4.5}$$

where $E[.]$ is the statistical expectation operator, $(.)^*$ denotes the complex conjugate operator, and $J_0(.)$ is the zero order Bessel function of the first kind.Note that the auto-correlation function of M-to-M channels ar the product of the two Bessel function in contrast to F-to-M channel which the corresponding functions involve single Bessel functions. Our goal is to reproduce this and match the results with the theoretical results.

4.3.2 Existing M-to-M SoS Simulation Models

The first to propose sum-of-sinusoids models for M-to-M were Patel et al [75], who used a double ring concept to derive the model. In their concept, they have assumed that the double rings model defines two rings of uniformly spaced fixed scatterers places, one around the transmitter and one around the receiver. They also assumed the omni-directional antennas at both ends, and the waves from the transmitter first arrive at the scatterers located on the transmitter ring. If you consider these fixed scatterers as virtual base station then the communication link from each virtual base station to the receiver is modeled as conventional F-to-M link.

The signals from each of virtual base station arrive at the receiver antenna uniformly from all direction in the horizontal plane due to isotropic plane due to isotropic scatterers located on the receiver end ring. Using this model, the received signal's complex faded envelope can be expressed as:

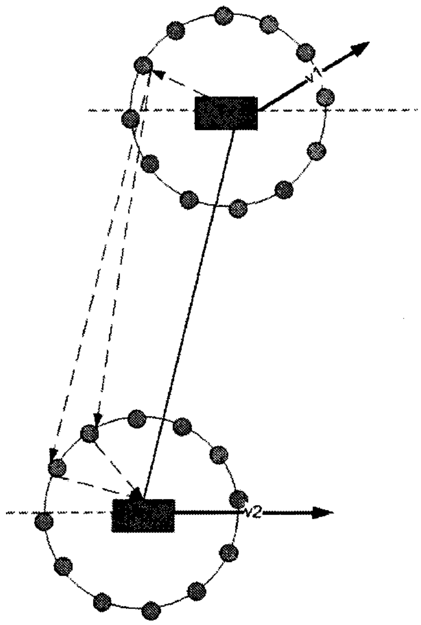

Figure 4.1: Ring Uniform scattering Right

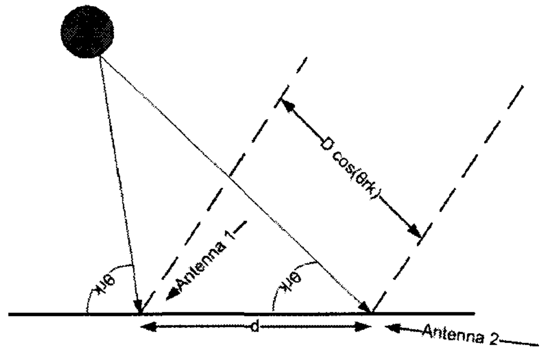

Figure 4.2: Signal at receive Antenna

$$g(t) = \sqrt{\frac{2}{N\ M}} \exp[j[\omega_1 t \cos(\alpha_n) + \omega_2 t \cos(\beta_m) + \phi_{nm}]]$$

Note that the single summation in equation 4.1 is replaced with a double summation, because each wave on its way from the transmitter to the receiver reflected twice. The channel characteristics remain the same as the reference model because each path will undergo a Doppler shift due to the motion of the transmitter and the receiver.

4.3.3 Two Ring Model

Figure ?? shows the physical scattering model for mobile-to-mobile MIMO communication system. The transmitter and the receiver are moving at the speed of V_1 m/s and V_2 m/s. There are I and K scatterers surrounding the transmitter and the receiver, respectively. θ_{ti} $(i = 1, 2, \ldots, I)$ denotes the angles of departure between vector V_1 and scattering paths and θ_{rk} $(k = 1, 2, \ldots, K)$ the angle of arrival between vector V_2 and the scattering paths. It is assumed that the departure angles θ_{ti} and the arrival angles θ_{rk} are independent and uniformly distributed over $[-\pi, \pi)$. The other figure shows the received signal at different receiving antenna. The antenna separation between each receiving antenna is denoted as d. The angle of arrival from k^{th} scatterers to receiving antenna 1 is θ_{rk}. Assume that the transmission distance from scatterer to antenna is much large than antenna separation. Therefore, the angle of arrival of the second receiving antenna will not be influence by the antenna separation and remain θ_{rk}. The transmission distance from the k^{th} scatterer to the second receiving antenna is $d\cos(\theta_{rk})$ which is longer than the distance from the scatterer to the first receiving antenna [83]

4.4 Channel Model

All the existing models have difficulties in producing time averaged auto and cross-correlation functions that matches those of the reference models. To solve this, they have introduced a new model using "two ring" or "double ring" concept and by choosing orthogonal functions for the in phase and quadrature components of the complex faded envelope. The following function is considered as the k^{th} complex faded envelope

$$g_k(t) = \sum_{n=1}^{N} \sum_{m=1}^{M} C \exp\{j[\omega_1 t \cos(\alpha_{nk}) + \omega_2 t \cos(\beta_{mk}) + \phi_{nmk}]\} \tag{4.6}$$

where $C = \frac{2}{\sqrt{NM}}$,ω_1,ω_2,α_{nk},β_{mk} and ϕ_{nmk} are the maximum radian Doppler frequencies, the random angel of departure, the random angle of arrival, and the random phase, respectively. It is assumed that P independent complex faded envelopes are required $k = 0, 1, \ldots, P-1$ each consisting of NM sinusoidal components. For the simulations, we can reduce the number of sinusoidal components to be $N_0 = N/4$ to be an integer,by taking into account shifts of the angles α_{nk} and ϕ_{nmk} we can split the equation 4.6 into the following terms:

$$
\begin{aligned}
g_k(t) &= C\sum_{m=1}^{M} e^{j\omega_2 t\cos(\beta_{mk})}\sum_{n=1}^{N} e^{j(\omega_1 t\cos(\alpha_{nk})+\phi_{nmk})} \\
&+ C\sum_{m=1}^{M} e^{j\omega_2 t\cos(\beta_{mk})}\sum_{n=1}^{N} e^{j(\omega_1 t\cos(\alpha_{nk})+\phi_{nmk}+\frac{\pi}{2})} \\
&+ C\sum_{m=1}^{M} e^{j\omega_2 t\cos(\beta_{mk})}\sum_{n=1}^{N} e^{j(\omega_1 t\cos(\alpha_{nk})+\phi_{nmk}+\pi)} \\
&+ C\sum_{m=1}^{M} e^{j\omega_2 t\cos(\beta_{mk})}\sum_{n=1}^{N} e^{j(\omega_1 t\cos(\alpha_{nk})+\phi_{nmk}+\frac{3\pi}{2})}
\end{aligned} \tag{4.7}
$$

Then the equation 4.7 simplifies to yield the following:

$$
\begin{aligned}
g_k(t) &= \frac{2}{\sqrt{N_0\ M}}\sum_{n=1}^{N_0}\sum_{m=1}^{M}\cos(\omega_2 t\cos(\beta_{mk}))\cos(\omega_1 t\cos(\alpha_{nk})+\phi_{nmk}) \\
&+ j\sum_{n=1}^{N}\sum_{m=1}^{M}\sin(\omega_2 t\cos(\beta_{mk}))\sin(\omega_1 t\sin(\alpha_{nk})+\phi_{nmk})
\end{aligned} \tag{4.8}
$$

equation (4.8) can be separated into the positive (in phase) part and the negative (quadrature) parts. It is shown as

$$
g_{ik}(t) = \frac{2}{\sqrt{N_0\ M}}\sum_{n=1}^{N_0}\sum_{m=1}^{M}\cos(\omega_2 t\cos(\beta_{mk}))\cos(\omega_1 t\cos(\alpha_{nk})+\phi_{nmk}) \tag{4.9}
$$

$$
g_{qk}(t) = \frac{2}{\sqrt{N_0\ M}}\sum_{n=1}^{N}\sum_{m=1}^{M}\sin(\omega_2 t\cos(\beta_{mk}))\sin(\omega_1 t\sin(\alpha_{nk})+\phi_{nmk}) \tag{4.10}
$$

It is assumed that P independent complex envelopes are desired, each having MN_0 sinusoidal terms in the I and Q components. The angle of departure and the angle of arrivals are chosen as follows:

$$\alpha_{nk} = \frac{2\pi\ n}{4N_0} + \frac{2\pi\ k}{4PN_0} + \frac{\theta - \pi}{4N_0} \tag{4.11}$$

$$\beta_{mk} = 0.5\left(\frac{2\pi\ m}{M} + \frac{2\pi\ k}{PM} + \frac{\psi - \pi}{M}\right) \tag{4.12}$$

for $n = 1, \ldots, N_0$,$m = 1, \ldots, M$,$k = 0, \ldots, P-1$. The angles of departures and the angles of arrivals in the k^{th} complex faded envelope are obtained by rotating the angles of departures and the angle of the arrival in the $(k-1)^{th}$ complex envelope by $(2\pi)/(4PN_0)$ and $)(2\pi)/(2PM)$. The parameters θ_{nmk},θ and ψ are independent random variables uniformly distributed on the interval $[-\pi, \pi)$. For the derivation of the autocorrelation is given in appendix B.

4.5 Simulation and Evaluation

Now that we have showed the theory behind the Mobile-to-Mobile channel design and its auto and cross correlations, we will compare results of our simulation to the theoretical results. In our case, for simplicity, we decided to make $f_1 = f_2$, a normalized sampling period of $f_1 T_s = 0.01$, where F is the maximum Doppler frequencies and the T_s is the sampling period. We also used $N_0 = M = 8$. There have been plenty of research done on different values of Doppler frequency values and the number of sinusoids values to have the better matched simulation results. For the readers to have better understanding of how the different number of simulation trials effect the results, we have decided to show all our results in different simulation trials. Since there is a space limit in this chapter for better presentation, we have decided to show only one trial values in this chapter but place all the other trial results in Appendix B.

As we can see in Figure 4.3, 4.4 and 4.5, our simulation results match the theoretical results for a large range of normalized time delays of $0 \leq f_s T_s \leq 7$. Now that we have a good matching results in the auto-correlation we will check the cross-correlation to make sure the results are what we have expected.

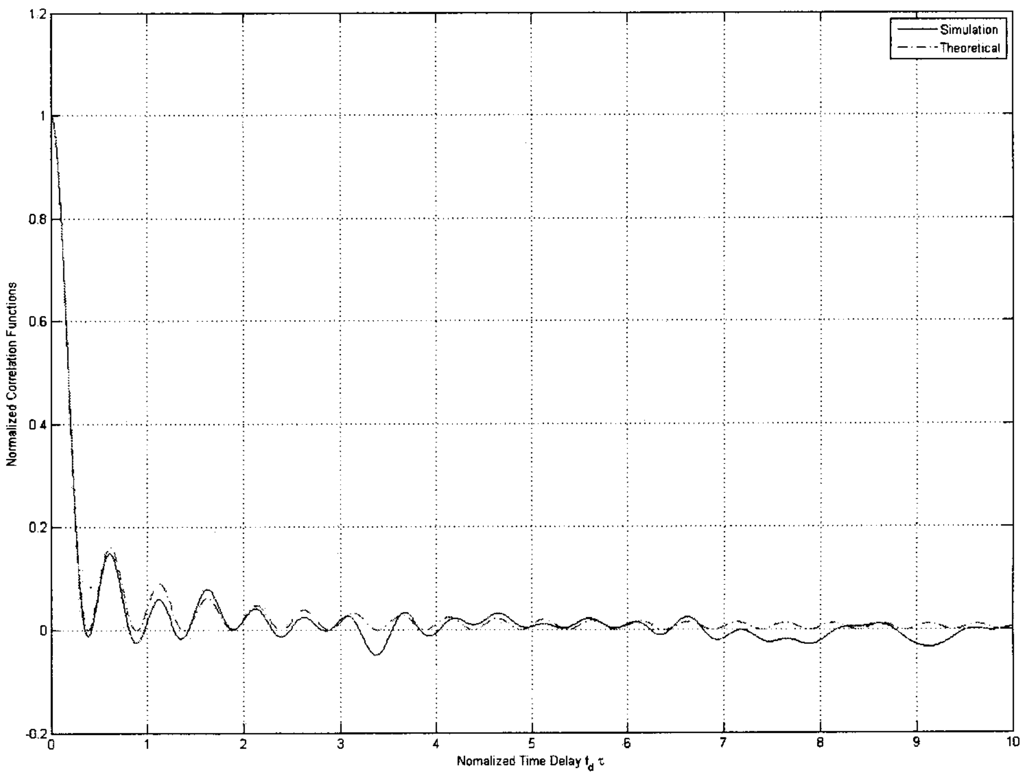

Figure 4.3: Theoretical and simulation (Number of simulation 100) auto-correlation function of in-phase component of the M2M model.

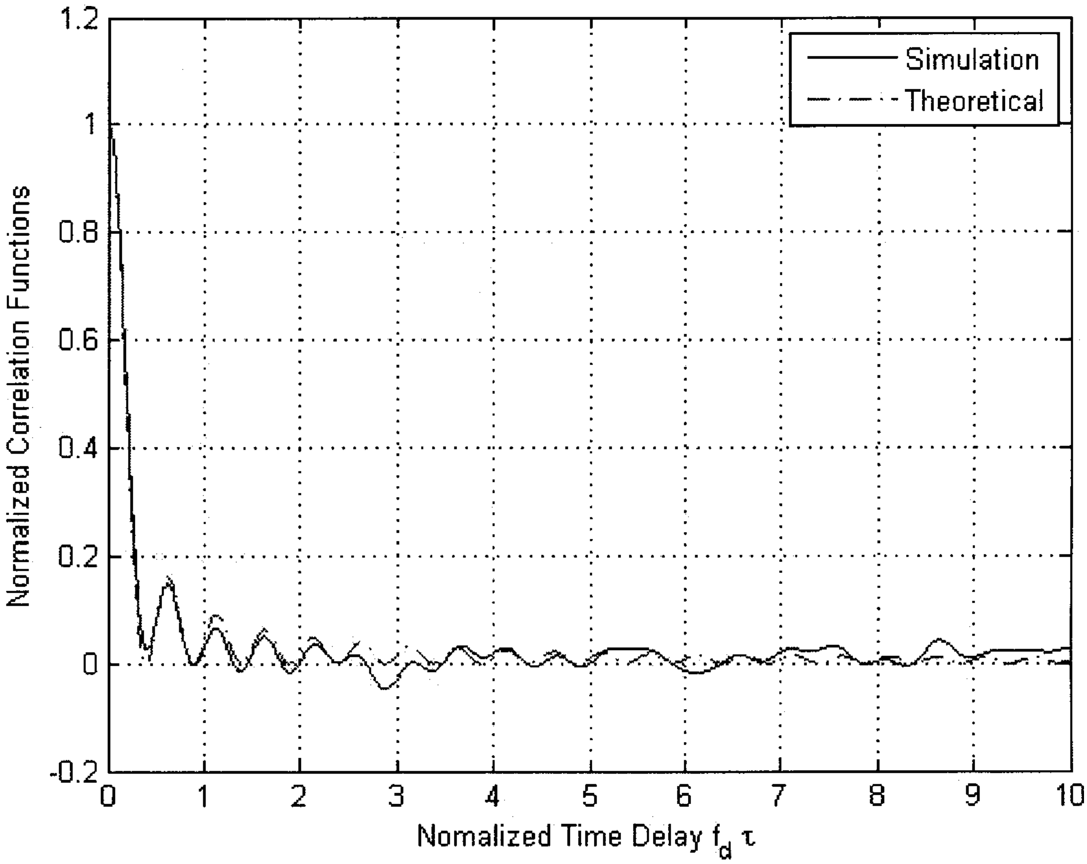

Figure 4.4: Theoretical and simulation (Number of simulation 100) auto-correlation function of quadrature component of the M2M model.

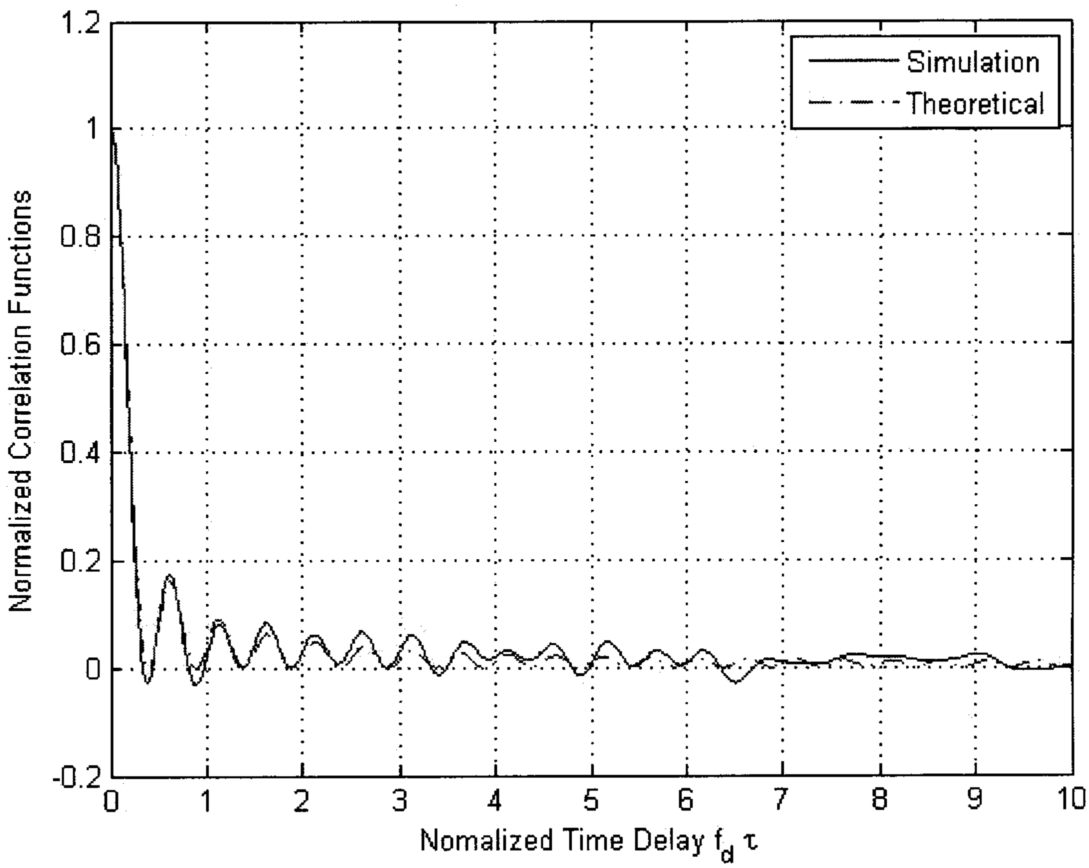

Figure 4.5: Theoretical and simulation (number of simulation 100) auto-correlation function of the main faded envelope of the M2M model.

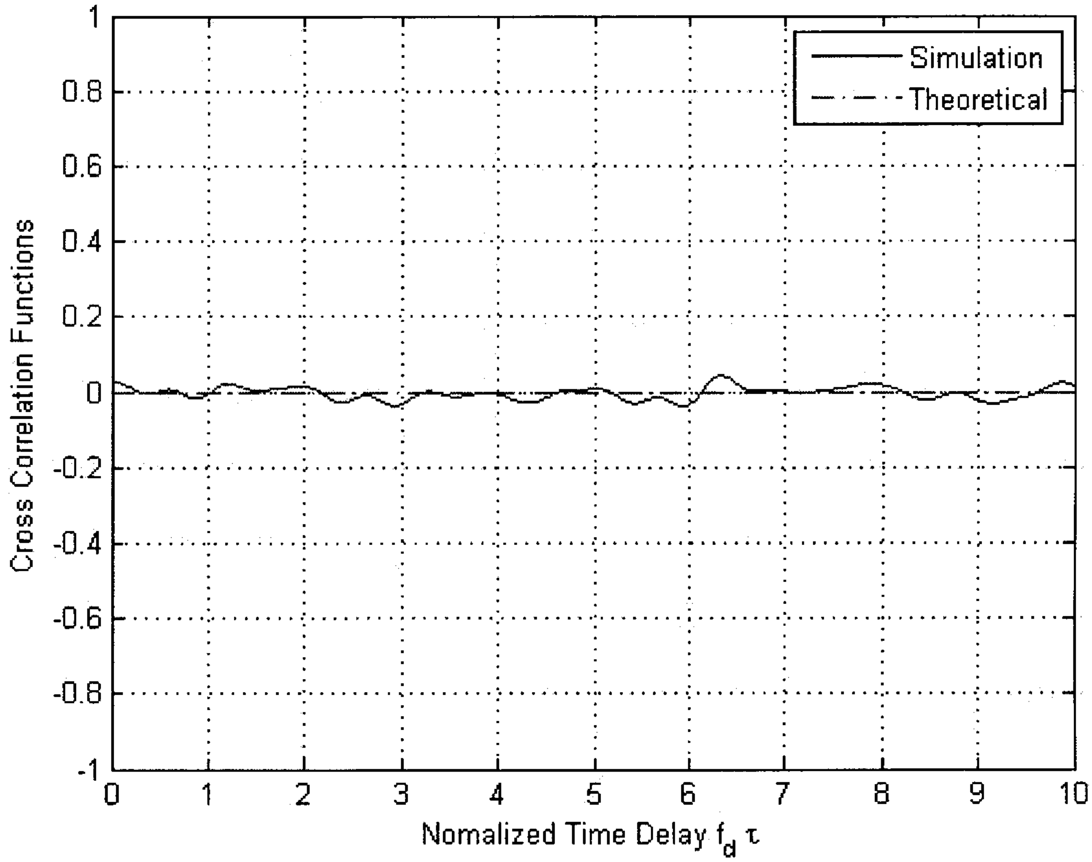

Figure 4.6: Theoretical and simulation (number of simulation 100) cross-correlation function of the in-phase and quadrature components of the M2M model.

We can see from figure (4.6), when we plotted the cross correlation of in phase and quadrature, the results is 0, which is what we have expected from the beginning. It shows that there is no correlation in these two components.

4.6 Conclusion

We can clearly see from our results that the auto correlation and the cross correlation of the M2M channel matches with the theoretical results in higher number of simulation trials. We presented our findings on mismatch between the simulation and the theoretical results for lower number of trails in appendix B.

Chapter 5
AR Channel Modeling

5.1 Introduction

In bandlimited Rayleigh fading process, the power spectral density is zero past the maximum Doppler frequency. The simulation of this channel design has been of theoretical and practical interest of the wireless communications community for many years. There are several articles published on how to model the correlated Rayleigh fading. Among these, simulators based on either a sum-of-sinusoids (SoS) approach or on the inverse discrete fourier transform algorithm have been popular [84][86] and [87]. There are several problems with SoS model; the classical Jake's simulator produces fading signals that are not in strict sense stationary. The IDFT is known to be a high quality and efficient fading generator. The main disadvantage of this method is that the samples are generated with a single FFT operation. Main problem why this method does not attract much attention is the need of a large storage space.

The paper that we will look at explains how to design a general autoregressive (AR) modeling approach for the accurate generation of correlated Rayleigh processes. AR models have been used with success to predict fading channel dynamics for the purposes of Kalman filter based channel estimation [88] [89] and for long-range channel forecasting [90]. There have been several authors who have used these models to simulate correlated Rayleigh fading. Even in the low order AR process, there is not a good match to the desired bandlimited correlation statistics. At the beginning of this research, I have used 3D correlation matrix to design an AR model, but due to some difficulty I have abandoned that project and moved on to somewhat similar one. In later sections, we will explain how the channel modeling is done and how the model was tested.

The received signal correlation functions and power spectra at the mobile station depend on the probability density function of the angle of arrival of a scattered wave. Most researchers use Clarke's two-dimensional isotropic scattering model that gives rise to the zero order Bessel function for the autocorrelation function and the U-shaped power spectrum for the complex envelope of multipath components at the mobile station. However, in real case, the scattering encountered in many environments is non-isotropic scattering resulting in a nonuniform PDF for AoA at the mobile station. There have been serval experiments and the results to back it up [91]- [100]. In paper [100], the assumption of a uniform PDF of the AoA introduces small errors on the first order statistics of the received signal, but a significant error on the second-order statistics, like correlation functions and level crossing rates.There are several papers [101][102], that explain how to derive the geometrically based AoA PDFs.

5.2 AoA Model and PSD

In mobile environment, the Doppler shift in the frequency domain is a finite quantity that is related to the speed of the car. Therefore, the power spectral density of the bandlimited Rayleigh fading process is zero past the maximum Doppler frequency. There are ways to perform real data measurements of the mobile radio channel; unfortunately at a high cost. Therefore, the system can be designed by using computer simulations taking into account the behavior of the channel.The classical fading simulations application is to generate a single sequence of correlated Rayleigh variates in accordance with Clarke's wide-sense stationary isotropic model.

Computer simulation of cross-correlated fading processes has become as important research topic due to the increased interested in using antenna arrays, both at the transmitter and at the receiver, to improve cellular radio communications. Simulators which can accurately capture that characteristics of correlated diversity channels are needed to enable realistic performance assessments of multiple-antenna systems.The simulation of narrow-band vector fading channels, in particular, requires the generation of cross-correlated Rayleigh and Rician sequences. Typically, the sequences must be specified for the auto-correlation and cross-correlation statistics.

5.2.1 Correlated Fading Model

The Gaussian WSS (wide sense stationary) uncorrelated scattering fading model is a complex Gaussian process. A Rayleigh characterization of the land mobile radio channel follows from the Gaussian wide-sense stationary uncorrelated scattering fading model, where the fading process is modeled as a completed Gaussian process. The variability of the wireless channel over time is reflected in the autocorrelation function of the independent in phase and quadrature Gaussian components. The second order statistic generally depends on the propagation geometry, the velocity of the mobile, and the antenna characteristics. In the assumption that the radio propagation path consists of a two dimensional isotropic scattering, the theoretical PSD associated with either in-phase or quadrature portion of the received fading signal has the well-known U-shaped bandlimited form [103]

$$\begin{aligned} S(f) &= \frac{1}{\pi f_d \sqrt{1-(\frac{f}{f_d})^2}}, \quad |f| \leq f_d \\ &= 0 \quad \text{elsewhere} \end{aligned} \tag{5.1}$$

where f_d is the maximum Doppler frequency in Hertz (Hz), derived by the user velocity v and the carrier wavelength λ according to $f_d = v/\lambda$. The corresponding normalized continuous time auto-correlation of the received signal under these condition is $R(\tau) = J_0(2\pi f_d \tau)$, where $J_0(.)$ is the zeroth-order Bessel function of the first kind [103]. For the purpose of discrete-time simulation of this model, the autocorrelation sequence becomes

$$R[n] = J_0(2\pi f_m |n|)$$

where $f_m = f_d T$ is the normalized Doppler frequency where $1/T$ is the sampling rate. We should note that in-phase and quadrature processes must be independent and each must have zero mean for Rayleigh fading and if is non-zero then the fading would be Rician fading. The method for simulating the channel gain is the sum-of-sinusoids approach, also known as the Jake's model. In [104],implemented a careful design to obtain the low pass discrete fading process. In [104], it was shown that the statistical properties of the fading process approach those of Clarke's isotropic model as the number of sinusoids considered N_s approaches infinity. A good approximation of the ensemble statistics has been reported for $N_s > 8$.

Exact generation of N Gaussian variates with an arbitrary correlation can be achieved in principle by decomposing the desired N x N covariance matrix $\mathbf{R} = \mathbf{G}\mathbf{G}^H$, where $\mathbf{G}^H$ denotes the Hermittian transpose of $\mathbf{G}$, then multiplying N independent Gaussian variates by $\mathbf{G}$. For bandlimited process, an approximation using a singular value decomposition is typically required due to numerical limitations arising from an ill-conditioned covariance matrix.Another method to generate Correlated Rayleigh variates is by filtering two zero-mean independent white Gaussian process then adding the outputs in the quadrature [105]. Another popular method for generating correlated Rayleigh variates is Smith's IDFT algorithm. In this case, the IDFT operation is applied to sequences of uncorrelated complex Gaussian variates, each sequence weighted by appropriate filter coefficients to shape the PSD. After considering the quality of the generated variates and the computational effort,a comparison of the IDFT generator with the sum-of-sinusoids technique and the exact J_0 FIR filter method concluded that the IDFT generator is superior.

One of the main assumptions of the WSS isotropic model is the uniform distribution of the angle of arrival of multipath components at the mobile receiver. It have been demonstrated that most of the scattering that we encounter in daily life is non-isotropic, condition that strongly affects the second order statistics and the power spectrum of the channel complex envelope [36]. We can also face strong cross-correlation in this case. As a consequence, the PSD in non-isotropic environments can be bandlimited but not symmetric. In it is shown that the received signal correlation and power spectra depend on the probability density function (PDF) of the AoA of the scattered wave. The von Mises PDF is shown to be a versatile and powerful instrument to describe a directional scattering environment. Now we will explain more about this.

5.2.2 Flexible PDF of the AoA

A PDF which spans range from uniform to a Gaussian was introduced in 1918 by Von Mises to study the deviations of measured atomic weights from integral values. The PDF plays a big role in statistical modeling and analysis of angular variables. Let the random variable Θ represent the AoA of the multipath component at the received at the Mobile station [106]. The von Mises PDF for the scatterer component is given by

$$P_{\Theta}(\theta) = \frac{exp[k\cos(\theta - \theta_p)]}{2\pi I_0(k)} \quad \theta \in [-\pi, \pi)$$

where $I_0(.)$ is the zero-order modified Bessel function, $\theta_p \in [-\pi, \pi)$ accounts for the mean direction of AOA of scatter components, and $k \geq 0$ controls the width of AoA of the scatter components. As we can see from the equation, when $k = 0$ we obtain $p_{\Theta} = 1/2\pi$ (isotropic scattering) while $k = \infty$ then $p_{\Theta} = \delta(\theta - \theta_p)$ (extremely non-isotropic scattering), where $\delta(.)$ is the Dirac delta function. For small k, this function approximates the cardioid pdf, which is rather similar to the cosine PDF, while for large k it resembles a Gaussian pdf with mean θ_p and the standard deviation $1/\sqrt{k}$ [107]. When we look at the Von Mises PDF in polar coordinates for the AoA of scatter components at the mobile station ($\theta_p = 0$), we can see that its a circular shape when the k is close to zero, but when the $k \geq 3$, it takes a unidirectional shape. The normalized auto-correlation function $\rho\tau$ of the mobile channel is associated to the distribution of AoA $P_{\Theta}(\theta)$ [103] as

$$\rho(\tau) = \int_{-\pi}^{\pi} \exp(j2\pi f_d \tau \cos(\theta)) p(\theta) d\theta$$

and we can expressed the auto correlation in discrete time as

$$R[n] = R_{II}[n] + jRIQ[n] = \frac{I_0(\sqrt{k^2 - z^2 + j2kz\cos(\phi)})}{I_0(k)}$$

where $z = 2\pi f_m |n|$,$R_{II}[n]$ and $R_{QQ}[n]$ denotes the sampled auto-correlation of the real in-phase and quadrature Gaussian process respectively, and $R_{IQ}[n]$ denotes the cross-correlation function.

There are other others that proposed an autoregressive (AR) modeling approach for the accurate generation of correlated Rayleigh process. In this case, we can find the covariance matrix by the Cholesky factorization.The exact generation of N gaussian variables with the desired correlation can be achieved in principle by decomposing the desired N x N covariance matric $\mathbf{R} = \mathbf{R}^{1/2}, \mathbf{R}^{1/2^H}$, where $\mathbf{R}^H$ indicates the Hermitian transpose of R, then multiplying N independent variables by $R^{1/2}$.

5.3 Channel Modeling

A complex AR process of order p (AR(p)) can be generated via the time domain recursion

$$x[n] = -\sum_{k=1}^{p} a_k \; x[n-k] + w[n]$$

where $w[n]$ is a complex white Gaussian noise process with uncorrelated real and imaginary components. For the Rayleigh variates generation, $w[n]$ has zero mean and the simulator output is $|x[n]|$.The AR model parameters consist of the filter coefficients $\{a_1, a_2, \ldots, a_p\}$ and the variance σ_p^2 of the driving noise process $w[n]$. The PSD of the AR(p) model can be expressed as

$$S_{xx}(f) = \frac{\sigma_p^2}{|1 + \sum_{k=1}^{p} a_k \exp(-j2\pi f_k)|^2}$$

Although the Doppler spectrum models proposed for mobile radio are not rational, an arbitrary spectrum can be closed approximated by an AR model of sufficiently large order. The relationship between the autocorrelation function and the AR(p) can be given as

$$\begin{aligned} R_{xx}[k] &= -\sum_{m=1}^{p} a_m m R_{xx}[k-m] \quad k \geq 1 \\ & \quad -\sum_{m=1}^{p} a_m \; R_{xx}[-m] + \sigma_p^2 \quad k = 0 \end{aligned} \tag{5.2}$$

We can also write these in matrix form for all different values of k

$$\mathbf{R}_{xx}\mathbf{a} = -\mathbf{v} \tag{5.3}$$

where R, a and v can be defined as

$$\mathbf{R}_{xx} = \begin{bmatrix} R_{xx}[0] & R_{xx}[-1] & \dots & R_{xx}[-p+1] \\ R_{xx}[1] & R_{xx}[0] & \dots & R_{xx}[-p+2] \\ \vdots & \vdots & \ddots & \vdots \\ R_{xx}[p-1] & R_{xx}[p-2] & \dots & R_{xx}[0] \end{bmatrix} \tag{5.4}$$

$$\mathbf{a} = \begin{bmatrix} a_1 & a_2 & \dots & a_p \end{bmatrix}^T \tag{5.5}$$

$$\mathbf{v} = \begin{bmatrix} R_{xx}[1] & R_{xx}[2] & \dots & R_{xx}[p] \end{bmatrix}^T \tag{5.6}$$

and

$$\sigma_p^2 = R_{xx}[0] + \sum_{k=1}^{p} a_k \; R_{xx}[k]$$

Based on the desired ACF, the AR filter coefficients can thus be determined by solving the set of p Yule-Walker equations in equation 5.3. These equations can be solved by using the Levinson-Durbin recursion. The R_{xx} is the autocorrelation, it is positive semidefinite and can be shown to be singular only if the process is purely harmonic and consists of p-1 or fewer sinusoids.In most of the cases, the inverse R_{xx}^{-1} exists and the Yule-Walker equations are guaranteed to have the unique solution. The generated AR(p) process has the ACF

$$\hat{R}_{xx}[k] = R_{xx}[k] \quad 0 \leq k \leq p \tag{5.7}$$

$$-\sum_{m=1}^{p} a_m \hat{R}_{xx}[k-m] \quad k > p \tag{5.8}$$

The simulated process has the attractive property that it sampled ACF up the lag p.

5.3.1 The ρ Conditioning of the Yule-Walker Equations

When we solve the Yule-Walker equations, the condition of the autocorrelation matrix is an important consideration in determining the accuracy of the solution. This condition is provided by the white noise variance parameter σ_p^2 and it can be expressed as

$$|R_{xx}| = \sum_{m=0}^{p-1} \sigma_m^2 \tag{5.9}$$

where $|R_{xx}|$ denotes the determinant of R_{xx} and σ_m^2 represents the driving white noise variance corresponding to an AR(m) model of the process. If the values of the σ_m^2 are small, R_{xx} is nearly singular so that significant errors in the simulated parameters are expected and unavoidable, regardless of the model used to solve the Yule-Walker equation.In these cases, the numerical problems in the solution typically yield unstable model filters. We will show how this result in our results. Another way to explain is that, for a single channel case, a spectral bias should be added for the vector AR simulation technique to work. The numerical problems that arise in these cases can be resolved by approximating any band-limited processes to be generated with non deterministic process by adding a very small positive bias to the zeroth lag of their ACFs. If the ill conditioning in R_{xx} is ignored, the algorithm typically produces a meaningless solution with either a covariance matrix Q that is not realized or a multichannel infinite-impulse response (IIR) filter that is unstable.

5.4 Performance and Evaluation

The following figures show the auto correlation of the fading process obtained by the AR filtering. We decided to show two different filter orders to demonstrate that we can have a better match in the higher order AR filter then lower filter orders. In this example, we have the value of k to be 0 (isotropic scattering) and we will have other results to show the effects of k values.For this case we assumed that the velocity of the mobile is about 20 m/s and the carrier frequency is 2GHz. Parameters

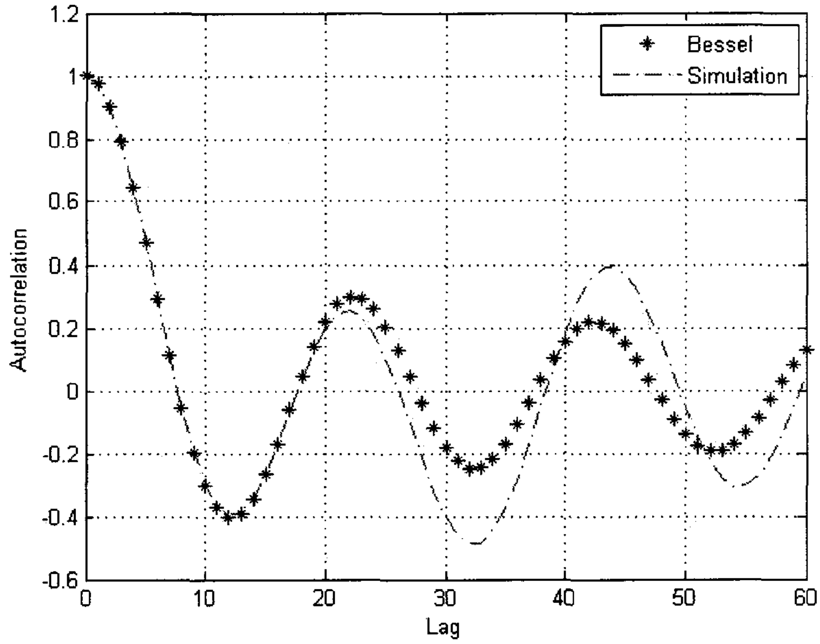

Figure 5.1: The auto-correlation of AR(10)- channel in-phase correlation R_{II} in isotropic scattering (k=0).

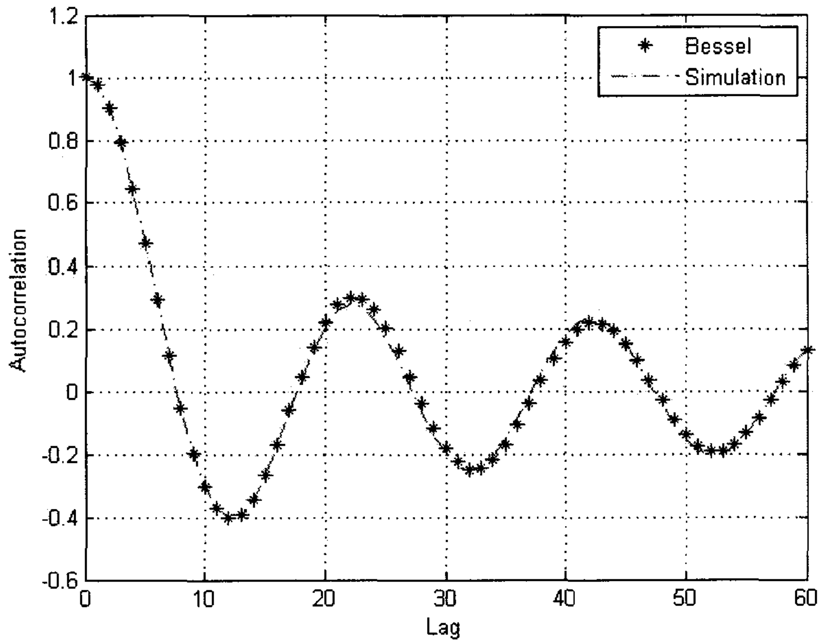

Figure 5.2: The auto-correlation of AR(100)- channel in-phase correlation R_{II}in isotropic scattering (k=0).

are chosen from [108] for the numerical comparison. The figure 5.1 and 5.2 shows the isotropic scattering for different values of filter size. For the theoretical we used equation 5.2.2 and labeled as Bessel in the figures. From figures 5.3 we can see that the

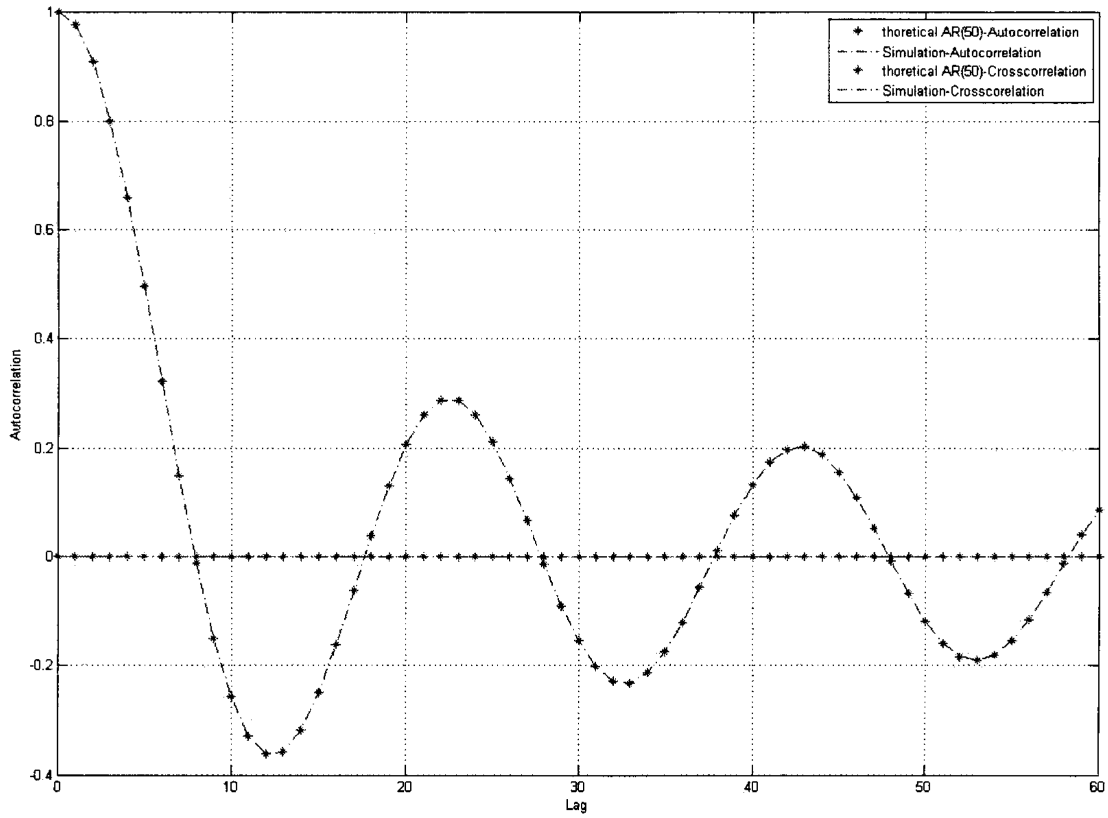

Figure 5.3: In-phase (autocorrelation) and quadrature (cross-correlation) from AR model between simulation and theoretical results for AR order of 50 at isotropic scattering (k=0).

autocorrelation and cross correlation matches between the theoretical and simulation results. We can also see this good match in figure 5.4 when we have directional scattering. We can see that, when we have directional scattering our cross-correlation is not exactly zero which means that there is cross correlation between the in-phase and quadrature components. Now we will show the results of auto-correlation and cross correlation results based on different scattering values (k values)but first we will show the results of 1 step prediction MMSE for the AR model. We can clearly see from figure 5.5 that when we decrease the bias value from 10^{-3} to very high

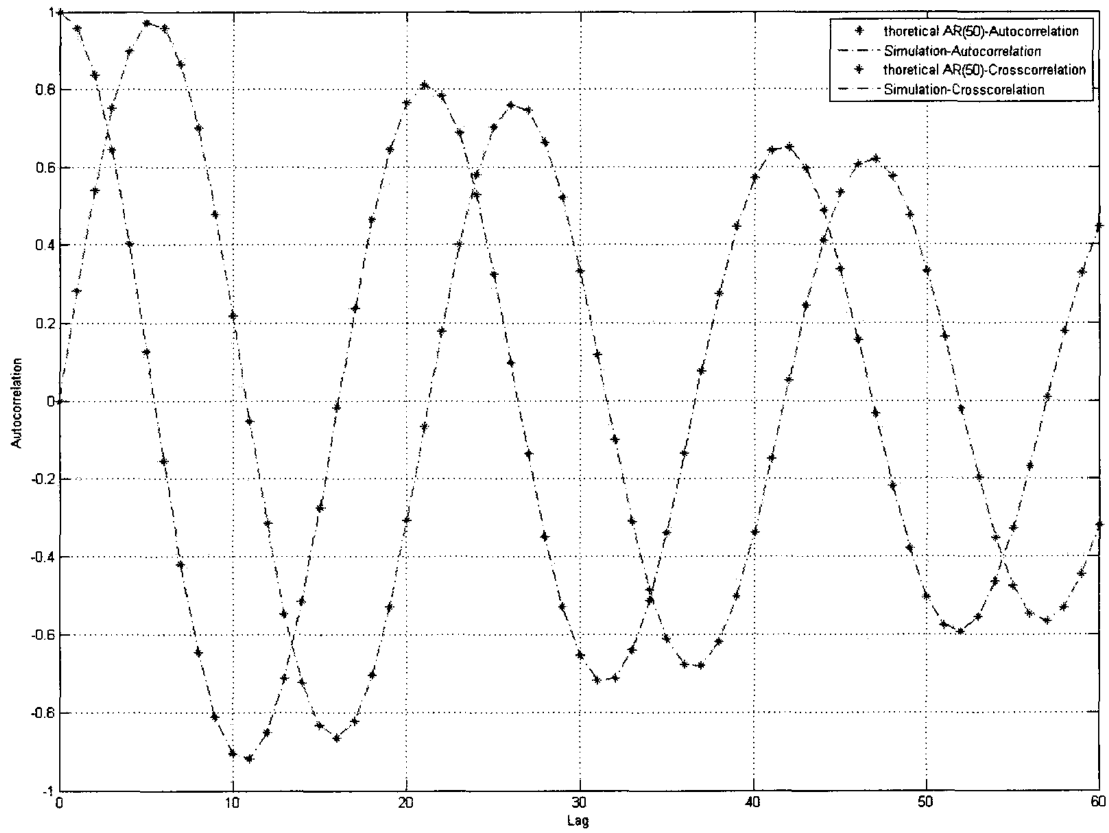

Figure 5.4: In-phase (autocorrelation) and quadrature (cross-correlation) from AR model between simulation and theoretical results for AR order of 50 at directional scattering (k=5).

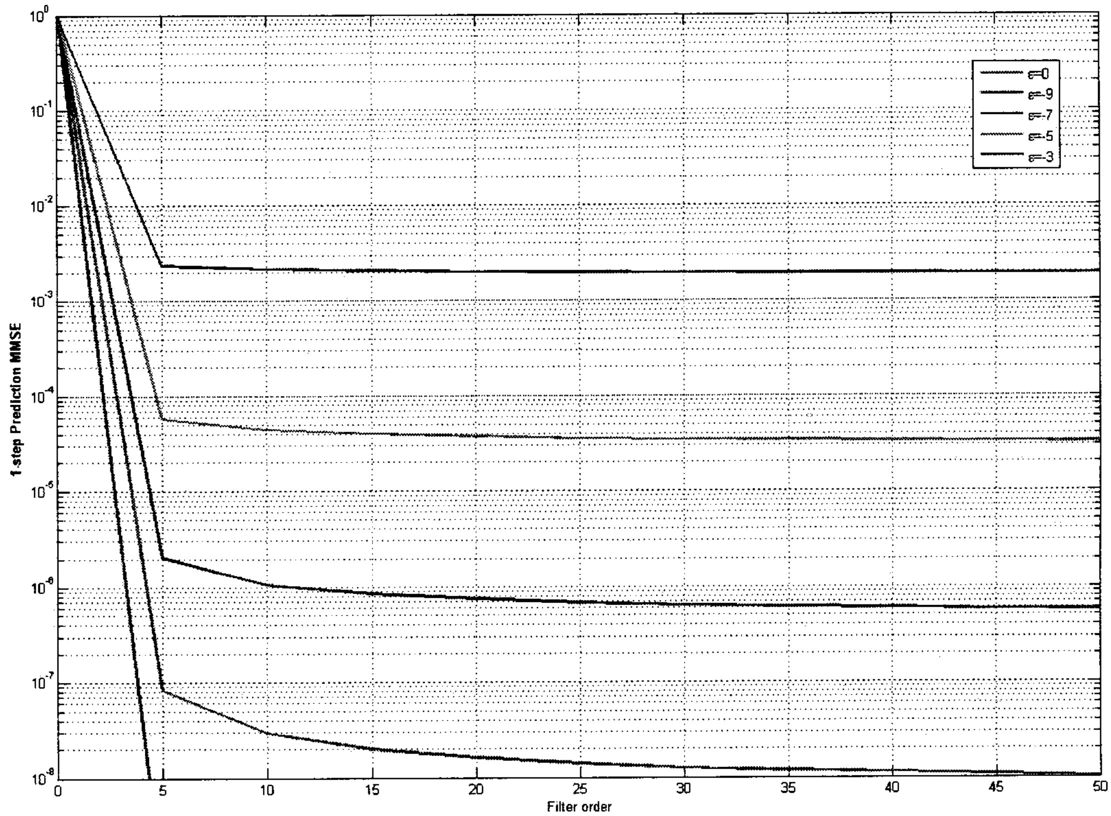

Figure 5.5: The 1-step prediction MMSE for the AR model with different bias values ε.

negative value, we can see that the system goes to out of control.The MMSE value also increase from 10^{-2} to all the way 10^{-8}. The results in figure 5.6 and 5.7 provide

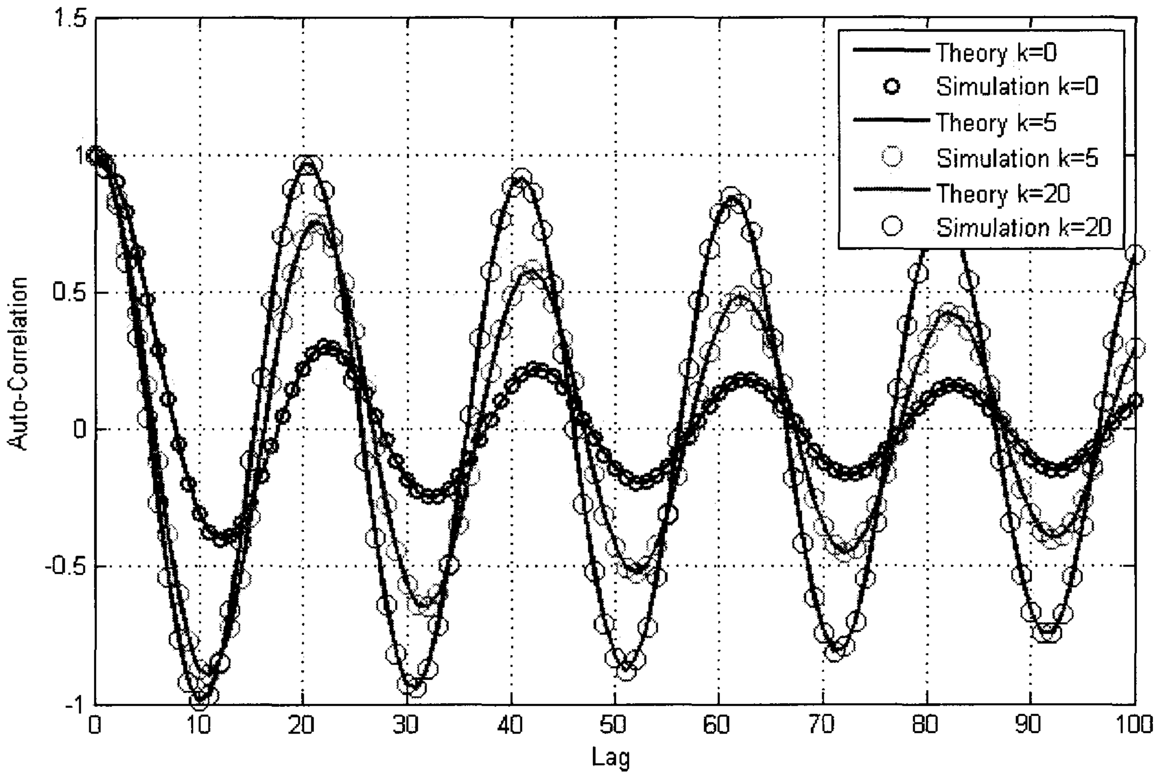

Figure 5.6: In-phase channel correlation of R_{II} of AR(50) from isotropic scattering(k=0) to very sharp directional scattering(k=20).

better understanding for those who wants to know how different k values change the auto and cross correlation in the channel design. All our simulation results matches according to its theoretical results. Now we will use the AR channel model and find out the Performance of the channel using Alamouti Scheme and Pair-Wise Probability of error.

5.5 Conclusion

We can conclude from our results that all the auto and cross correlation results matches according to theoretical results and also what we have expected. We can also

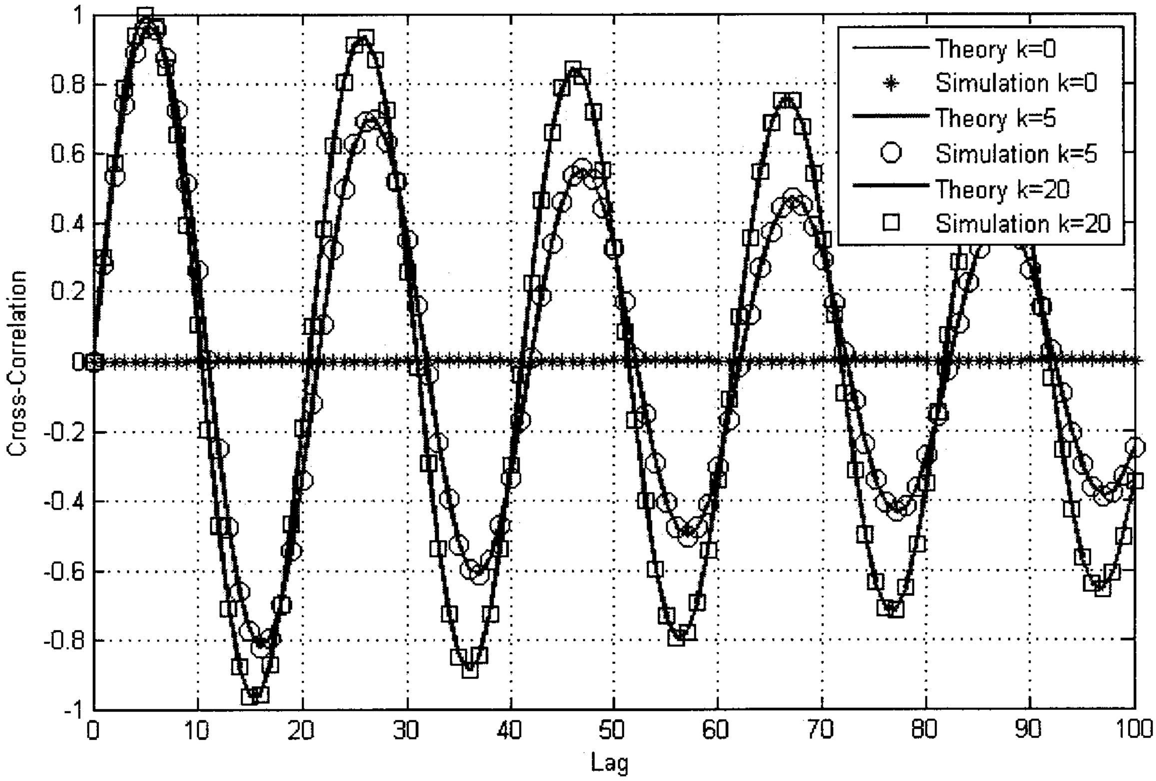

Figure 5.7: Cross-Correlation of R_{IQ} of AR(50) from isotropic scattering (k=0) to very focus directional scattering (k=20).

see how the value of k effect (iso or non-isotropic scattering) changes the results. We can also see the effect of ill-conditioning in the results.

Chapter 6
Capacity of MIMO Channels

6.1 Channel Capacity

Following the work of Telatar [109], [110], Foschini [111] and Gans and many others, it is well know that multi-element wireless system based on MIMO channels, can attain capacities many time grater than the Shannon Limit for SISO channels. Shannon Limit for SISO is well explained in the capacity of MIMO systems in the introduction chapter of the thesis. It has been well established that these capacities depend critically upon the multipath environment in which the system operates and in particular on the number of resolvable multipath components, their amplitudes, and their spatial distributions.

As we all know, the increase in spectral efficiency offered by MIMO system is based on the utilization of space diversity at both the transmitter and receiver. With the MIMO system, the data stream from a single user is de-multiplexed into N_T separate sub-streams, where N_T is number of transmitters. With this scheme, there is a linear increase in spectral efficiency compared to a logarithmic increase in more traditional systems utilizing received diversity or no diversity [112]. The high spectral efficiencies attained by a MIMO system are enabled by the fact that in a rich scattering environment the signals from each individual transmitter appear highly uncorrelated at each of the receive antennas. The receiver can use these differences in spatial signature, simultaneously and at the same frequency separate the signals that originated from different transmit antennas. At the input of a communication system, discrete source symbols are mapped into a sequence of channel symbols. The channel symbols are then transmitted though a wireless channel that by nature is random and we will have random noise which has a characteristics of Gaussian with zero mean and some variance. A measure of how much information that can be transmitted and received with a negligible probability of error is called the channel capacity.

In order for us to determine the performance achievable over this channel, let us assume that the channel encoder receives a source symbol every T_s second. With an optimal source code, the average code length of all source symbols is equal to the entropy rate of the source. If S represents the set of all source symbols and the entropy rate of the source is written as $H(S)$ and the channel encoder will receive on average $\frac{H(S)}{T_s}$ information bits per second. If the channel codeword leaves the channel encoder every T_C second then in order to transmit all the information from the source, there must be,

$$R - \frac{H(S)T_C}{T_s}$$

information bits per channel symbol. The number R is called the information rate of the channel encoder. The maximum information rate that can be used causing negligible probability of errors at the the output is called the capacity of the channel. By transmitting information with rate R, the channel is used every T_C seconds. The channel capacity is then measured in bits per channel use. Assuming that the channel has bandwidth, W, in the input and output can be represented by samples taken $T_s = \frac{1}{2W}$ seconds apart. With a band limited channel, the capacity is measured in information bits per second. The channel capacity is measured in bits/s/Hz. The input and output of the wireless channel with the random variables X and Y respectively, the channel capacity is defined as

$$C = \max_{p(x)} I(X, Y)$$

where $I(X, Y)$ represents the mutual information between X and Y. The above equation states that the mutual information is maximized with respect to all possible transmitter statistical distribution $p(x)$.Mutual information is a measure of the amount of information that one random variable contains about another variable. The mutual information between X and Y can also be written as

$$I(X, Y) = H(Y) - H(Y|X)$$

where $H(Y|X)$ represents the conditional entropy between the random variables X and Y. The entropy of a random variable can be described as a measure of the amount of information required on average to describe the random variable. It can also be described as a measure of the uncertainty of the random variable.

6.1.1 Capacity of MIMO Channels

In this section we will discuss different types of channel capacities that we studied in order to gain insight into our problem. We looked in to the following topics - Shannon's capacity, transformation of the MIMO channel into n-SISO channels, Capacity of SIMO and MISO channels, MIMO capacity with Rice and Rayleigh Channels and finally, MIMO channel matrix for Rician propagation conditions. We divided at our capacity types into three different sections and they are as follows:

- Capacity scaling for rich scattering
- Capacity scaling for correlated scattering
- Time evolution of capacity

6.1.1.1 Shannon's Capacity

Shannon's capacity formula provides theoretically the maximum achievable transmission rate for a given channel with bandwidth B, transmitted signal power P and single side noise spectrum N_0 based on the assumption that the channel is white Gaussian

$$C = B \ \log_2 \left(1 + \frac{P}{N_0 B}\right)$$

This Shannon formula is developed for SISO case. This equation provides an upper limit for the achievable error free SISO transmission rate. If the transmission rate is less than C then an appropriate coding scheme exists that could lead to a reliable and error free transmission. If the transmission rate is more than C, the the received signal will involve errors. Now we will see how a capacity of SISO channel will transform into a capacity for MIMO channel.

For MIMO, we consider an antenna array with N_T elements at the transmitter and an antenna array with N_R elements at the receiver. The impulse response of the channel between the j^{th} transmitter and the i^{th} receiver element is denoted as $h_{i,j}(\tau,t)$. Then the MIMO channel can be described as

$$\mathbf{H}(\tau,t) = \begin{bmatrix} h_{1,1}(\tau,t) & h_{1,2}(\tau,t) & \dots & h_{1,N_T}(\tau,t) \\ h_{2,1}(\tau,t) & h_{2,2}(\tau,t) & \dots & h_{2,N_T}(\tau,t) \\ \vdots & \vdots & \ddots & \vdots \\ h_{n,1}(\tau,t) & h_{n,2}(\tau,t) & \dots & h_{N_R,N_T}(\tau,t) \end{bmatrix} \tag{6.1}$$

The input and output notation of the MIMO system can be express as:

$$y(t) = \mathbf{H}(\tau,t) \otimes s(t) + u(t)$$

where $\otimes$ denotes convolution. If we assume that the transmitted signal bandwidth is narrow enough that the channel response can be treated as flat across frequency, then the previous equation can be written in discrete form as:

$$r_\tau = \mathbf{H}\ s_\tau + u_\tau$$

The capacity of MIMO channel can be estimated as

$$C = \max_{tr(R_{ss} \leq P)} \log_2 \left[\det(\mathbf{I} + \mathbf{H}\ \mathbf{R}_{SS}\mathbf{H}^H)\right] \tag{6.2}$$

6.1.1.2 Transformation of the MIMO Into Parallel-SISO Subchannels

Suppose that the aforementioned channel matrix this transformation is given by

$$H = \mathbf{U}\mathbf{D}\mathbf{V}^H \tag{6.3}$$

where the matrices $\mathbf{U}, \mathbf{V}$ are unitary while $\mathbf{D}$ is a non negative diagonal matrix. The diagonal elements of matrix $\mathbf{D}$ are the singular values of the channel matrix $\mathbf{H}$. The operations that lead to the linear transformation of the channel into $n = \min\ (n_r, n_t)$

SISO subchannels are described as follow [112]. First the transmitter multiplies the signal to be transmitted x_T with the matrix,$\mathbf{V}$, the receiver multiplies the received signal r_T and noise with the conjugate transpose of the matrix $\mathbf{U}$. We can express them in the following equation forms:

$$s_T = \mathbf{V} X_T \tag{6.4}$$

$$y_T = \mathbf{U}^H r_T \tag{6.5}$$

$$n_T = \mathbf{U}^H u_T \tag{6.6}$$

By rearranging the equation we will get

$$y_T = D\ x_T + n_T$$

Then we can write each of the received vector component as

$$y_T^k = \varepsilon_k\ x_T^k + n_T^k$$

where ε_k are the singular values of matrix $\mathbf{H}$ according to the transformation. The above equation basically tells us that, the initial MIMO system has been transformed into $n = \min(n_r, n_t)$ SISO subchannels. The total capacity of n-SISO subchannels is the sum of the individual capacities and as a result the total MIMO capacity is

$$C = \sum_{k=1}^{n} \log_2 \left(1 + p_k \varepsilon_k^2\right) \tag{6.7}$$

where p_k is the power allocated to the k^{th} subchannels and ε_k^2 is its power gain [113].

6.1.1.3 Capacity of SIMO and MISO Channels

Single-Input Multi-Output (SIMO) and Multi-Input Single-Output (MISO) channels are special cases of MIMO channels. In this paragraph,we discuss the capacity formulas for the case of SIMO and MISO channels. For a SIMO channel, we only have one transmit antenna therefore the CSI at the transmitter does not effect the SIMO channel capacity:

$$C_{SIMO} = \log_2 \left(1 + p\varepsilon_1^2\right) \tag{6.8}$$

For MISO channel, we only have one receiver, therefore with no CSI at the transmitter, the capacity formula can be expressed as:

$$C_{MISO} = \log_2 \left(1 + \frac{p}{n_t}\varepsilon_1^2\right) \tag{6.9}$$

6.1.1.4 MIMO Channel with Rice and Rayleigh Channels

In this section, we will look at the capacity expression for the cases of Rayleigh and Rician channels, as well as when spatial fading correlation is included to the signal due to the limited distance between the array elements. When the wireless environment is characterized by strong multipath activity, then the number of paths between the transmitter and receiver allows the use of the central limit theorem and the envelope of the received signal follows the Rayleigh distribution. In the case of line of sigh in this scattering effects, then the Rician distribution is more suitable. The receiver in that scenario sees a dominant signal component along with lower power components caused by multipath. The dominant component that reaches the receiver may not be the result of LOS propagation. The Rician K factor of the channel is defined as the ratio of the powers of the dominant and the fading components.

$$K = \frac{A^2}{2\sigma^2} \tag{6.10}$$

if $K = 0$ shows a Rayleigh fading channel while $K \to \infty$ shows a non fading channel. Now we will look in the capacity of individual channel conditions. First we will start with Rayleigh fading condition. In cases where the wireless channel is submitted to Rayleigh fading and the array antennas do not introduce additional correlation to the transmitted received signal, the channel matrix becomes spatially white. The ergodic capacity formula under the assumption of Rayleigh channel and equal power allocation is:

$$C = E\left[\log_2\left(\det\left(\mathbf{I} + \frac{p}{n_t}\mathbf{H}_w\mathbf{H}_w^H\right)\right)\right] \tag{6.11}$$

Now under the assumption of $n_t = n_r = n$, it would be interesting to study the case of $n \to \infty$. Using the strong law of large numbers we get

$$\begin{aligned}
\frac{1}{n}\mathbf{H}_w\mathbf{H}_w^H &\to I_n \\
C &\to \log_2[\det(I_n + pI_n)] = \log_2[(1+p)^n] = n\log_2(1+p) \\
C &\to n\log_2(1+p)
\end{aligned}$$

From these equations, we can see two things:

1. Capacity does not depend on the nature of the channel matrix, as it increases linearly with n for a fixed SNR.
2. Every 3dB increase of SNR corresponds to an n bits/sec/Hz increase in capacity.

6.1.1.5 MIMO Channel Matrix for Rician Propagation Conditions

In the presence of a dominant component between the transmitter and receiver, the wireless channel can be modeled as the sum of a constant and a variable component caused by scattering

$$\mathbf{H}_{rice} = \sqrt{\frac{K}{K+1}}e^{j\phi_0}H_{LOS} + \sqrt{\frac{1}{K+1}}H_{Rayleigh} \tag{6.12}$$

The $\mathbf{H}_{\text{Rayleigh}}$ is spatially white, and its structure was described earlier. Let assume, R is the distance between the transmitter and the receiver and d is the inter element distance. The matrix of H_{LoS} is given by

$$\mathbf{H}_{LOS} = \begin{bmatrix} 1 & e^{j\theta} & \dots & e^{j(n_t-1)\theta} \\ e^{-j\theta} & 1 & \dots & \vdots \\ \vdots & \vdots & \ddots & e^{j\theta} \\ e^{-j(n_r-1)\theta} & e^{-j(n_r-2)\theta} & \dots & 1 \end{bmatrix}$$

where θ is the angle corresponding to phase shift between the neighbor array elements. In order to simplify this, we will assume that the distance between receiver and transmitter is larger then the distance between each antenna.In that case, H_{LOS} is a matrix with one as elements.

6.1.2 Capacity scattering for rich scattering for large number of antennas

For this part, we will assume that elements of the matrix $\mathbf{H}$ are i.i.d zero mean complex random variables. The time correlation is not consider therefore, independent samples can be used. We will show how to find the mean value, the variance, the skewness and the kurtosis(also known as 1st to 4th order statistics of the capacity) for starting from 1×1 to 9×9 antenna. Once we contain the results, we will compare the results to the theoretical equation which was contain form [114].

For theoretical the paper assumed a MIMO link with rich scattering. It also assumed that both side of the system contains large number of antennas therefore, the capacity distribution is approximately Gaussian, with the mean and variance is given as follows:

$$\begin{aligned} \frac{\bar{C}}{N_R} &= \beta \ln\left[1 + \frac{\gamma}{\beta} - \frac{1}{4}F\left(\frac{\gamma}{\beta}, \beta\right)\right] \\ &+ \ln\left[1 + \gamma - \frac{1}{4}F\left(\frac{\gamma}{\beta}, \beta\right)\right] - \frac{\beta}{4\gamma}F(\frac{\gamma}{\beta}, \beta) \\ \sigma_C^2 &= -\ln\left(1 - \beta\left[\frac{1}{4\gamma}F\left(\frac{\gamma}{\beta}, \beta\right)\right]\right) \end{aligned} \tag{6.13}$$

$$F(x, z) = \left[\sqrt{x(1+\sqrt{z})^2 + 1} - \sqrt{x(1-\sqrt{z})^2 + 1}\right]^2 \tag{6.14}$$

The paper also give us 2 different sets of equation based on the size of the SNR. For example, for the small value of SNR γ, these equations can be simplified to produce

$$\frac{\bar{C}}{N_R} = \gamma - \frac{1}{2}\frac{\beta+1}{\beta}\gamma^2 \tag{6.15}$$

$$\sigma_C^2 = \gamma - \frac{1}{2}\frac{\beta+2}{\beta}\gamma^2 \tag{6.16}$$

but for the large SNR γ, the approximation ($\beta = 1$) is as follows:

$$\frac{\bar{C}}{N_R} \approx \ln\frac{\gamma}{e} + \frac{2}{\sqrt{\gamma}} - \frac{1}{\gamma} \tag{6.17}$$

$$\sigma_C^2 \approx \frac{1}{2}\left(\ln\frac{\gamma}{4} + \frac{2}{\sqrt{\gamma}} - \frac{1}{4\gamma}\right) - 0.193 \tag{6.18}$$

To complete our goal, we will start by generating the channel matrix H which are i.i.d zero-mean complex random variables. Once we generated that we will find the mean, the variance, the skewness and the kurtosis of each channels to see the performance and compare that to the theoretical values. The results are presented in figure (6.1)

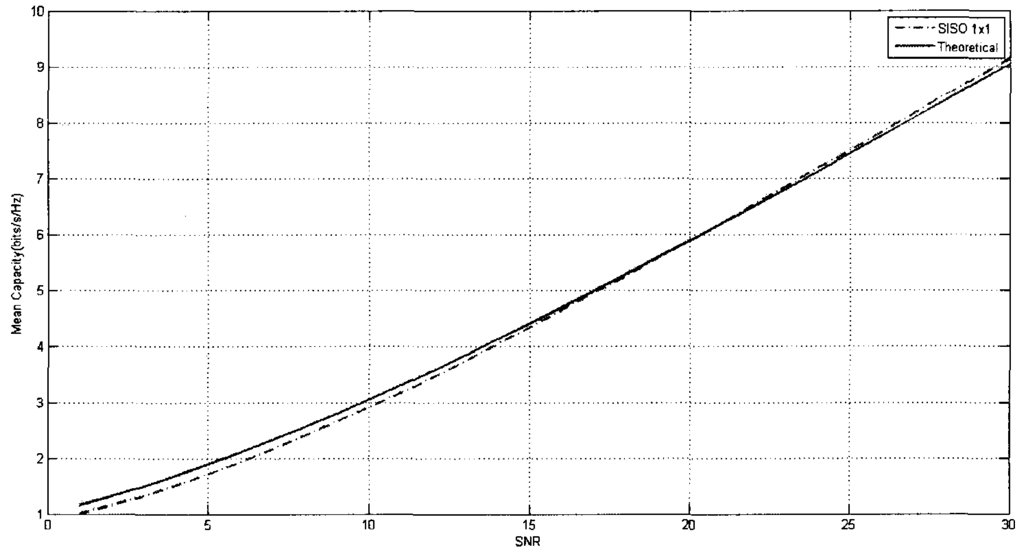

Figure 6.1: The mean capacity of 1x1 i.i.d zero-mean complex random channel.

As we can see in figure 6.1, the red dotted line represents our simulation result and the blue straight line represents the theoretical result using the equation (6.17). The graph shows us that, our simulation and the theoretical values were very close. We have plotted SNR on the x axis from 1dB SNR to 30 dB SNR against the capacity value on the y axis starting from 1 bit/s/Hz to 10 bit/s/Hz in this case. We can see that the capacity grew from 1 bit/s/Hz to 9 bit/s/Hz fairly constantly in this case. We will use this 1 $\times$ 1 case as a bench mark and show the readers how it increases as we increase the antenna values on both sides. If we look at figures 6.2 and 6.3

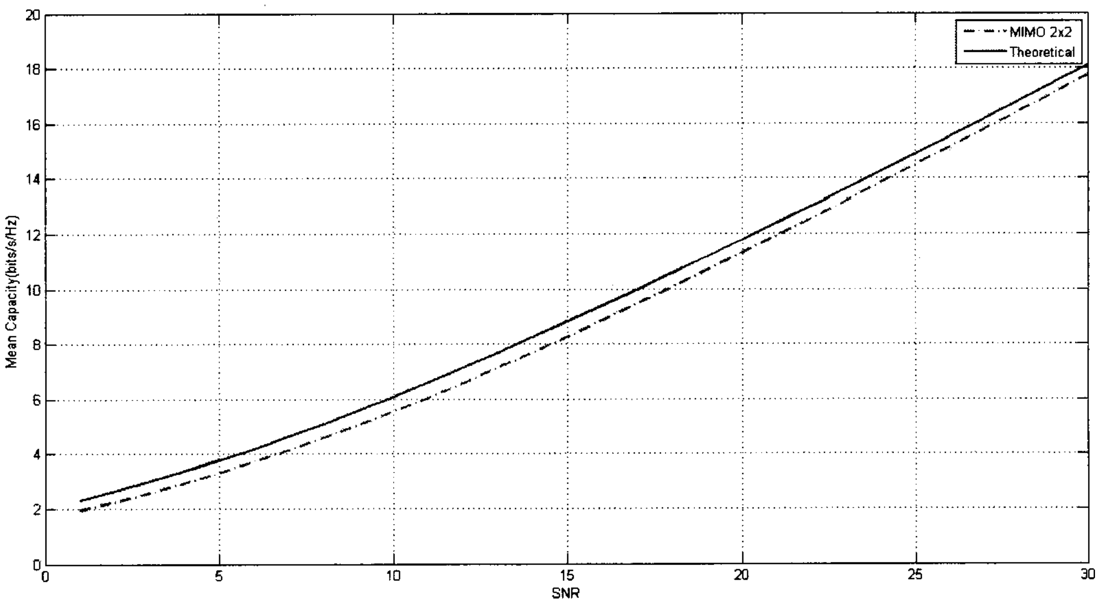

Figure 6.2: The mean capacity of $2x2$ i.i.d zero-mean complex random channel.

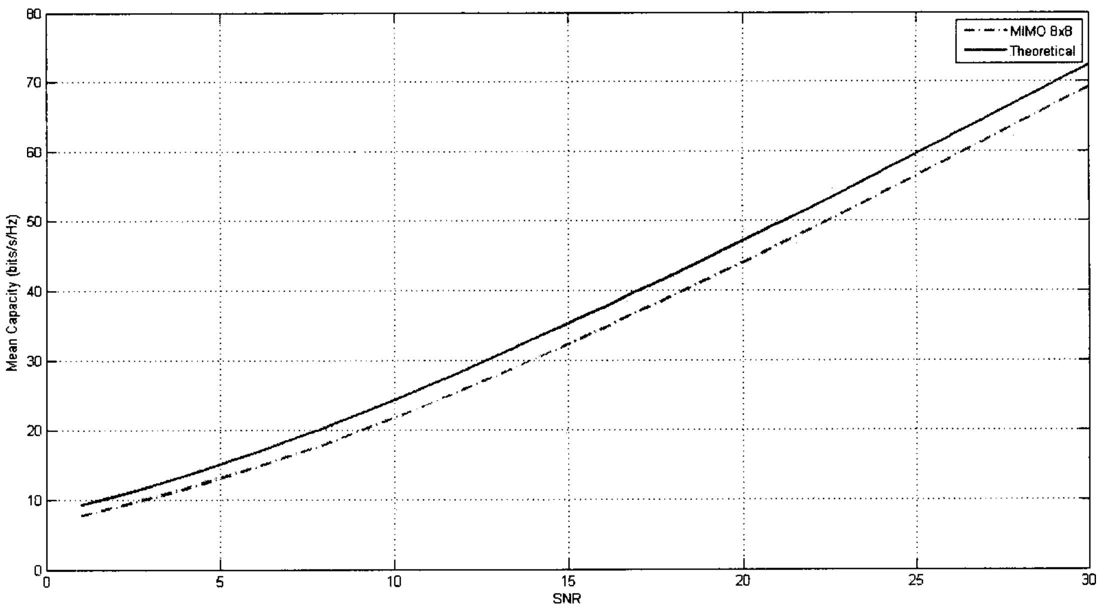

Figure 6.3: The mean capacity of $8x8$ i.i.d zero-mean complex random channel.

we can see that our simulation results and the theoretical values were very close and have the same shape. These graphs were plotted in a similar way as in figure 6.1 so that comparison is possible of the capacity values for the increased antenna values on both sides. In figure 6.2 the capacity started out to be at 2bit/s/Hz at 1dB SNR and goes up to 18 bit/s/Hz at 30 dB SNR. In Fig. 6.3 we can see that the capacity at 1dB SNR is about 10 bit/s/Hz and at 30 dB SNR its about 70 dB. These results show us that the capacity grew linearly when the amount of antenna is increased using independent channel. The figure (6.4) shows the resemblance of shapes as the

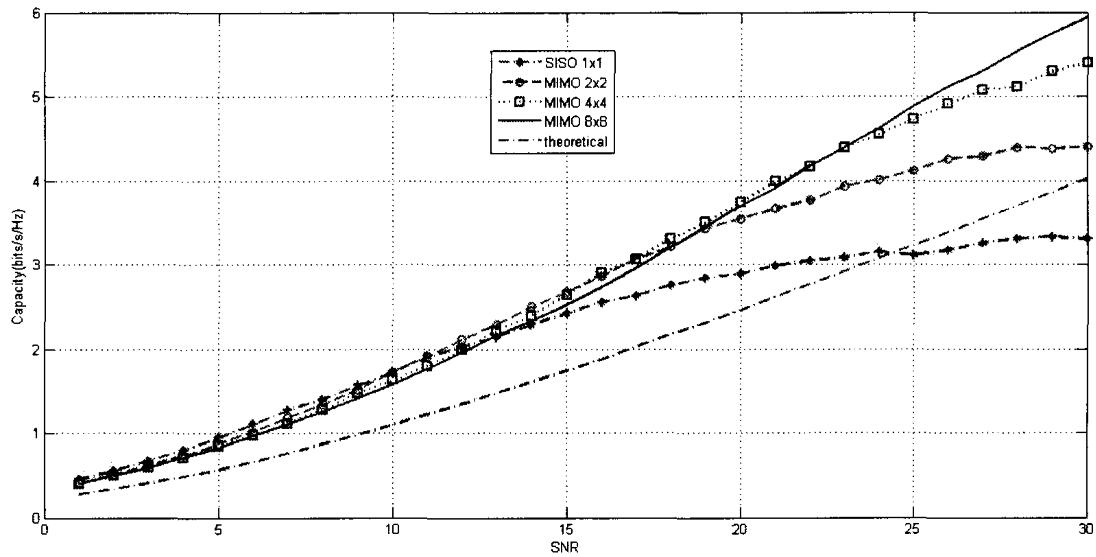

Figure 6.4: The variance of different antenna sizes and theoretical values for i.i.d zero-mean complex random channel.

theoretical result. For all the different amount of antennas, all the variance were same from 0-15 dB of SNR.They started to deviate after 15dB of SNR up to 30 dB of SNR. The figure 6.5 show that for all different types of number of antennas, the kurtosis is about 3.

The figure 6.6 shows the skewness of our capacity for different antenna values. As we know, skewness is the third standardized moment. We can see that the skewness for all the antennas started out from the small positive value and end up at the negative values. From the negative skewness we can say that the left tail is longer and the mass of the distribution is concentrated on the right of the figure. Now that

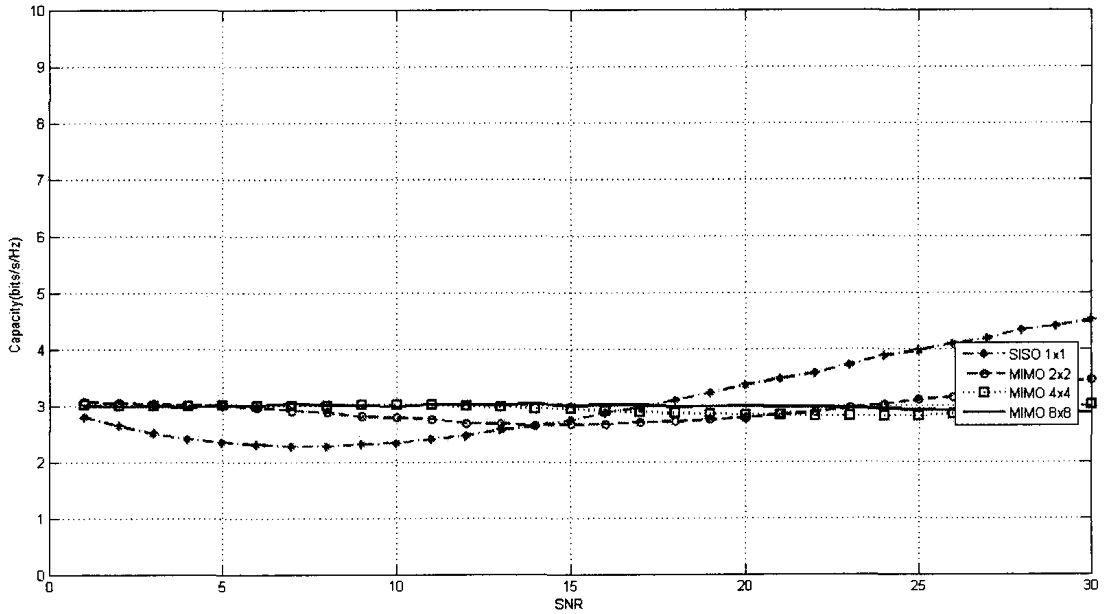

Figure 6.5: The kurtosis of different antenna sizes for i.i.d zero-mean complex random channel.

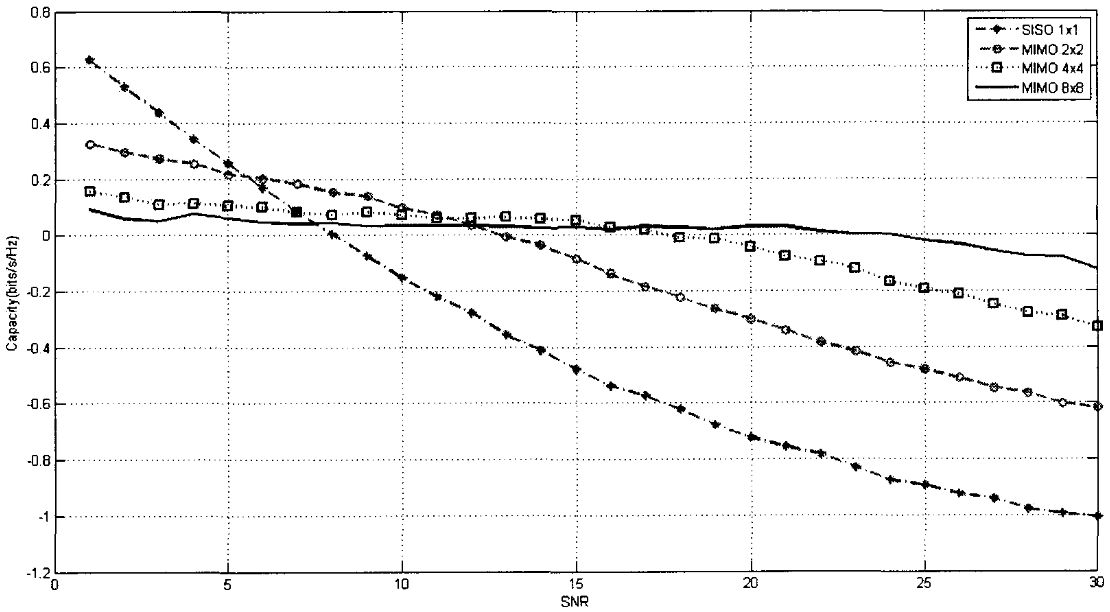

Figure 6.6: The skewness of different antenna sizes for i.i.d zero-mean complex random channel.

we have successfully simulated and tested out the performance of capacity scaling for rich scattering we will move on to testing the performance of capacity scaling for correlated scattering.

6.1.3 Capacity scaling for correlated scattering

For this section we will be using the UIU channel model that we have designed in the pervious section, but we will change some assumptions from the design of the model. We will assume that the average AoD 20° and the average AoA 40°, and the distributions of AoA and AoD are independent uniform distributions in the range of $[-20^\circ, 20^\circ]$ around corresponding mean values. We should note that, we will use samples that are independent in time which means that we can generate channel for each time sample. Figure (6.7) shows the assumption made and the output of the joint uniform PDF function.

Next step will be regenerating the UIU channel model that we have shown before, using the uniform joint PDF instead of Gaussian PDF. We will find the mean, the variance, the skewness and the kurtosis of the different set of antennas using the new UIU channel coefficients to show that the correlation in this case does not increase linearly as it did in capacity scaling for rich scattering. Due to the space limit, we will only provide two sets of results that will give the best understanding of correlation for correlated scattering.

From Fig. 6.8 and Fig. 6.9 we can easily see that all the shapes were very similar to what we have expected. From Fig. 6.8 we can see that the mean values increased from 1 to 11 while in Fig. 6.9 the mean value increased from 1 to 15. We can clearly conclude in this case that the mean of the capacity did not really increase linearly in this case as we have expected before. We can also notice that the variance and the skewness decreased a lot in 11×11 antenna case then 5×5. However, the kurtosis of the 11x11 goes up more than 5×5 case. As the final case for the capacity, we will study the time evolution of capacity in the next section.

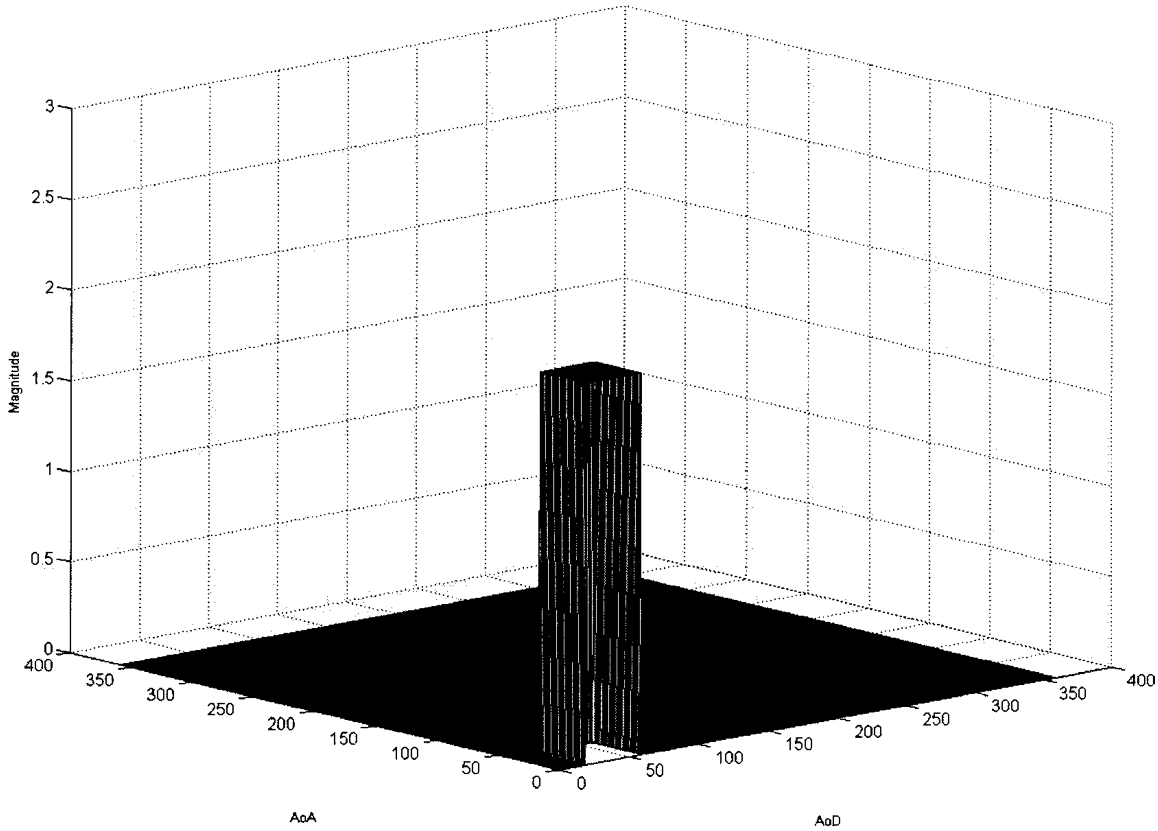

Figure 6.7: The uniform PDF for the average AoD is 20° and the average AoA is $40^\circ$and the distributions of AoA and AoD are independent uniform distributions in the range of $[-20^\circ, 20^\circ]$ around corresponding mean values.

6.1.4 Time Evolution of Capacity

Our task for this section is to use the same UIU model that we have created before to find out the following quantities related to the instantaneous capacity $C(t)$:

- Covariance function $R_{CC}(\tau)$
- Level Crossing Rate (LCR)
- The average outage duration (AoD)

and then we will find out how well the covariance function is approximated by a single exponent function in this case.

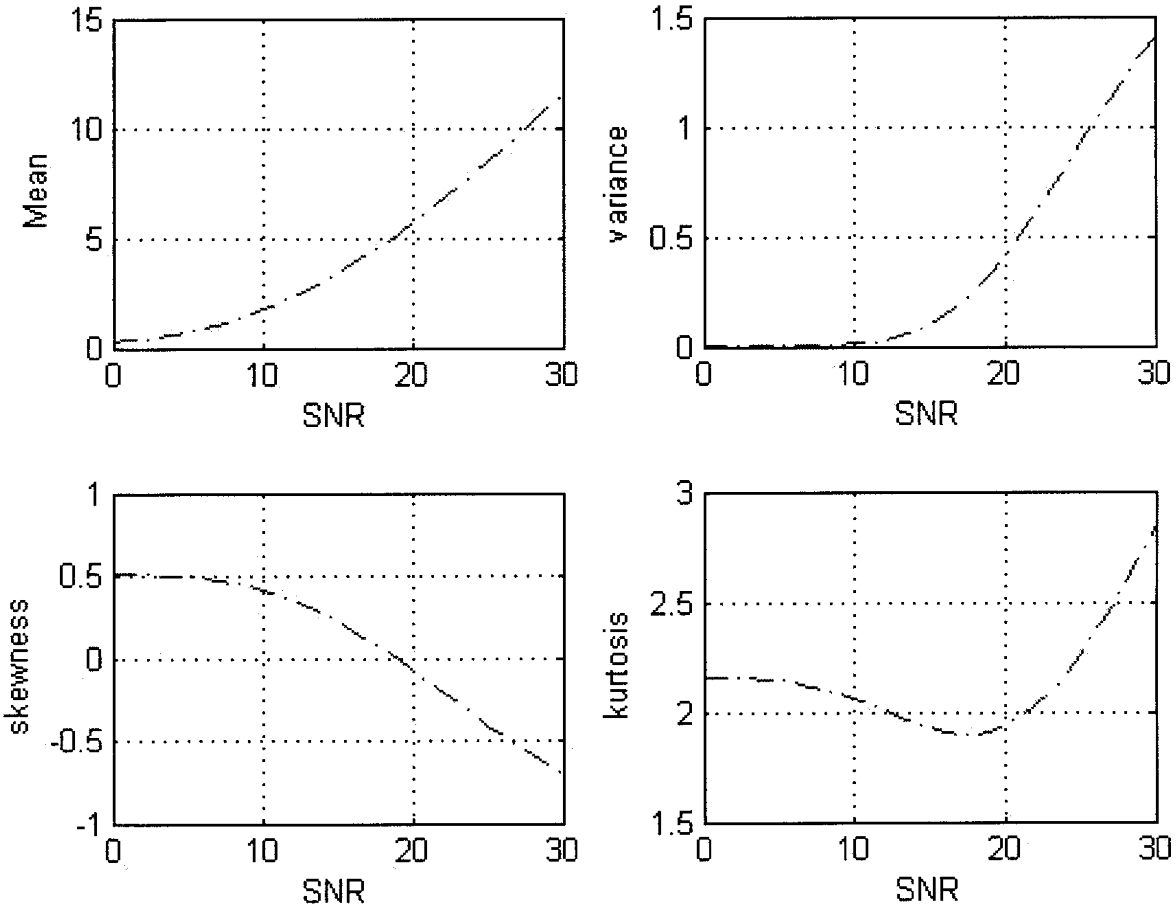

Figure 6.8: The mean, the variance, the skewness and the kurtosis for 5transmitter and 5 receiver using uniform PDF in UIU model.

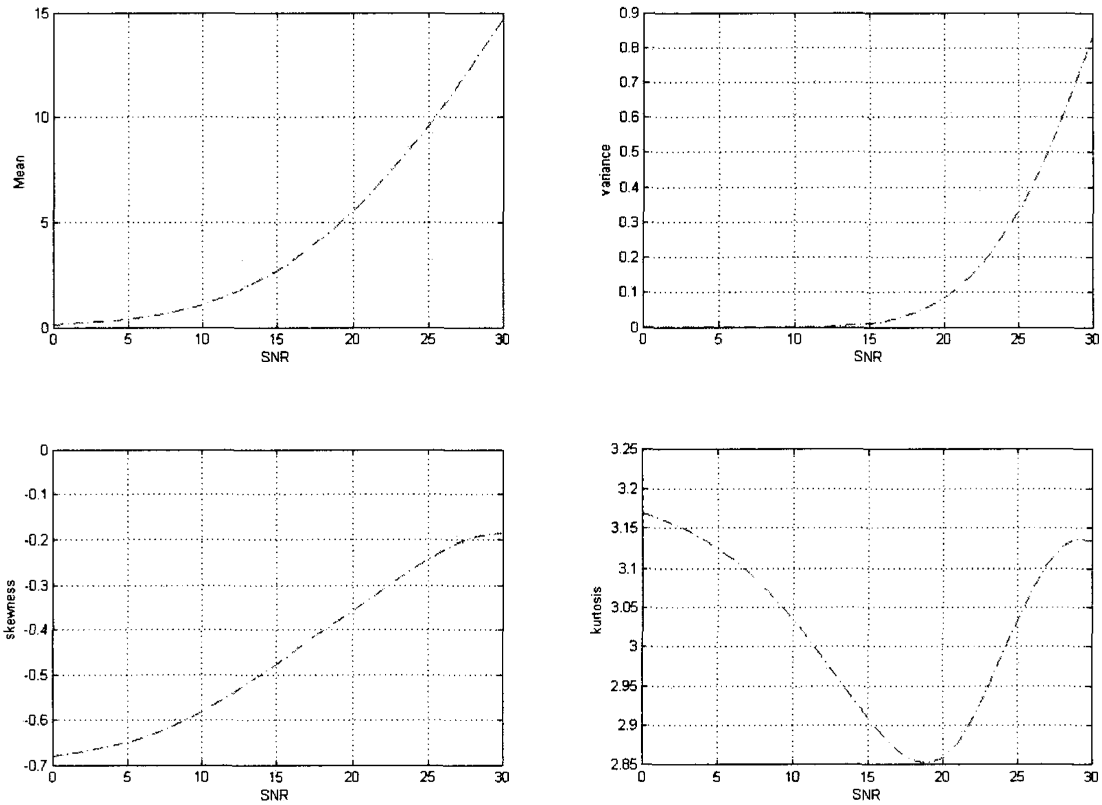

Figure 6.9: The mean, the variance, the skewness and the kurtosis for 11 transmitter and 11 receiver using uniform PDF in UIU model.

First we will find out how the channel evolves over time. For this we will use 15 Transmit antennas and 15 receive antennas with the noise to power ratio of 30dB SNR. The Figure show how the instantaneous capacity looks like for the given case. As we can see that, in this graph, the medium of the instantaneous capacity is around

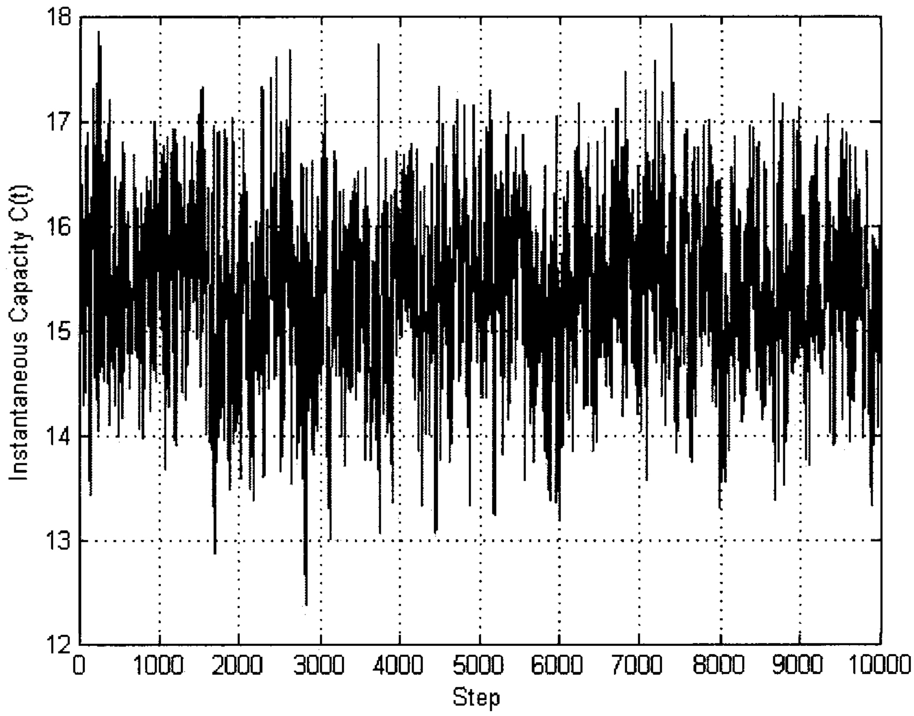

Figure 6.10: The instantaneous capacity of an UIU model using 15 transmit antennas and 15 receive antennas with the 30dB SNR of signal to nose ratio.

15.5 but it varies based on the SNR values. Our next goal is to find the covariance function of the instantaneous capacity and find the exponent function that is as close as to our covariance results. We can conclude that from figure (6.11) the single exponential function of $-0.25\exp$ follows the shape and decays with the same slope as our covariance results from the instantaneous capacity. For the final part of this chapter we will find out the level crossing rate and the average outage durations for the instantaneous capacity. The level crossing rate is a measure of the rapidity of the fading. It quantifies how often the fading crosses some threshold, usually in the positive-going direction. The average outage duration, also known as the average fade duration, quantifies how long the signal spends below the threshold. The figure 6.12

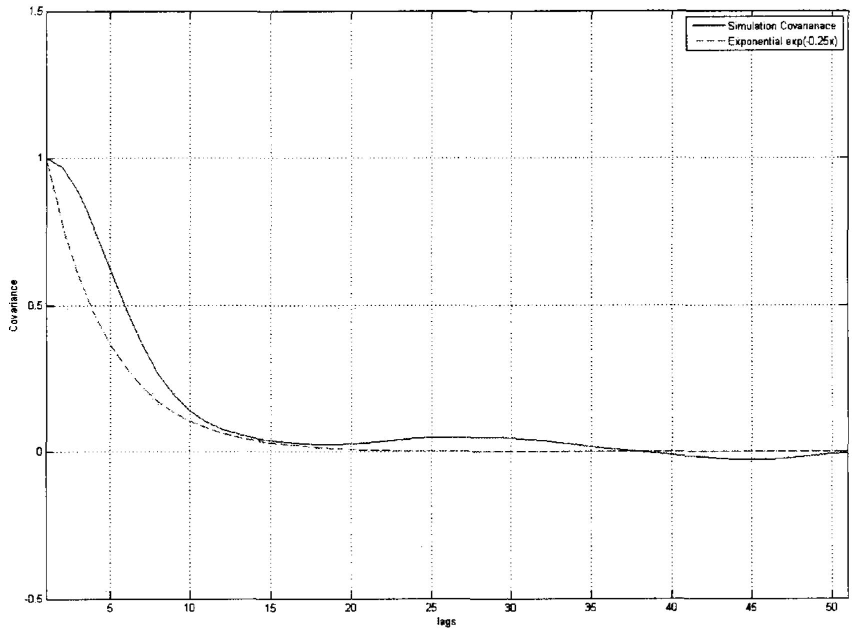

Figure 6.11: The covariance function of the instantaneous capacity of an UIU model with the 30dB SNR of signal to nose ratio with the best fit of single exponential function.

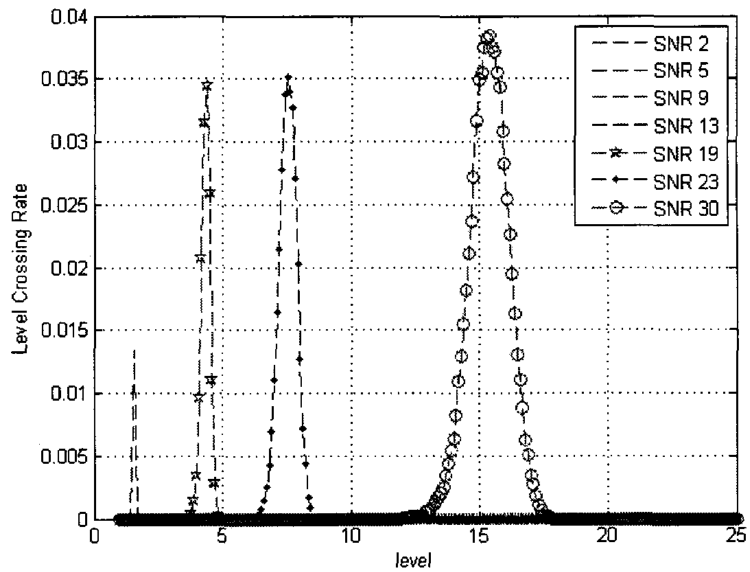

Figure 6.12: The level crossing rate of the instantaneous capacity of an UIU model with different SNR values and threshold levels.

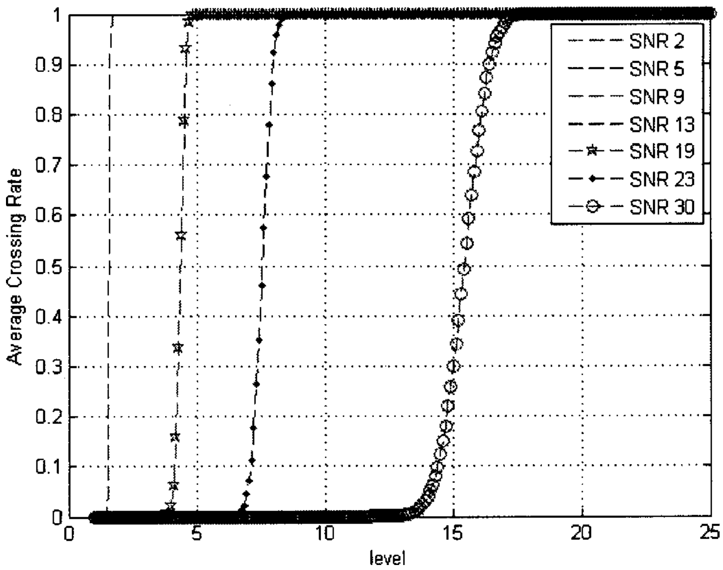

Figure 6.13: The average fade duration (The average outage duration) of the instantaneous capacity of an UIU model with different SNR values and threshold levels.

gave us different results based on different SNR values at a given level. For example, if we look at SNR 30dB, we can see that there is no changes till the threshold is between 12-18. We can also see that fact from the figure 6.10 that there is no effect when the threshold is less than 12 and no effects when it is above 18. The results from Figure 6.13 tells us that how long does the signal fades.For our better understanding, we can have look at the results from SNR 30dB. As we all know there is no level crossing outside of level between 12-18.When the threshold is around level 15, we have about 20% fading duration. As we increase the threshold, we can see that our signal is below the threshold level more and more until the threshold is set above level 19 then we have 100% fading duration. This concludes our discussion on the time evolution of capacity.

6.2 Conclusion

In this chapter, we have demonstrated the UIU channel modeling using [19] and the performance of the channel. The autocorrelation of the simulated results clearly matched with the theory results. We also tested the channel performance using Alamouti and PPE and the results were better then expected. Three different types of capacity and its results were shown in the later section of this chapter. The results show good agreement when comparing to theory and our predictions.

Chapter 7
Effect of Channel Estimation Error on Performance of Alamouti OSTBC

7.1 Introduction

Over the last decade, the space time coding has gained attention from both the research field and the industrial field. There have been many papers published and use this scheme in parts of future wireless communication standards. However, space-time coding schemes with large diversity gains require a greater number of transmit antennas which is generally not the case in practice. Therefore, in order to achieve the bit error rate performance levels requires in most wireless systems, the space time codes are often used in concatenation with channel codes or trellis coded modulations[115], [116], [117] and [118].

The Alamouti space time code was proposed in 1998 and has generated significant interest due to the low complexity linear combining Space-Time Decoder (LC-STD) suggested by Alamouti [119]. The linear combining Space-Time Decoder was designed so that under the perfect channel state information (CSI) and quasi-static fading assumptions, it can completely eliminate inference from the other symbol in the codeword and achieve the same performance as the more complex Maximum Likelihood Space-Time Decoder (ML-STD). When the channels are not quasi-static, the channel and self interference is not completely eliminated by the linear combiner, even with the perfect CSI. A performance degradation due to imperfect estimation of the channel is caused by the imperfection in CSI [120]. Under this condition, the ML symbol detector [121] and ML Space-Time Decoder should be used to reduce the effect due to reduce the effect of time varying fading channel. In addition to worsening the system performance though self interference, the time varying fading also increases the system channel estimation error and then degrades performance.

Other factors that can significantly degrade the performance of the Alamouti space time code are noisy CSI, which is caused by noise in the pilot symbols or time varying fading channels, and spatial correlation of the transmit antennas. When the CSI is noisy, the LC-STD can not correctly eliminate the signal contribution from the other symbol resulting in interference even in the quasi-static channels [122],[123], [124] and [125]. These degradations are known to limit performance regardless of the space-time decoding scheme employed. When then channels fade rapidly at a high Doppler frequency, the channel estimates derived from the received pilot signals become more unreliable, thus degrading the performance of the coherent detection scheme. Given the close relationship between the Doppler frequency and the channel estimation error and their effect on the interference in the system, it is important to evaluate the performance of such a system by taking into account these factors. In this chapter, we will use the two decoding schemes for the conventional alamouti space time coded systems are considered, namely, the low complexity LC-STD and the high complexity ML-STD. Two decoding schemes for the CCA are evaluated, namely, the LC-STD with an ML convolutional decoder (LC-ML) and the joint Alamouti and convolutional ML decoder (JML).

7.2 System Model

The system under consideration is a down-link Binary Phase Shift Keying (BPSK) DS-CDMA system with two transmit antennas and one receive antenna. In the following section, the transmitter, the receiver and the transmitter are discussed properly.

7.2.1 Transmitter

The two consecutive symbols for the concatenated system, or two un-coded symbols for the conventional Alamouti system, are then encoded by the Alamouti space-time encode. Since we have assumed BPSK modulation, the complex conjugates of signals used in the Alamouti code can be ignored. We have used the techniques that is suggested in [120]to evaluate the performance of the Alamouti STC. There are two pilot sequences, one from each transmit antenna, where each antenna uses a distinct orthogonal code. There are also two data sequences, but unlike the pilot sequences, both transmit antennas use the same orthogonal code for the data sequences. The symbol rate baseband representation of this system is shown in Figure 7.1, where s_k denotes the data symbol during the symbol time index k,E_s and E_p denotes the transmit energy per data symbol and pilot symbol (equivalent to $E_s/2$ and $E_p/2$ per symbol per antenna), respectively. The signal corresponding to the symbol time index 1 are show in parentheses and the signals corresponding to the symbol time index 2 are shown in square brackets.

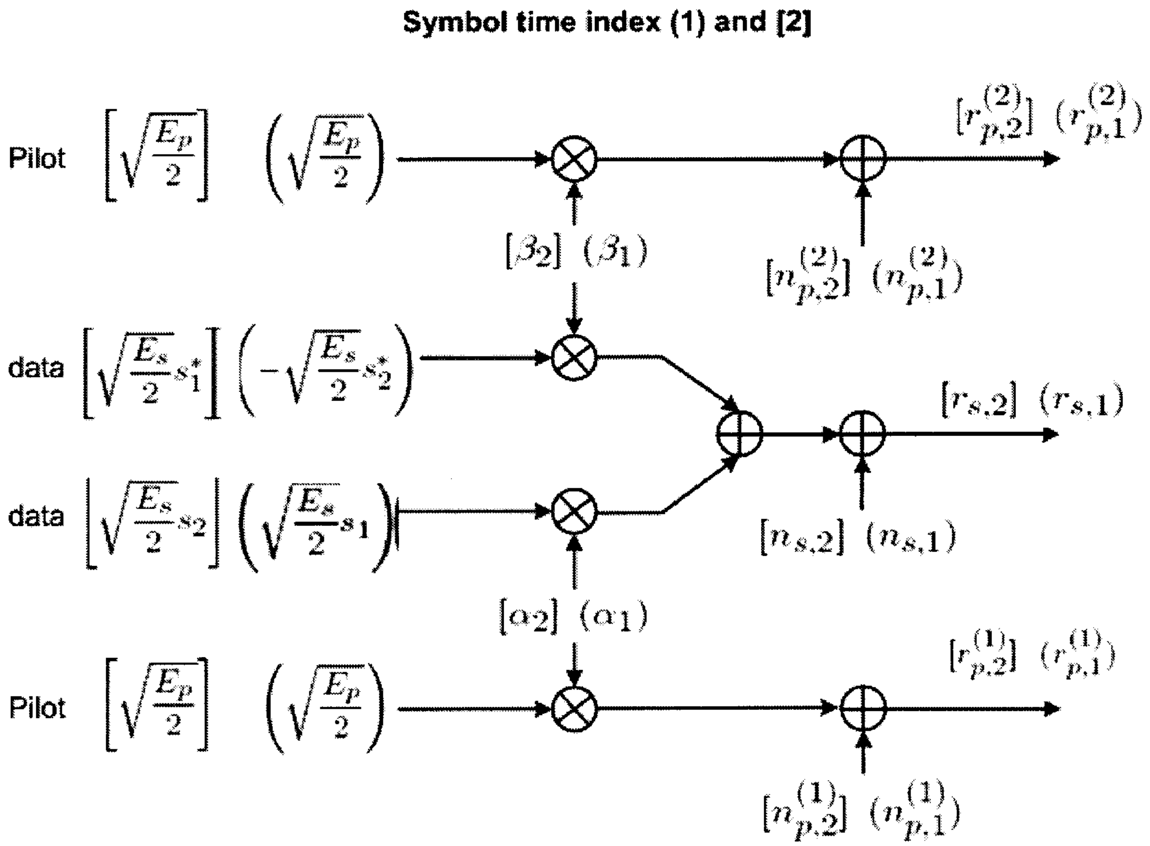

Figure 7.1: The System Diagram of STTD over two-symbol period

7.2.2 Channel

In this case, both channels are assumed to be time varying Rayleigh flat fading channels. The fading coefficient corresponding to the channel between transmit antenna A and the receiver antenna during the symbol time index k is denoted by α_k and the fading coefficient corresponding to the channel between the transmitter antenna B and the receive antenna during the symbol time index k is denoted by β_k. Since we have assumed that the Rayleigh fading, α_k and β_k are circularly symmetric zero-mean complex Gaussian random variable. We also assume that α_k and β_k have identical autocorrelation function $0.5E[\alpha_k\alpha^*_{k-m}] = 0.5E[\beta_k\beta^*_{k-m}] = \sigma_c^2 R(m\tau)$, where$R(0) = 1$. In our simulations, we generated these coefficients using SISO channel design that was explained in Chapter 4 of this thesis. We can also assume that the correlation between α_k and β_k can be written as $0.5E[\alpha_k\beta^*_{k-m}] = \rho\sigma_c^2 R(m\tau)$, where ρ is a real value indicating the spatial correlation between the two transmit antennas. We should note that, since we assume time varying channel, we are limiting ourself to the case when the channels change slowly enough that the fading coefficients appears to be constant over one symbol period τ. The noise from the pilot channels from transmit antenna A, transmit antenna B, and the data channel at the symbol time index k, denoted by $n^1_{p,k}$,$n^2_{p,k}$ and $n_{s,k}$ are zero-mean circularly symmetric complex white Gaussian variables with variances σ_p^2,σ_p^2 and σ_s^2, respectively.

7.2.3 Receiver

The discrete baseband representation of the received signals over one Alamouti code block can be expressed as

$$\mathbf{r}_{s,2k+1} = \begin{bmatrix} r_{s,2k+1} \\ r^*_{s,2k+2} \end{bmatrix} = \sqrt{\frac{E_s}{2}} \begin{bmatrix} \alpha_{2k+1} & -\beta_{2k+1} \\ \beta^*_{2k+2} & \alpha^*_{2k+2} \end{bmatrix} \begin{bmatrix} S_{2k+1} \\ S^*_{2k+2} \end{bmatrix} + \begin{bmatrix} n_{s,2k+1} \\ n^*_{s,2k+2} \end{bmatrix} \quad (7.1)$$

$$r^{(1)}_{p,k} = \sqrt{\frac{E_p}{2}}\alpha_k + n^{(1)}_{p,k} \rightarrow \mathbf{r}^{(1)}_{p,k} = [r^{(1)}_{p,k-M} \cdots r^{(1)}_{p,k} \cdots r^{(1)}_{p,k+M}]^T \quad (7.2)$$

$$r^{(2)}_{p,k} = \sqrt{\frac{E_p}{2}}\beta_k + n^{(2)}_{p,k} \rightarrow \mathbf{r}^{(2)}_{p,k} = [r^{(2)}_{p,k-M} \;\cdots\; r^{(2)}_{p,k} \;\cdots\; r^{(2)}_{p,k+M}]^T \tag{7.3}$$

where $r_{s,k}$denotes the received data signal during the symbol time index k, $r^{(1)}_{p,k}$ and $r^{2}_{p,k}$ denote the received pilot signals from transmit antennas A and B, respectively, during the symbol time index k.At the receiver, the channel estimation is performed by $(2M+1)$ tap FIR filters.We used one filter for reach resolvable path. The channel estimates, which are the output of the FIR filters, can be expressed as

$$\hat{\alpha}_k = \mathbf{h}^H \, \mathbf{r}^{(1)}_{p,k} \tag{7.4}$$

$$\hat{\beta}_k = \mathbf{h}^H \, \mathbf{r}^{(2)}_{p,k} \tag{7.5}$$

where $\mathbf{h} = [h_M \;\ldots\; h_0 \;\ldots\; h_{-M}]^T$ denotes the filter coefficient vector $\hat{\alpha}_k$ and $\hat{\beta}_k$ denote the channel estimates corresponding to the channel from the transmit antennas A and B, respectively. The figure (7.3) illustrate the basic idea of filtering using pilots.

7.3 The Linear Combining Scheme

The simple space time decoder originally suggested by Alamouti [126] is known as the linear-combining space-time decoder (LC-STD). It is the most likely scheme to be implemented in practice due to its low complexity [115], [116], [117] and [118]. In this section, we will show the derivation of the bit error probability of the conventional Alamouti space-time code when the LC-STD is used.

The linear combining scheme performed over an Alamouti space time code block corresponding to the symbol time index 1 and 2 can be written in a matrix form as

$$\begin{bmatrix} z_1 \\ z_2^* \end{bmatrix} = \begin{bmatrix} \hat{\alpha}_1^* & \hat{\beta}_2 \\ -\hat{\beta}_1^* & \hat{\alpha}_2 \end{bmatrix} \mathbf{r}_{s,1} = \sqrt{\frac{E_s}{2}}\, \mathbf{G}_1 \begin{bmatrix} s_1 \\ s_2^* \end{bmatrix} + \begin{bmatrix} \tilde{n}_{s,1} \\ \tilde{n}_{s,2} \end{bmatrix} \tag{7.6}$$

where z_1 and z_2 are the output of the linear combiner corresponding to the first and the second data symbols, respectively and $\tilde{n}_{s,1} = \hat{\alpha}_1^* n_{s,1} + \hat{\beta}_2 \, n^*_{s,2}$, $\tilde{n}_{s,2} = -\hat{\beta}_1^* n_{s,1} +$

$\hat{\alpha}_2 \ n_{s,2}^*$ and the matrix $\mathbf{G}$ can be defined as

$$\mathbf{G} = \begin{bmatrix} \alpha_1\hat{\alpha}_1^* + \beta_2^*\hat{\beta}_2 & \alpha_2^*\hat{\beta}_2 - \beta_1\hat{\alpha}_1^* \\ \beta_2^*\hat{\alpha}_2 - \alpha_1\hat{\beta}_1^* & \beta_1\hat{\beta}_1^* + \alpha_2^*\hat{\alpha}_2 \end{bmatrix}$$

In an ideal environment, where CSI is perfect and channels are quasi-static, we have $\hat{\alpha}_1 = \hat{\alpha}_2 = \alpha_1 = \alpha_2$ and $\hat{\beta}_1 = \hat{\beta}_2 = \beta_1 = \beta_2$. Now we can eliminate interference within the code block completely and $\mathbf{G}$ becomes

$$\mathbf{G}_{perfect} = \begin{bmatrix} |\alpha_1|^2 + |\beta_1|^2 & 0 \\ 0 & |\alpha_1|^2 + |\beta_1|^2 \end{bmatrix} = \left(|\alpha_1|^2 + |\beta_1|^2\right) I_2$$

where $\mathbf{I}_2$ is 2 x 2 identity matrix. We will show how we can derive the bit error probability, denoted by P_b, and the block error probability of the Alamouti space-time code, denoted by $P_{Alamouti}$ which is upper bounded by

$$P_{Alamouti} \leq 2P_b \tag{7.7}$$

Since the bit error probabilities of the first symbol and the second symbol are equal, we can focus on the bit error probability of the first symbol only. Without loss of generality, we can assume that $s_1 = s_2 = 1$. It follows from equation 7.6 that the output of the linear combiner corresponding to the first symbol is $z_1 = \hat{\alpha}_1^* r_{s,1} + \beta_2 r_{s,2}^*$. The real part of z_1 can be written in the quadratic form $Re[z_1] = \mathbf{x}^H\mathbf{Q}\mathbf{x}$ where [127]

$$\mathbf{x} = \begin{bmatrix} r_{s,1} & r_{s,2} & \hat{\alpha}_1 & \hat{\beta}_2 \end{bmatrix}^T \tag{7.8}$$

$$\mathbf{Q} = \frac{1}{2}\begin{bmatrix} \mathbf{0}_2 & \mathbf{I}_2 \\ \mathbf{I}_2 & \mathbf{0}_2 \end{bmatrix} \tag{7.9}$$

Using the ML symbol detector, an error occurs when Rez_1 or $\mathbf{x}^H\mathbf{Q}\mathbf{x}$ is less than zero. The bit error probability P_b can then be expressed as

$$P_b = P_r[\mathbf{x}^H\mathbf{Q}\mathbf{x}]$$

In addition, we can show that x_1 is a zero-mean complex Gaussian random vector. In order to find the characteristics function of $\Re z_1$ can be found but it requires the knowledge of the covariance matrix of $\mathbf{x}$. The covariance matrix , found in [120], can be expressed as

$$\sum = \begin{bmatrix} \mathbf{A} & \mathbf{C} \\ \mathbf{C}^H & \mathbf{B} \end{bmatrix} \tag{7.10}$$

$$\mathbf{A} = E_s\,\sigma_c^2(1+\bar{\gamma}_s^{-1})\mathbf{I}_2 \tag{7.11}$$

$$\mathbf{B} = \sigma_c^2\mathbf{h}^H\left(\frac{\mathbf{D}_0}{2}+\bar{\gamma}_p^{-1}\mathbf{I}_{2M+1}\right)\mathbf{h}\,\mathbf{I}_2 \tag{7.12}$$

$$\mathbf{C} = \frac{\sqrt{E_s\,\sigma_c^2}}{2}\begin{bmatrix} \mathbf{w}_0^H\,\mathbf{h} & -\mathbf{w}_1^H\,\mathbf{h} \\ \mathbf{w}_{-1}^H\,\mathbf{h} & \mathbf{w}_0^H\,\mathbf{h} \end{bmatrix} \tag{7.13}$$

where $\bar{\gamma}_p$ and $\bar{\gamma}_s$ are the average pilot SNR and the average data SNR, respectively. D_e is a square matrix of order $2M+1$ with $\mathbf{D}_e(m,n) = R((e+m-n)\tau)$ and w_e is the $(M+1)^{th}$ column of $\mathbf{D}_e$. With the knowledge of the characteristic function of $\mathbf{x}$. Knowing $\sum$, P_b can be found using the residue theorem, which is given in the appendix. Although the analysis allows any values of h, for simplicity, the $(2M+1)$ tap Winer filter will be used in this case.Using the Wiener filter as the pilot filter, the filter coefficients become

$$h = \frac{1}{\sqrt{2}}\left(\frac{\mathbf{D}_0}{2}+\bar{\gamma}_p^{-1}I_{2M+1}\right)^{-1}\mathbf{w}_0 \tag{7.14}$$

Now, we can substitute equation 7.14 into the above equations and we will get a simpler covariance matrix:

$$\sum = \sigma_c^2\begin{bmatrix} E_s(1+\bar{\gamma}^{-1})\mathbf{I}_2 & \sqrt{\frac{E_s}{8}}\begin{bmatrix} \varepsilon_0 & -\varepsilon_1 \\ \varepsilon_1 & \varepsilon_0 \end{bmatrix} \\ \sqrt{\frac{E_s}{8}}\begin{bmatrix} \varepsilon_0 & \varepsilon_1 \\ -\varepsilon_1 & \varepsilon_0 \end{bmatrix} & \frac{\varepsilon_0}{2}\mathbf{I}_2 \end{bmatrix} \tag{7.15}$$

where

$$\varepsilon_0 = \mathbf{w}_0^H(\mathbf{D}_0/2 + \gamma_p^{-1}\mathbf{I}_{2M+1})^{-1}\mathbf{w}_0 \tag{7.16}$$
$$\varepsilon_1 = \mathbf{w}_1^H(\mathbf{D}_0/2 + \gamma_p^{-1}\mathbf{I}_{2M+1})^{-1}\mathbf{w}_0 \tag{7.17}$$

Using the residue theorem, the paper found out the bit error probability as

$$P_b = \frac{1}{4}(2+\Upsilon)(1-\Upsilon)^2 \tag{7.18}$$

where Υ was defined in the paper as

$$\Upsilon = \left[\frac{4(1+\bar{\gamma}_s^{-1})}{\varepsilon_0} - \left(\frac{\varepsilon_1}{\varepsilon_0}\right)^2\right]^{-1/2}$$

For the perfect CSI case, the one sets $\bar{\gamma}_p \to \infty$. Since $\mathbf{D}_0^{-1}\mathbf{D}_0 = \mathbf{I}_{2M+1}$ and $\mathbf{w}_0$ is the $(M+1)^{th}$ column of D_0, we get $\mathbf{D}_0^{-1}\mathbf{w}_0 = [0\ \ldots\ 0\ 1\ 0\ \ldots\ 0]^T$ (with one in the $(M+1)^{th}$ row). Therefore, the values of $\varepsilon_0, \varepsilon_1$ and Υ when $\bar{\gamma}_p \to \infty$ are equal to 2,2 and $2R(\tau)$ respectively. This results in changes to Υ and it becomes

$$\Upsilon = \left(2 + \frac{2}{\bar{\gamma}_s} - R^2(\tau)\right)^{-1/2}$$

When we substitute the Υ into the equation (7.18), we can obtain the closed-form expression of the bit error probability with the Wiener filter as the channel estimator. In the limit when $R(\tau) = 0$ (very fast fading) or $R(\tau) = 1$ (static channel,very slow fading) with perfect CSI the bit error probability can be written in compact forms as

$$R(\tau) = 0 \;\rightarrow\; P_b = \frac{1}{4}\left(2 + \sqrt{\frac{\bar{\gamma}_s}{2\bar{\gamma}_s + 2}}\right)\left(1 - \sqrt{\frac{\bar{\gamma}_s}{2\bar{\gamma}_s + 2}}\right) \tag{7.19}$$
$$R(\tau) = 1 \;\rightarrow\; P_b = \frac{1}{4}\left(2 + \sqrt{\frac{\bar{\gamma}_s}{\bar{\gamma}_s + 2}}\right)\left(1 - \sqrt{\frac{\bar{\gamma}_s}{\bar{\gamma}_s + 2}}\right) \tag{7.20}$$

and the substitutions steps that was taken to drive this probability of error can be found in the appendix A. Although the bit probability of s_1 and s_2 are equal, they are not independent. The approach suggested here does not lead to the exact sequence error probability of $[s_1\ s_2]$. Nevertheless, the upper bound of the error probability of the code sequence $[s_1\ \ s_2]$,P_2 can be found by the union bound of the bit error probability of s_1 and s_2, i.e.,

$$P_2 \leq 2\ P_b \tag{7.21}$$

7.4 ML Decoder

The Maximum Likelihood (ML) decoder is the optimal decoder. Unlike the LC-STD, the ML-STD does not assume that the channels are quasi-static. It chooses the code-word, which is the most likely to be transmitted given the received signals. Without loss of generality, we assume that the transmitted sequence is $[s_1\ s_2] = [1\ 1]$ and let $P_{[\hat{s}_1\ \hat{s}_2]}$ be the probability that the ML space-time decoder picks $[\hat{s}_1\ \hat{s}_2]$ given the transmitted sequence is [1 1]. The union bound of the sequence error, which is the summation of all possible error patterns, can be written as,

$$P_2 \leq P_{[1\ -1]} + P_{[-1\ 1]} + P_{[-1\ -1]} \tag{7.22}$$

For clear presentation we can define $\tilde{P}_1 = P_{[1\ -1]}$,$\tilde{P}_2 = P_{[-1\ 1]}$ and $\tilde{P}_3 = P_{[-1\ -1]}$, the probabilities $\tilde{P}_i$ for $i = 1, \ldots, 3$ can be simplified to

$$P_i = Pr\{\Re\{z^i < 0\}\} \tag{7.23}$$

where z^i for $i = 1, \ldots, 3$ can be defined as

$$\begin{aligned}
z^1 &= -\sqrt{\frac{E_s}{2}}\left(r_{s,1}\hat{\beta}_1^* - r_{s,2}\hat{\alpha}_2^*\right) + \frac{E_s}{2}\left(\hat{\alpha}_1\hat{\beta}_1^* - \hat{\alpha}_2\hat{\beta}_2^*\right) && (7.24)\\
z^2 &= \sqrt{\frac{E_s}{2}}\left(r_{s,1}\hat{\alpha}_1^* + r_{s,2}\hat{\beta}_2^*\right) + \frac{E_s}{2}\left(\hat{\alpha}_1\hat{\beta}_1^* - \hat{\alpha}_2\hat{\beta}_2^*\right) && (7.25)\\
z^3 &= \sqrt{\frac{E_s}{2}}\left(r_{s,1}(\hat{\alpha}_1 - \hat{\beta}_1)^*\right) + \sqrt{\frac{E_s}{2}}\left(r_{s,2}(\hat{\alpha}_2 + \hat{\beta}_2)^*\right) && (7.26)
\end{aligned}$$

Using the same approach used in previous section, we let

$$\mathbf{x}_{ML} = \begin{bmatrix} r_{s,1} & r_{s,2} & \sqrt{\frac{E_s}{2}}\hat{\alpha}_1 & \sqrt{\frac{E_s}{2}}\hat{\alpha}_2 & \sqrt{\frac{E_s}{2}}\hat{\beta}_1 & \sqrt{\frac{E_s}{2}}\hat{\beta}_2 \end{bmatrix}^T \tag{7.27}$$

The matrix $\mathrm{Re}\{z^i\}$, means real part of the z, corresponding to each error pattern can then be written in the quadratic form $\mathrm{Re}\{\mathbf{x}_{ML}^H \mathbf{Q}_i \mathbf{x}_{ML}\}$, where $i = 1, \ldots, 3$ and matrix Q for different corresponding i can be define as

$$Q_1 = \frac{1}{2}\begin{bmatrix} 0 & 0 & 0 & 0 & -1 & 0 \\ 0 & 0 & 0 & 1 & 0 & 0 \\ 0 & 0 & 0 & 0 & 1 & 0 \\ 0 & 1 & 0 & 0 & 0 & -1 \\ -1 & 0 & 1 & 0 & 0 & 0 \\ 0 & 0 & 0 & -1 & 0 & 0 \end{bmatrix}$$

$$Q_2 = \frac{1}{2}\begin{bmatrix} 0 & 0 & 1 & 0 & 0 & 0 \\ 0 & 0 & 0 & 0 & 0 & 1 \\ 1 & 0 & 0 & 0 & 1 & 0 \\ 0 & 0 & 0 & 0 & 0 & -1 \\ 0 & 0 & 1 & 0 & 0 & 0 \\ 0 & 1 & 0 & -1 & 0 & 0 \end{bmatrix}$$

$$Q_3 = \frac{1}{2}\begin{bmatrix} 0 & 0 & 1 & 0 & -1 & 0 \\ 0 & 0 & 0 & 1 & 0 & 1 \\ 1 & 0 & 0 & 0 & 0 & 0 \\ 0 & 1 & 0 & 0 & 0 & 0 \\ -1 & 0 & 0 & 0 & 0 & 0 \\ 0 & 1 & 0 & 0 & 0 & 0 \end{bmatrix}$$

We can again use the same approach as the linear combination scheme and derive the covariance matrix for the ML decoder as well. The covariance matrix of $\mathbf{x}$ can be found to be

$$\sum = \begin{bmatrix} \mathbf{A}_{ML} & \mathbf{C}_{ML} & \mathbf{D}_{ML} \\ \mathbf{C}_{ML}^H & \mathbf{B}_{ML} & \mathbf{0}_2 \\ \mathbf{D}_{ML}^H & \mathbf{0}_2 & \mathbf{B}_{ML} \end{bmatrix} \tag{7.28}$$

where

$$\begin{aligned}
A_{ML} &= E_s\sigma_c^2(1+\bar{\gamma}_s^{-1})\mathbf{I}_2 \\
B_{ML} &= \frac{E_s\sigma_c^2}{2}\begin{bmatrix} \mathbf{h}^H\left(\frac{\mathbf{D}_0}{2}+\bar{\gamma}_p^{-1}\delta_0\right)\mathbf{h} & \mathbf{h}^H\left(\frac{\mathbf{D}_{-1}}{2}+\bar{\gamma}_p^{-1}\delta_{-1}\right)\mathbf{h} \\ \mathbf{h}^H\left(\frac{\mathbf{D}_1}{2}+\bar{\gamma}_p^{-1}\delta_1\right)\mathbf{h} & \mathbf{h}^H\left(\frac{\mathbf{D}_0}{2}+\bar{\gamma}_p^{-1}\delta_0\right)\mathbf{h} \end{bmatrix} \\
C_{ML} &= \frac{E_s\sigma_c^2}{2\sqrt{2}}\begin{bmatrix} \mathbf{w}_0^H\mathbf{h} & \mathbf{w}_1^H\mathbf{h} \\ \mathbf{w}_{-1}^H\mathbf{h} & \mathbf{w}_0^H\mathbf{h} \end{bmatrix} \\
D_{ML} &= \frac{E_s\sigma_c^2}{2\sqrt{2}}\begin{bmatrix} -\mathbf{w}_0^H\mathbf{h} & -\mathbf{w}_1^H\mathbf{h} \\ \mathbf{w}_{-1}^H\mathbf{h} & \mathbf{w}_0^H\mathbf{h} \end{bmatrix}
\end{aligned}$$

where δ_e is a square matrix of size $2M+1$ with ones on the e^{th} diagonal, $\mathbf{w}_e$ and D_e are the same as defined before.

7.5 Simulation and Evaluation

In this section, the numerical examples are presented to illustrate the effect of the Doppler spread and the channel estimation error on the performance of the conventional Alamouti space-time code. The system estimation performance is tested for SISO case where SISO channel was designed in M2M case. The design of this channel is presented in the chapter where we discuss more about Mobile to Mobile communication. Throughout this section, unless stated otherwise, we assume that the fading autocorrelation function is the zeroth-order Bessel function of the first kind $J_0(2\pi f_d\tau)$, which is derived from Jakes' PSD, where f_d denotes the normalized

Doppler frequency. We have given the transmitter and receiver scheme of this alamouti estimation in the figure (7.2) for the readers to have better understanding of what we did in our simulations.

As we have mentioned above, we have two transmitters and one receiver in Alamouti scheme. Figure (7.2) shows how pilots are inserted for individual data scheme for given transmitter. Transmitter 1 corresponding to the channel coefficient α_i where $i = 1, \ldots, N$ (N is the total length) and transmitter 2 corresponds to β_i. At first time interval, we transmit both pilot1 (P_1) and pilot2 (P_2) from each transmitter using the equation (4.2) and (4.3). For the second time interval, we transmit one bit form each antenna, Alamouti scheme uses 2 pair of data to transmit over the antennas,using equation 4.1. On the receiver side, we will have 2 different pilots followed by 8 different received bits. They will be place as shown in the figure and we will follow this procedure till the whole sequences are transmitted. As the second step, we will

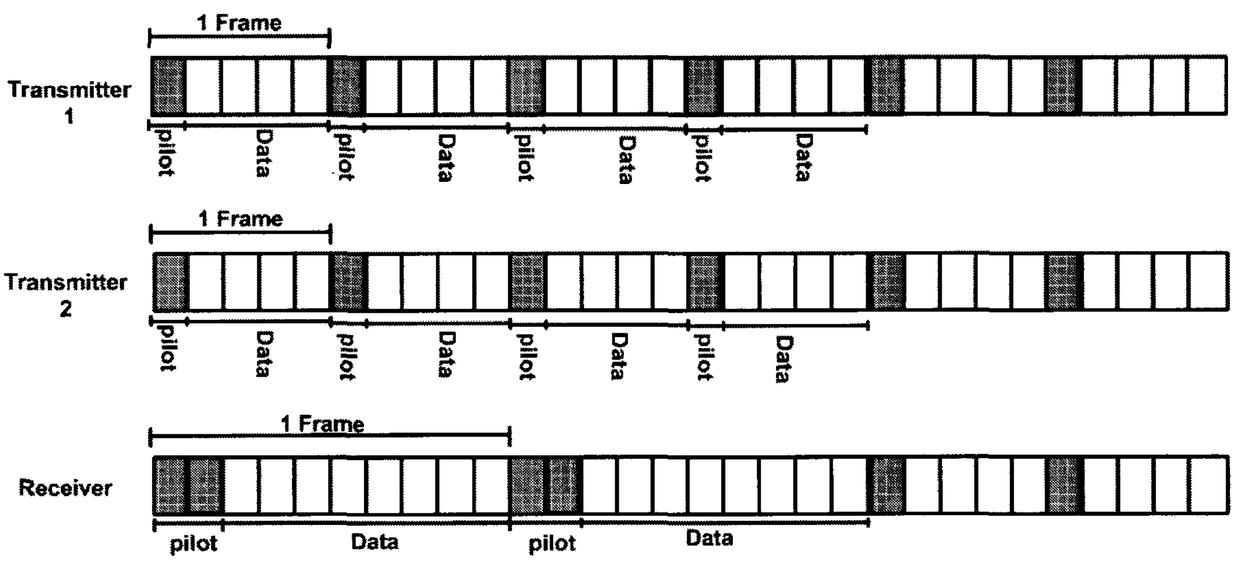

Figure 7.2: Transmission and 4eceiver structure.

show how the channel estimation is done using Wiener filtering.The figure 7.3 shows how we did the filtering for individual resolvable paths, mentioned in the paper. We used 11-tap Wiener filter (following [120]), given in equation 7.14, using 5 tap as the reference size, we can achieve this design. In this part, we will explain how we can

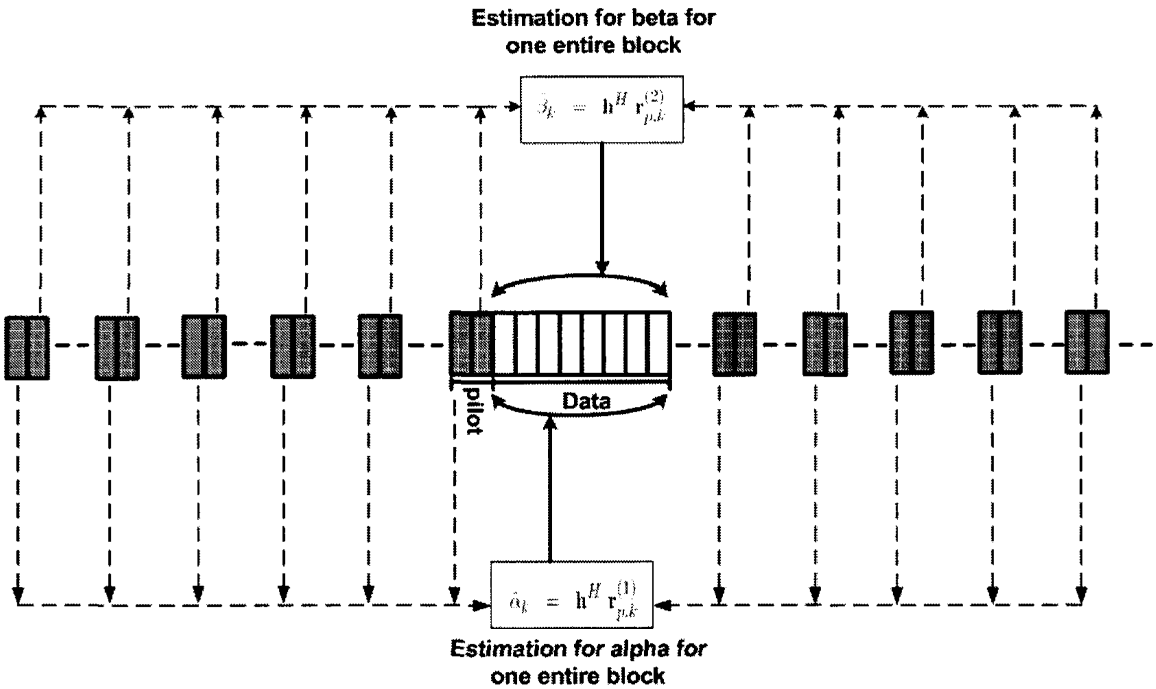

Figure 7.3: Channel estimation diagram using the filter coefficients.

estimate one path,$\hat{\alpha}_i$. By using the equation 7.4, we can calculate each α and β for individual blocks. We should note that, we have done simulation for the block fading case, were the channel only update for block by block.It is not only easy to simulate but also it has never been done using these schemes.

For our simulations, we have used $f_d\tau = 0.03, 0.05, 0.0005$, to see the effect of different normalized Doppler effects on the channel, and also the noise of the channel from 0 dB to 30 dB. We have used a wide range of noise level to understand the performance of the simulation results. We also generated the individual variance for two pilots and a channel. We used two different values for the SNR for data (10dB and 30dB) to see the difference in the error performance with different SNR values. The results for different $f_d\tau$ with different channel SNR are given bellow.

Figure 7.4 show comparisons of the autocorrelation of channel1 vs. theoretical and channel2 vs theoretical. As we can see in the figure, our simulations results for both channel 1 and channel 2 matches very closely to the theoretical results. Figure 7.5 shows as the cross correlation between channel 1 and channel 2 against theoretical value. Since we have generated the channel without correlation, spacing

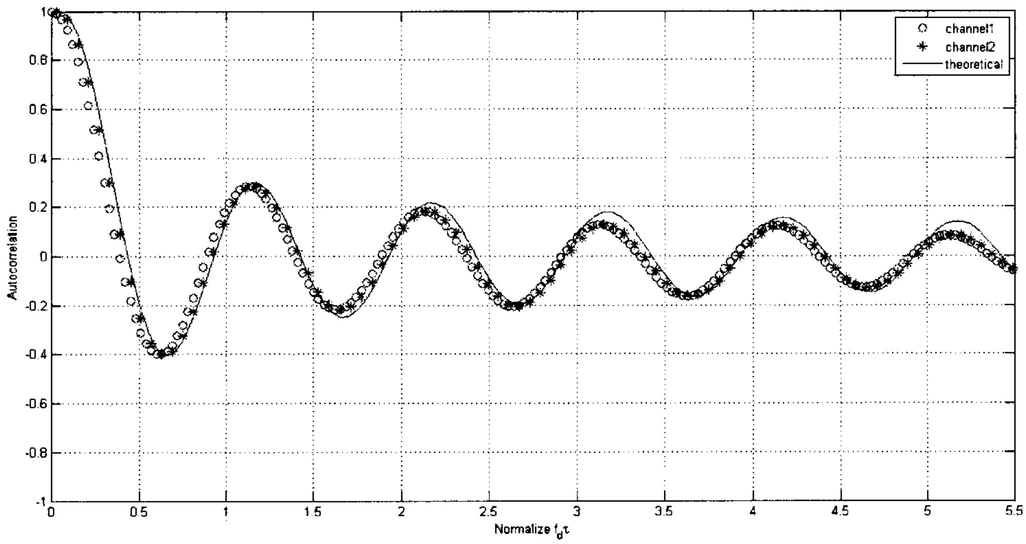

Figure 7.4: Simulation results of each channel auto-correlation vs. theoretical results.

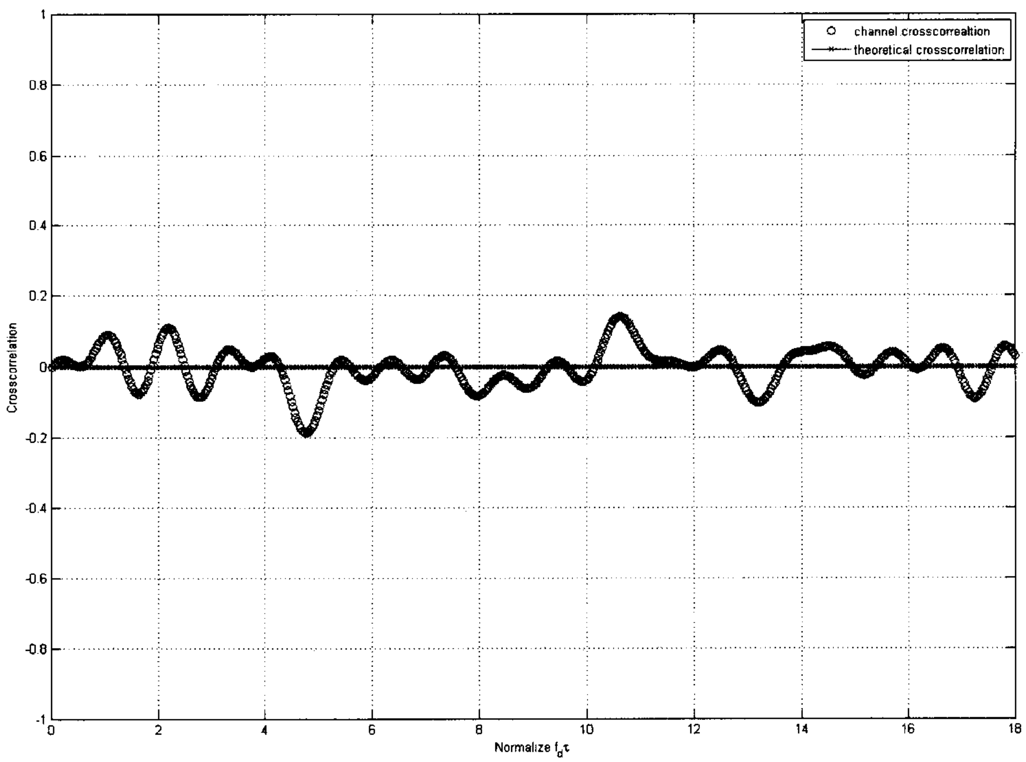

Figure 7.5: Simulation results of cross-correlation of channel1 and channel 2 vs. theoretical results.

between antennas are far enough to have any effects, the cross correlation should be close to zero and we can see that it it true in our simulation results.

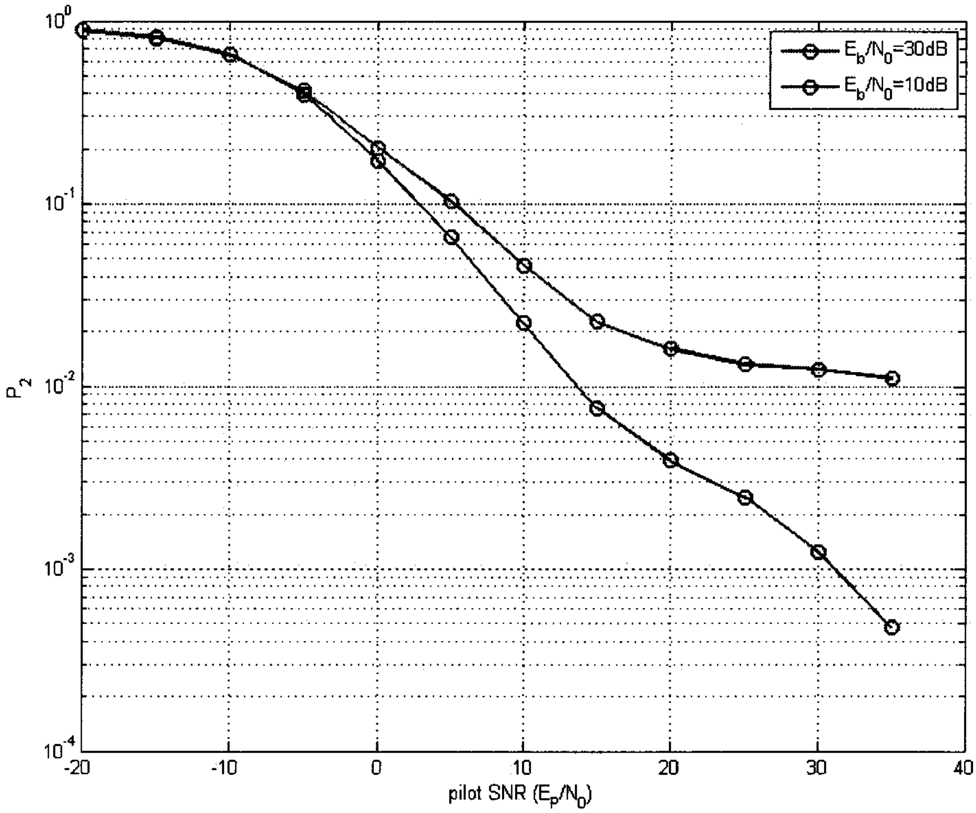

Figure 7.6: Performance of the Alamouti space-time code with the LC-STD with 11-tap Wiener Filter and The channel with normalized Doppler frequency of 0.05 with different channel SNR where the blue line represents the data SNR of 10dB and the red line represents the data SNR of 30dB.

Let us compare the results from figure 7.6 7.6 and 7.8. First we will discuss the performance of the channel estimation at data SNR of 10dB.We can see that when the normalized Doppler frequency is high, at 0.03 and 0.05 the probability of error is round 10^{-2} but when the normalized Doppler frequency decreases to 0.0005, where we can make the estimations due to the slow changes in the channel, we can see the probability of error is about 10^{-3}. Now let us compare the situation where the data SNR is 30dB. At the Doppler frequency 0.05, fast changing channel, we have about 10^{-2} of probability of error but once the normalized doppler frequency decreases we can see that the results started to improve up to 10^{-5}. These results

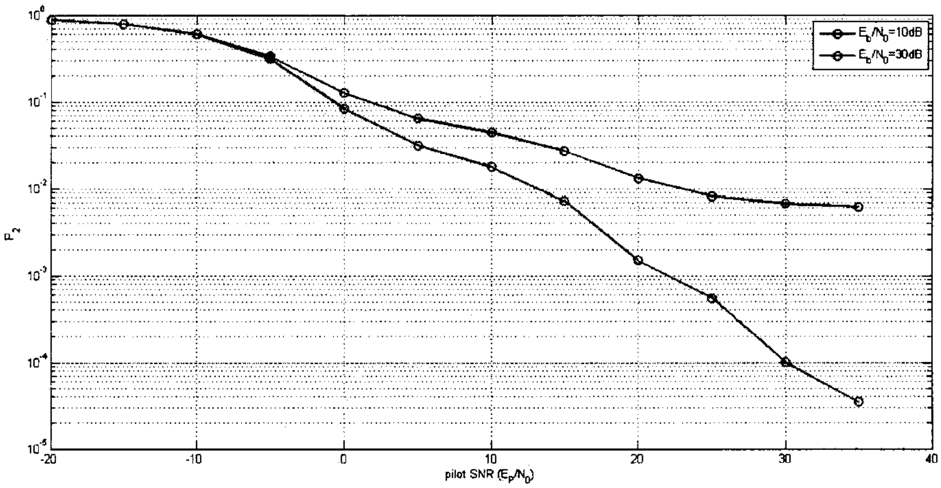

Figure 7.7: Performance of the Alamouti space-time code with the LC-STD with 11-tap Wiener Filter and The channel with normalized Doppler frequency of 0.03 with different channel SNR where the red line represents the data SNR of 10dB and the blue line represents the data SNR of 30dB.

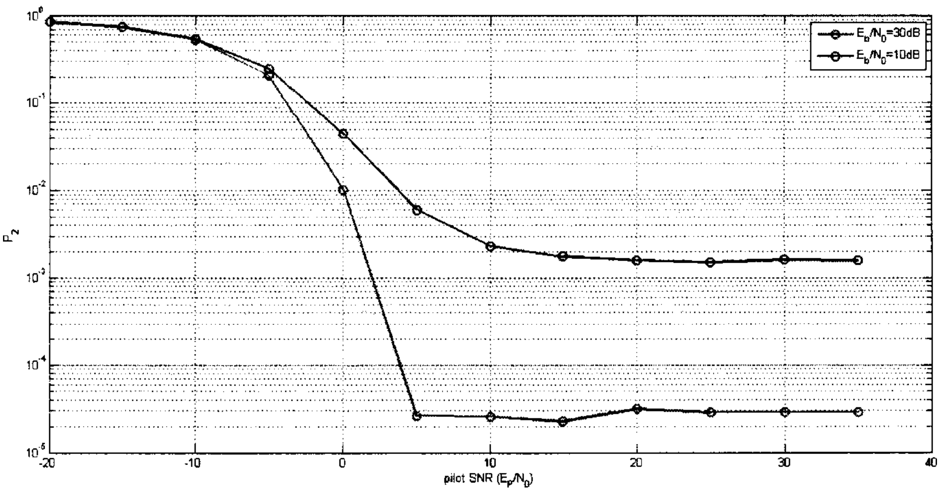

Figure 7.8: Performance of the Alamouti space-time code with the LC-STD with 11-tap Wiener Filter and The channel with normalized Doppler frequency of 0.0005 with different channel SNR where the blue line represents the data SNR of 10dB and the red line represents the data SNR of 30dB.

show us that, when the channel is slow changing, we can perform better estimation i.e, low probability of error. When the data SNR is high, we can receiver bits better and do better estimations with lower error rates.

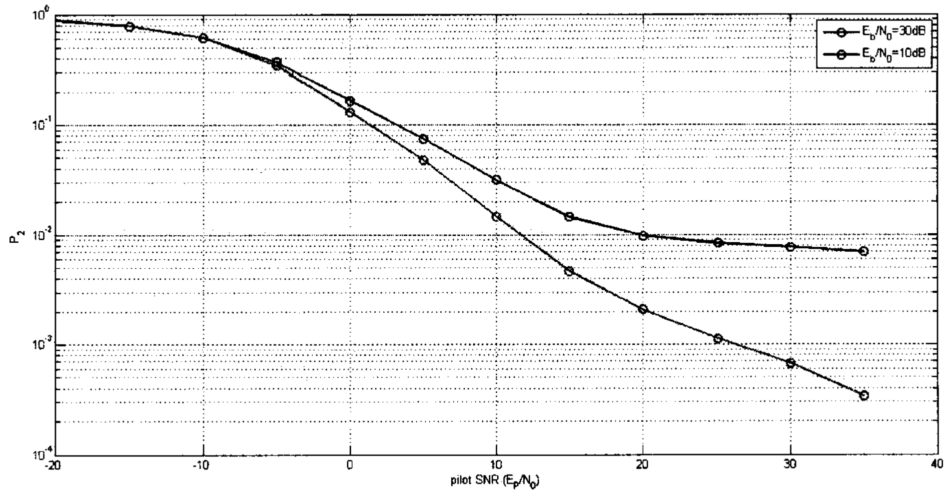

Figure 7.9: Performance of the Alamouti Space-time code with the ML-STD with 11-tap Wiener Filter and the channel with Doppler frequency of 0.05 with different channel SNR where the blue line represents the data SNR of 10dB and the red line red line represents the data SNR of 30dB

In the case of ML-STD case, we can clearly see that, when the doppler frequency decreases from 0.05 to 0.03 or 0.0005 at data SNR of 10dB, we can see the improvement in the probability of error. This mean that we can do channel estimation with less error when the channel changes slowly. This case apply to the data SNR of 30dB as well. We can see the results in figure (7.10, 7.9 and 7.8).

As the second step, we proceeded to do simulations using the UIU channel model that we have presented in one of the chapters in the thesis to see the effect of spatial correlation on performance of the Alamouti. We did exact same procedure as using the SISO model but instead of using SISO in this case, we used the different type of channel model. The results can be divided into two groups - Linear combination and ML detection. The results for linear combination schemes are as follows:

As we can see from the results, there is a big difference in the error performance once the doppler frequency decreased from 0.03 to 0.0005, which means that, we can do better channel estimations without causing a huge amount of errors. We will also

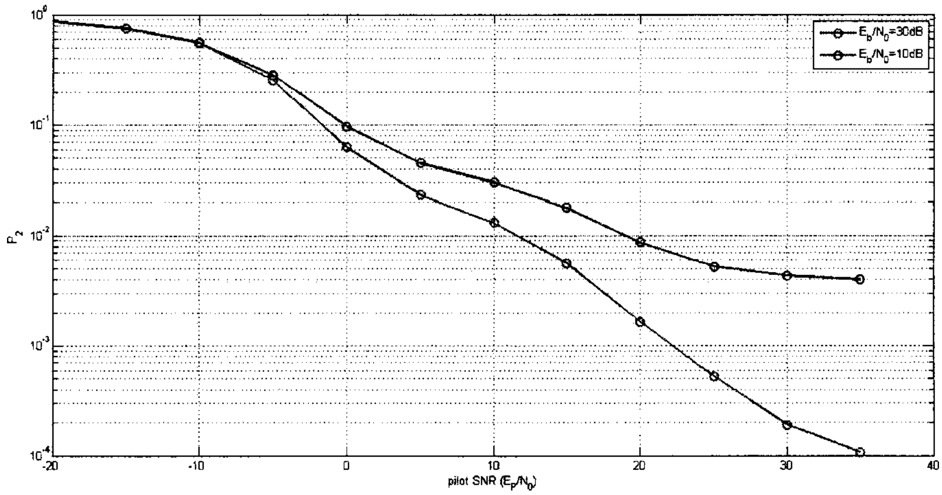

Figure 7.10: Performance of the Alamouti Space-time code with the ML-STD with 11-tap Wiener Filter and the channel with Doppler frequency of 0.03 with different channel SNR where the blue line represents the data SNR of 10dB and the red line red line represents the data SNR of 30dB

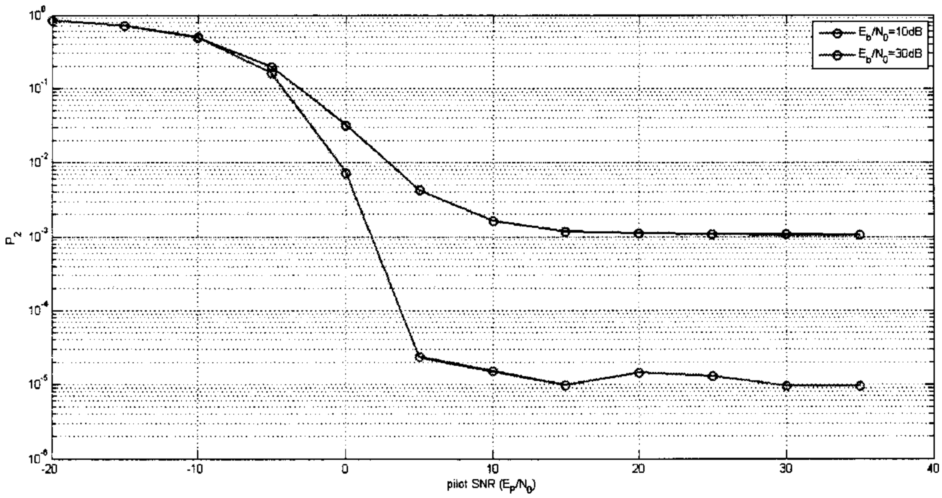

Figure 7.11: Performance of the Alamouti Space-time code with the ML-STD with 11-tap Wiener Filter and the channel with Doppler frequency of 0.0005 with different channel SNR where the blue line represents the data SNR of 10dB and the red line red line represents the data SNR of 30dB

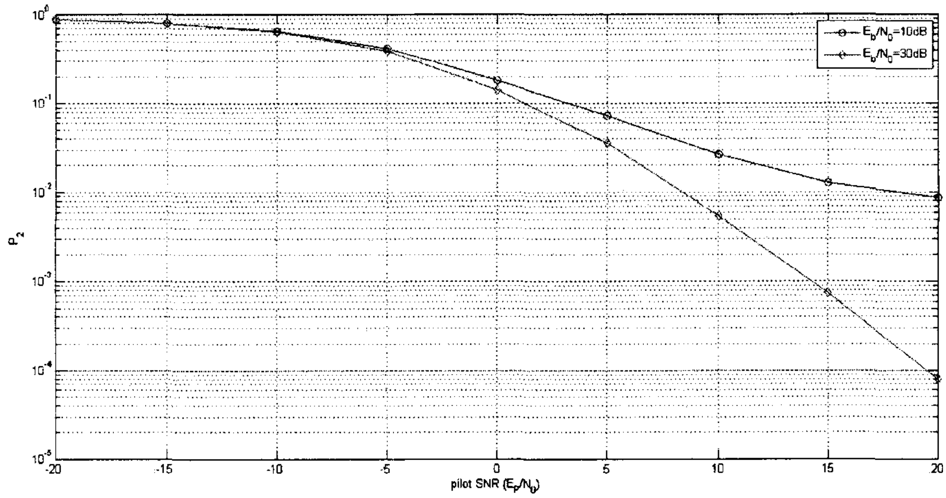

Figure 7.12: Performance of the Alamouti space-time code with the LC-STD with 11-tap Winer filter and the UIU channel with Doppler frequency of 0.05 with different channel SNR where the blue line represents the data SNR of 10dB and the red line represents the data SNR of 30dB

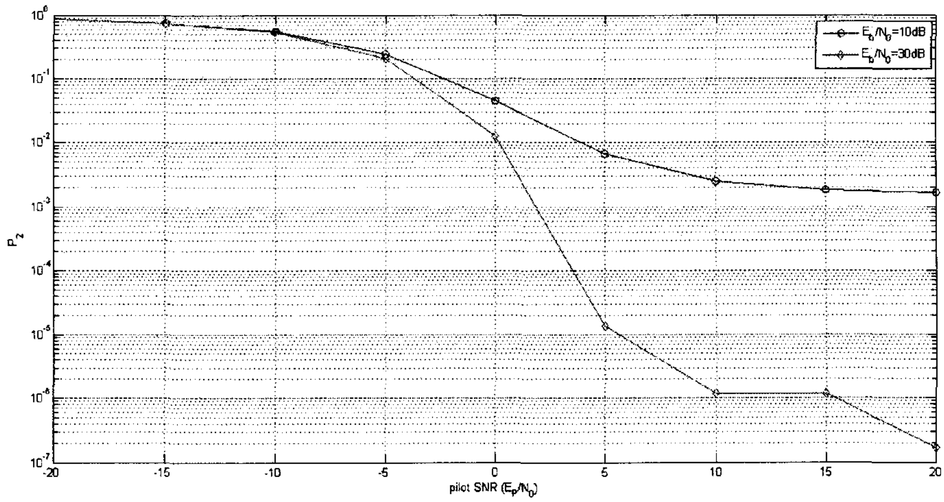

Figure 7.13: Performance of the Alamouti space-time code with the LC-STD with 11-tap Winer filter and the UIU channel with Doppler frequency of 0.0005 with different channel SNR where the blue line represents the data SNR of 10dB and the red line represents the data SNR of 30dB

check the ML detection using UIU model to make sure these results hold in that case as well.

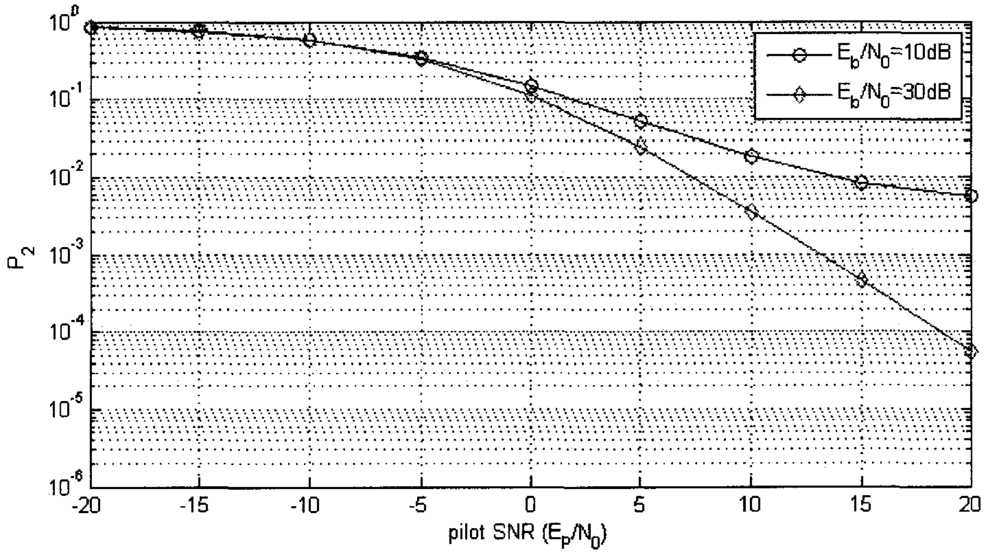

Figure 7.14: Performance of the Alamouti space-time code with the ML-STD with 11-tap Winer filter and the UIU channel with Doppler frequency of 0.05 with different channel SNR where the blue line represents the data SNR of 10dB and the red line represents the data SNR of 30dB.

We can clearly see in figure 7.14 and 7.15 that, there is better performance when the doppler frequency decreased from 0.05 to 0.0005 in other words, the channel is changing very slowly. The results matches with what we have predicted before the simulations. Now as the final step, we will do simulations using different antenna spacing in UIU model, which will show as the effect and the changes in each estimation.

7.6 Effects of Estimation Based in case of antenna correlation

In this section, we will use the same UIU channel Model design from the previous section using different sizes of antenna spacing, which will show as the correlation effect in our channel estimation. Due to the space limit in the thesis, we will only provide results for the Doppler frequency of 0.05 for LC-STD and ML-STD with data SNR of 10 and 30dB.

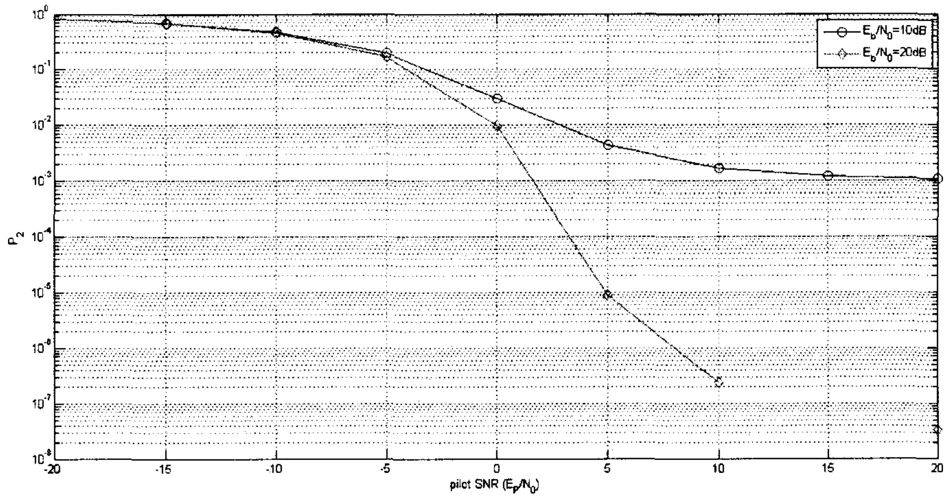

Figure 7.15: Performance of the Alamouti space-time code with the ML-STD with 11-tap Winer filter and the UIU channel with Doppler frequency of 0.0005 with different channel SNR where the blue line represents the data SNR of 10dB and the red line represents the data SNR of 30dB.

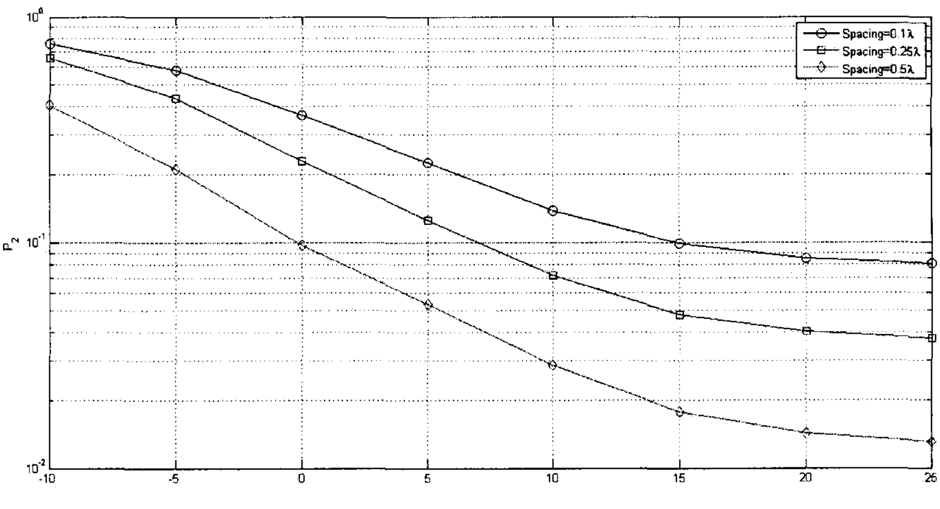

Figure 7.16: Performance of the Alamouti space-time code with the LC-STD with 11-tap Winer filter and the UIU channel with Doppler frequency of 0.05 with channel SNR of 10dB.

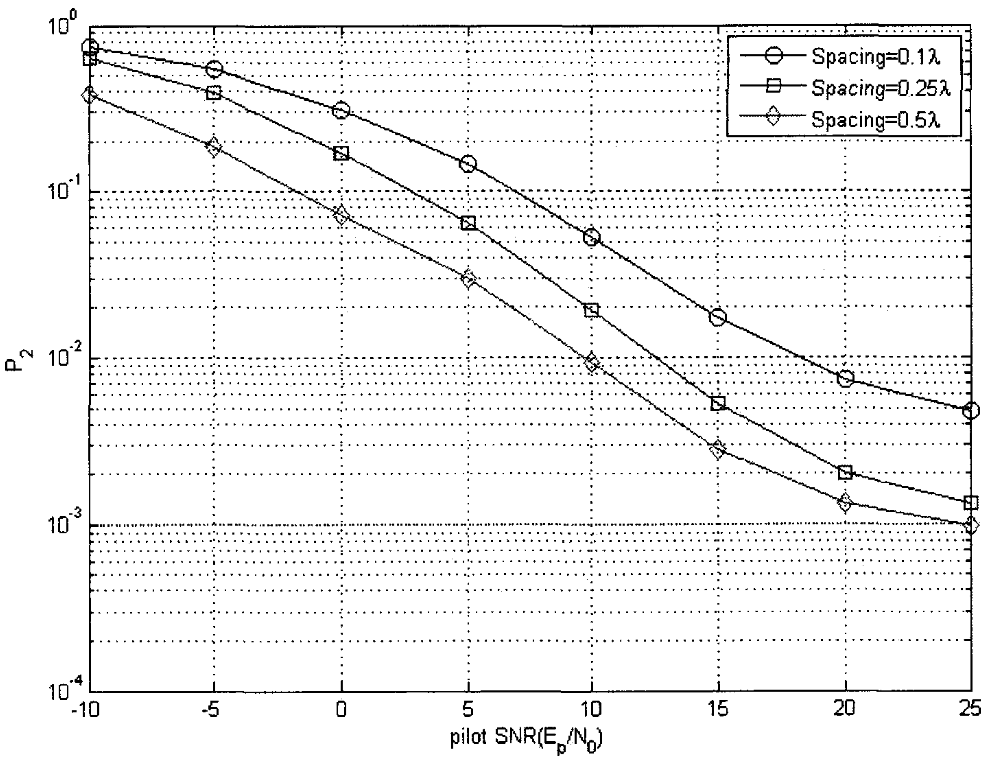

Figure 7.17: Performance of the Alamouti space-time code with the LC-STD with 11-tap Winer filter and the UIU channel with Doppler frequency of 0.05 with channel SNR of 30dB.

We can clearly see from Figure 7.17 that, when the antenna spacing is 0.1λ apart the probability of error is 10^{-1} but when its increase to 0.5λ, in other words there is no correlations in the antennas, the probability of error goes up to 10^{-2}. We can clearly see that, there is an effect in the probability of error in the channel estimation due to the antenna spacing. We can again see that effect in the Figure 7.16 where the data SNR increases to 30dB. For the completeness, we will show the results form ML-STD for the same scenario. The results from Figure 7.19 and 7.18 shows that, our simulations results matches with what we have predicted.

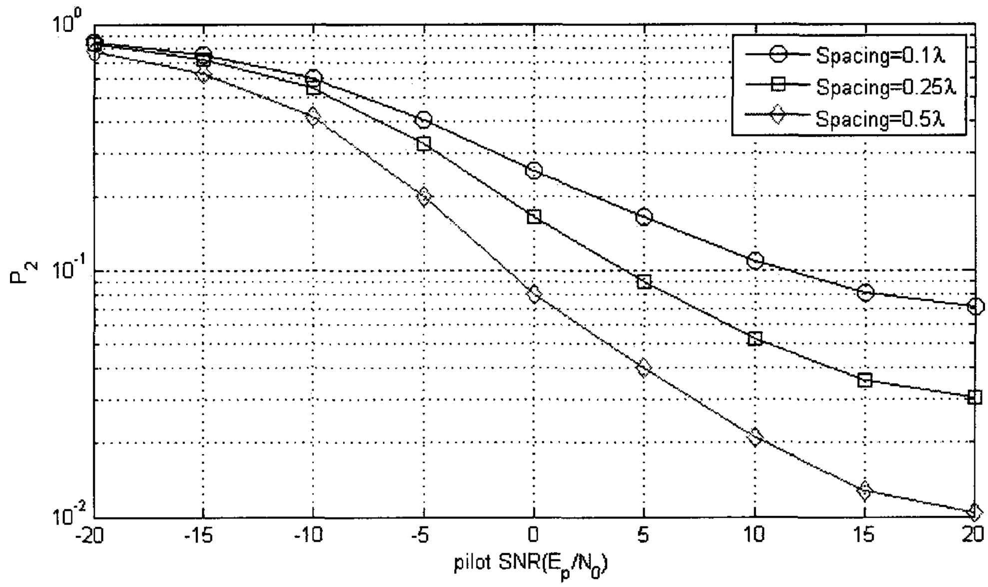

Figure 7.18: Performance of the Alamouti space-time code with the ML-STD with 11-tap Winer filter and the UIU channel with Doppler frequency of 0.05 with channel SNR of 10dB.

7.7 Conclusion

This chapter explained us how the error performance can be done on the estimation of the channel. In our case, we have show the estimation using Linear combination scheme and ML decoding scheme. We can clearly see that from our result figures, when the bit data is low in SNR we have more errors then when the bit SNR is high. This means that the channel can estimate better when we have high bit SNRs. We can

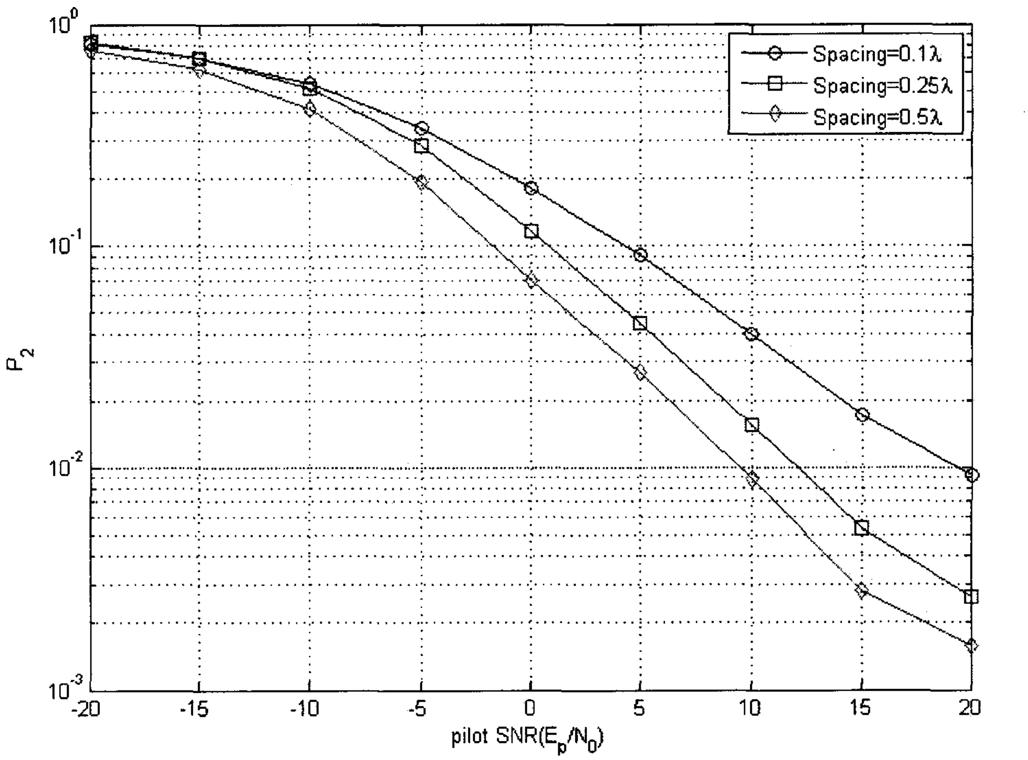

Figure 7.19: Performance of the Alamouti space-time code with the ML-STD with 11-tap Winer filter and the UIU channel with Doppler frequency of 0.05 with channel SNR of 30dB.

also see that the error performance is much better in ML decoding due to its design. As the next step in this chapter, we have shown the effects of these performance based on the spacing of the antennas. When the antennas are 0.1λ the performance is the lowest compare where the antennas are 0.25λ or 0.5λ.

Chapter 8 Performance of OSTBC in M2M & AR Channel

8.1 Performance

In this section, we will perform two test using the channel design that we just explained in prior sections of this chapter. Our test will be based on Space-Time coding and pairwise probability of errors.

8.1.1 Introduction

Analysis by Foschini (1996) and by Telatar (1999) shows that multiple antennas at the transmitter and receiver enable very high rate wireless communication. Space-time codes, introduced by Tarokh et al (1998), improve the reliability of communication over fading channels by correlating signals across different transmit antennas. We will discuss the performance analysis and design criteria for space time codes. In this chapter, we present space-time block codes and evaluate their performance on MIMO fading channels, specially in this chapter we will use the MIMO channel that is design for Mobile-to-Mobile communication. We first introduce the Alamouti code, which is a simple two branch transmit diversity scheme. The main goal about this scheme is that it achieves a full diversity gain with a simple maximum-likelihood decoding algorithm. We will also show the design of the space time block codes with large number of transmit antennas based on the orthogonal designs. The decoding algorithms for both space time block codes with both real and complex signal constellations are discussed.

The space time code (STC) is a method to improve the reliability of the data

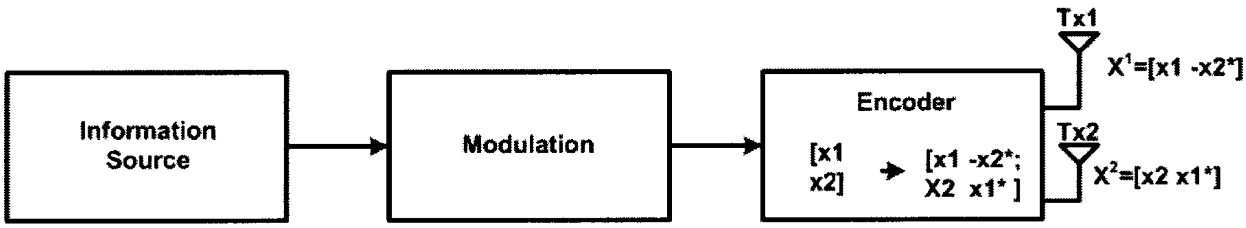

Figure 8.1: A black diagram of the Alamouti space-time encoder

transmission in wireless using multiple transmit antennas. STC basically allow us to send several copies, redundant copies of a data stream to the receiver in the hope that at least one of them may survive the obstacles between the transmitter and receiver in good condition so that they can decode it. There are two main types of STC:

1. Space time block codes (STBC)

2. Space time trellis codes (STTC)

STBC act on a block of data at once and provide a diversity gain, but they are less complex in implementation. STTC distribute a trellis code over multiple antennas and multiple time slots and provide both coding and diversity gain. We will look at STBC in more details in future sections and show our simulation results.

8.1.2 Alamouti Space-Time Code

The Alamouti scheme is historically the first space-time block code to provide full transmit diversity for systems with two transmit antennas. It is worthwhile to mentioned that delay diversity scheme can also achieve a full diversity, but they introduce interference between symbols and complex detectors required at the receiver. In this section, we present Alamouti's encoding and decoding algorithms and its performance.

8.1.2.1 Alamouti Space-Time Encoding

Figure 8.1 shows the block diagram of the Alamouti space-time encoder. Now let us assume that the M-ary modulation scheme is used, where $m = \log_2 M$. Then the encoder takes a block of two modulated symbols x_1 and x_2 in each encoding operation and maps them to the transmit antennas according to a code matrix given by

$$\mathbf{X} = \begin{bmatrix} x_1 & -x_2^* \\ x_2 & x_1^* \end{bmatrix}$$

The encoder outputs are transmitted in two consecutive transmission periods from two transmit antennas. During the first transmission period, two signals x_1 and x_2 are transmitted simultaneously from antenna one and antenna two, respectively. In the second transmission period, signal $-x_2^*$ is transmitted from transmit antenna one and signal x_1^* from antenna two, where x_1^* is the complex conjugate of x_1.We can see that the encoding is done both in space and time domains. Let us denote the transmit sequence from antennas one and two by $\mathbf{x}^1$ and $\mathbf{x}^2$, respectively.

$$\begin{aligned} \mathbf{x}^1 &= [x_1, -x_2^*] \\ \mathbf{x}^2 &= [x_2, x_1^*] \end{aligned}$$

The main feature of the Alamouti scheme is that the transmit sequences from the two transmit antennas are orthogonal, since the inner produce of the sequences $\mathbf{x}^1$ and $\mathbf{x}^2$ is zero,i.e.,

$$\mathbf{x}^1 \cdot \mathbf{x}^2 = x_1 x_2^* - x_2^* x_1 = 0$$

The code matrix has the following property

$$\begin{aligned} \mathbf{X} \cdot \mathbf{X}^H &= \begin{bmatrix} |x_1|^2 + |x_2|^2 & 0 \\ 0 & |x_1|^2 + |x_2|^2 \end{bmatrix} \\ &= (|x_1|^2 + |x_2|^2)\mathbf{I}_2 \end{aligned}$$

where $\mathbf{I}_2$ is 2 x 2 identity matrix. Now let us assume that one receive antenna is used at the receiver. The block diagram of the receiver for the Alamouti scheme is shown in Figure 8.2. The fading channel coefficients from the first and the second transmit antennas to the receive antenna at time t are denoted by $h_1(t)$ and $h_2(t)$,respectively. Assuming that the fading coefficients are constant across two consecutive symbol transmission periods, they can be expressed as follows

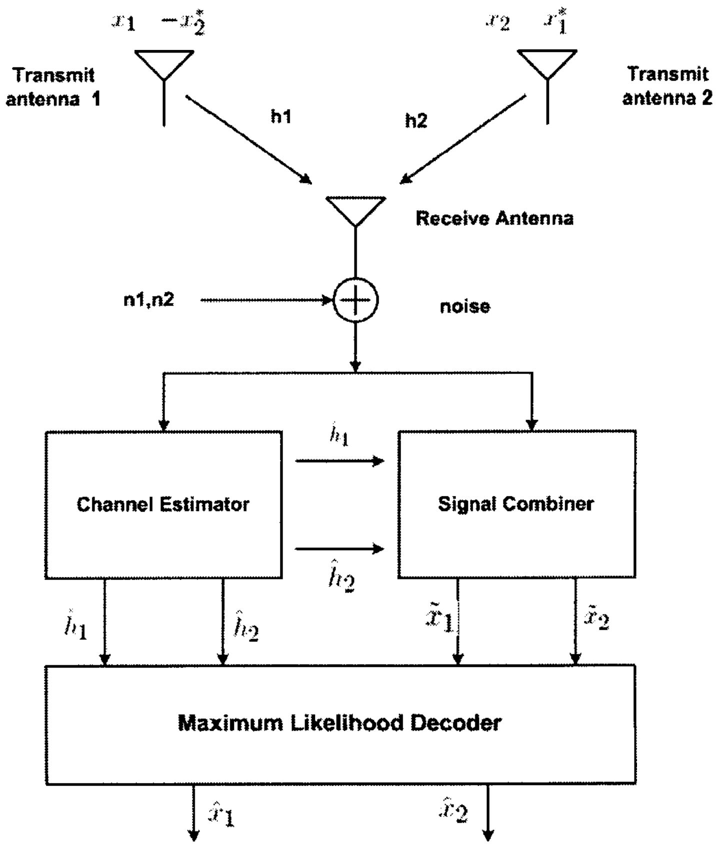

Figure 8.2: Receiver for the Alamouti Scheme

$$
\begin{aligned}
h_1(t) &= h_1(t+T) = h_1 = |h_1|e^{j\theta_1} \\
h_2(t) &= h_2(t+T) = h_2 = |h_2|e^{j\theta_2}
\end{aligned}
$$

where $|h_i|$ and θ_i,$i = 0, 1$ are the amplitude gain and phase shift for the path from transmit antenna i to the receive antenna, and T is the symbol duration. At the receive antenna, the received signals over two consecutive symbol periods, denoted by r_1 and r_2 for time t and $t + T$, respectively, can be expressed as

$$r_1 = h_1 x_1 + h_2 x_2 + n_1 \tag{8.1}$$

$$r_2 = -h_1 x_2^* + h_2 x_1^* + n_2 \tag{8.2}$$

where n_1 and n_2 are independent complex variables with zero mean and power spectral density $N_0/2$ per dimension, representing additive white Gaussian noise samples at time t and $t+T$, respectively.

8.1.2.2 Combining and Maximum Likelihood Decoding

If we can recover the channel fading coefficients, h_1 and h_2 perfectly, the decoder will use them as the channel states information. Assuming that all the signals in the modulation constellation are equiprobable, a maximum likelihood decoder chooses a pair of signals $(\hat{x}_1, \hat{x}_2)$ from the signal modulation constellation to minimize the distance metric

$$d^2(r_1, h_1\hat{x}_1 + h_2\hat{x}_2) + d^2(r_2, -h_1\hat{x}_2^* + h_2\hat{x}_1^*) = |r_1 - h_1\hat{x}_1 - h_2\hat{x}_2|^2 + |r_2 + h_1\hat{x}_2^* - h_2 x_1^*|$$

over all possible values of $\hat{x}_1$ and $\hat{x}_2$. IF we substitute r_1 and r_2 into the above equation, we can rewrite the maximum likelihood decoding as

$$(\hat{x}_1, \hat{x}_2) = \arg\ \min_{(\hat{x}_1, \hat{x}_2) \in\ C}(|h_1|^2 + |h_2|^2 - 1)(|\hat{x}_1|^2 + |\hat{x}_2|^2) + d^2(\tilde{x}_1, \hat{x}_1) + d^2(\tilde{x}_2, \hat{x}_2)$$

where C is the set of all possible modulated symbol pairs $(\hat{x}_1, \hat{x}_2)$, $\tilde{x}_1$ and $\tilde{x}_2$ are two decision statistics constructed by combining the received signals with channel state information. The decision statistics are given by

$$\tilde{x}_1 = h_1^* r_1 + h_2 r_2^*$$

$$\tilde{x}_2 = h_2^* r_1 - h_1 r_2^*$$

Again, we can substitute all the values of r_1 and r_2 into the above equation and we will get the decision statistics as

$$\begin{aligned}\tilde{x}_1 &= (|h_1|^2 + |h_2|^2)x_1 + h_1^* n_1 + h_2 n_2^* \\ \tilde{x}_2 &= (|h_1|^2 + |h_2|^2)x_2 - h_1 n_2^* + h_2^* n_1\end{aligned}$$

For a given channel h_1 and h_2, the decision statistics $\tilde{x}_i$,$i = 1, 2$, is only a function of x_i. Thus, the maximum likelihood decoding rule can be separated into two independent decoding rules for x_1 and x_2, given by

$$\hat{x}_1 = arg\ min_{\tilde{x}_1 \in\ S}(|h_1|^2 + |h_2|^2 - 1)|\hat{x}_1|^2 + d^2(\tilde{x}_1, \hat{x}_1) \tag{8.3}$$

and

$$\hat{x}_2 = arg\ min_{\tilde{x}_2 \in\ S}(|h_1|^2 + |h_2|^2 - 1)|\hat{x}_2|^2 + d^2(\tilde{x}_2, \hat{x}_2) \tag{8.4}$$

For M-PSK signal constellation,$(|h_1|^2 + |h_2|^2 - 1)|\hat{x}_i|^2$,$i = 1, 2$ are constant for all signal points, given the channel fading coefficients.Therefore, the decision rules in equation 8.3 and 8.4 can be simplified to

$$\begin{aligned}\hat{x}_1 &= arg\ min_{\hat{x}_1 \in\ S}\ d^2(\tilde{x}_1, \hat{x}_1) && (8.5) \\ x_2 &= arg\ min_{\hat{x}_2 \in\ S}\ d^2(\tilde{x}_2, \hat{x}_2) && (8.6)\end{aligned}$$

8.1.2.3 The Alamouti Scheme with Multiple Receive Antennas

The Alamouti scheme can be applied for a system with two transmit and n_R receive antennas. The encoding and transmission for this configuration is identical to the case of a single receive antenna. Let us denote by r_1^j and r_2^j the received signals at the j^{th} receive antenna at time t and $t + T$, respectively.

$$\begin{aligned}r_1^j &= h_{j,1}x_1 + h_{j,2}x_2 + n_1^j \\ r_2^j &= -h_{j,1}x_2^* + h_{j,,2}x_1^* + n_2^j\end{aligned}$$

where $h_{j,i}$, $i = 1, 2$, $j = 1, 2, \ldots, n_R$, is the fading coefficient for the path from transmit antenna i to receive antenna j, and n_1^j and n_2^j are the noise signals for receive antenna j at the time t and $t + T$, respectively.

The receiver constructs two decision statistics based on the linear combination of the received signals. The decision statistics, denotes by $\tilde{x}_1$ and $\tilde{x}_2$ are given by

$$\begin{aligned}
\tilde{x}_1 &= \sum_{j=1}^{n_R} h_{j,1}^* r_1^j + h_{j,2}(r_2^j)^* \\
&= \sum_{i=1}^{2}\sum_{j=1}^{n_R} |h_{j,i}|^2 \; x_1 + \sum_{j=1}^{n_R} h_{j,1}^* n_1^j + h_{j,2}(n_2^j)^* \\
\tilde{x}_2 &= \sum_{j=1}^{n_R} h_{j,2}^* r_1^j - h_{j,1}(r_2^j)^* \\
&= \sum_{i=1}^{2}\sum_{j=1}^{n_R} |h_{j,i}|^2 \; x_2 + \sum_{j=1}^{n_R} h_{j,1}^* n_1^j - h_{j,1}(n_2^j)^*
\end{aligned}$$

The maximum likelihood decoding rules for the two independent signals x_1 and x_2 are given by

$$\begin{aligned}
\hat{x}_1 &= arg\ min_{\hat{x}_1 \in\ S} \left[\left(\sum_{j=1}^{n_R} (|h_{j,1}|^2 + |h_{j,2}|^2 - 1) \right) |\hat{x}_1|^2 + d^2(\tilde{x}_1, \hat{x}_1) \right] \\
\hat{x}_2 &= arg\ min_{\hat{x}_2 \in\ S} \left[\left(\sum_{j=1}^{n_R} (|h_{j,1}|^2 + |h_{j,2}|^2 - 1) \right) |\hat{x}_2|^2 + d^2(\tilde{x}_2, \hat{x}_2) \right]
\end{aligned}$$

As for completeness and the better understanding for the readers, we will explain one section on Space-Time Block Coding,which will explain better in PPE error.

8.1.2.4 Orthogonal Space-Time Block Codes

Orthogonal STBC is an important subclass of linear STBC. The orthogonal space-time block codes (OSTBC) guarantees that the ML detection of different symbols is decoupled and at the same time achieves a diversity order equal to $n_r n_t$. The simplest form of OSTBC is the Alamouti code and it has been adopted in the third generation cellular standard W-CDMA.

The OSTBC is a linear space time block code that has the following unitary property:

$$\mathbf{X}\mathbf{X}^H = \sum_{n=1}^{n_s} |s_n|^2 \mathbf{I}$$

This is the main property why the OSTBC is very well known. To understand why the code matrices $\mathbf{X}$ in OSTBC are proportional to unitary matrices guarantee that the detection of s_n is decoupled. The following are one of the few examples that are given in the literature for 3 and 4 transmit antennas.

(1) OSTBC for $n_t = 3$: Following code is an Orthogonal STBC for $n_t = 3$, $N = 4$, $n_s = 4$

$$X = \begin{bmatrix} s_1 & 0 & s_2 & -s_3 \\ 0 & s_1 & s_3^* & s_2^* \\ -s_2^* & -s_3 & s_1^* & 0 \end{bmatrix}$$

This code has a rate of 3/4. An alternative OSTBC for $n_t = 3$

$$X = \begin{bmatrix} s_1 & -s_2^* & s_3^* & 0 \\ s_2 & s_1^* & 0 & -s_3^* \\ s_3 & 0 & -s_1^* & s_2^* \end{bmatrix}$$

(2)OSTBC for $n_t = 4$:Following code is an Orthogonal STBC for $n_t = 4$, $N = 4$, $n_s = 3$

$$X = \begin{bmatrix} s_1 & 0 & s_2 & -s_3 \\ 0 & s_1 & s_3^* & s_2^* \\ -s_2^* & -s_3 & s_1^* & 0 \\ s_3^* & -s_2 & 0 & s_1^* \end{bmatrix}$$

All these code have code rate of 3/4. We can also find OSTBC for $n_t = 8$ in the literature but we will not express it in here because our goal is to use 4 x 4 OSTBC

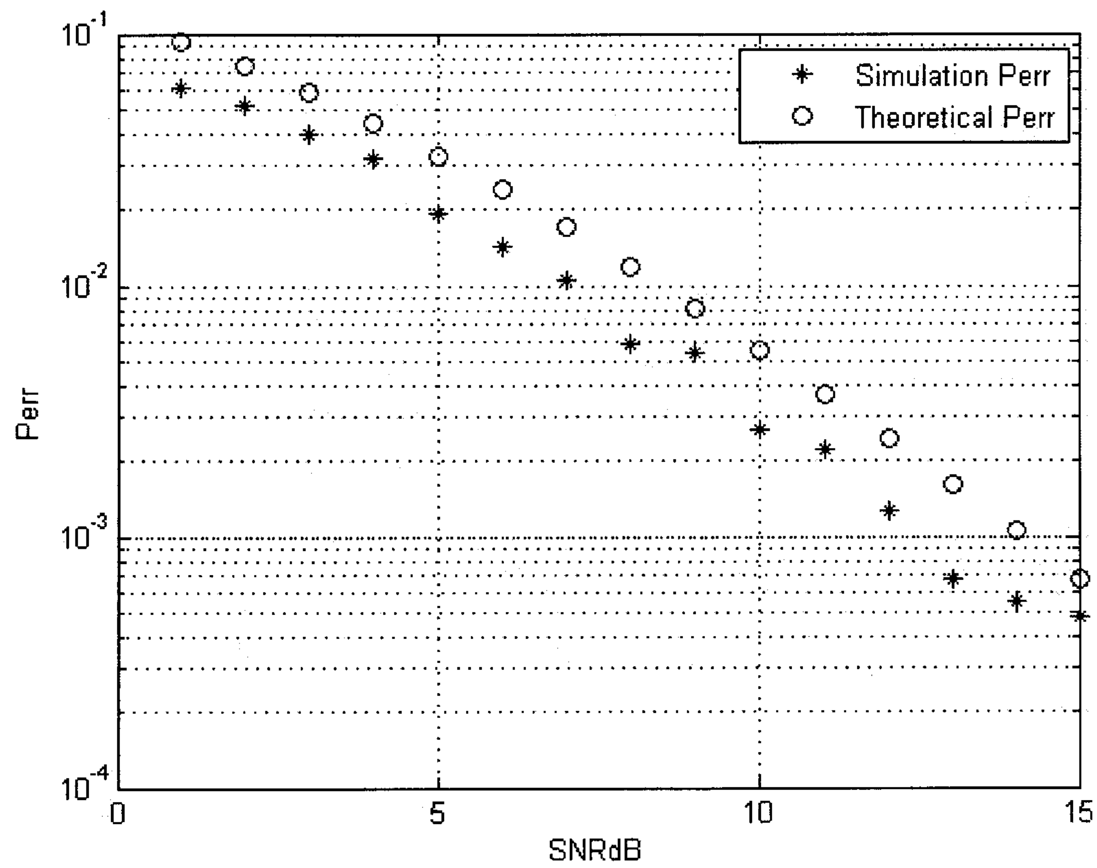

Figure 8.3: Probability of error on Alamouti Scheme using i.i.d Gaussian channel.

and find it pairwise probability of error.

8.1.2.5 Performance of the Alamouti Scheme

As the first step, we will test out the performance of the Alamouti scheme using BPSK on i.i.d channel. We have to accomplish this step to see how the Alamouti scheme outperform the theoretical results and then as the next step, we will do similar simulation using M-to-M channel.

The figure 8.3 shows that our simulation results out performed the theoretical results. In this case, we have used a channel to be i.i.d Gaussian channel to test the performance. The results from using the Mobile-to-Mobile channel is as follows:

The Fig. 8.5, shows us that, when we do simulation or testing in real life, we will have different results based on different type of vehicle speeds. In our case, both

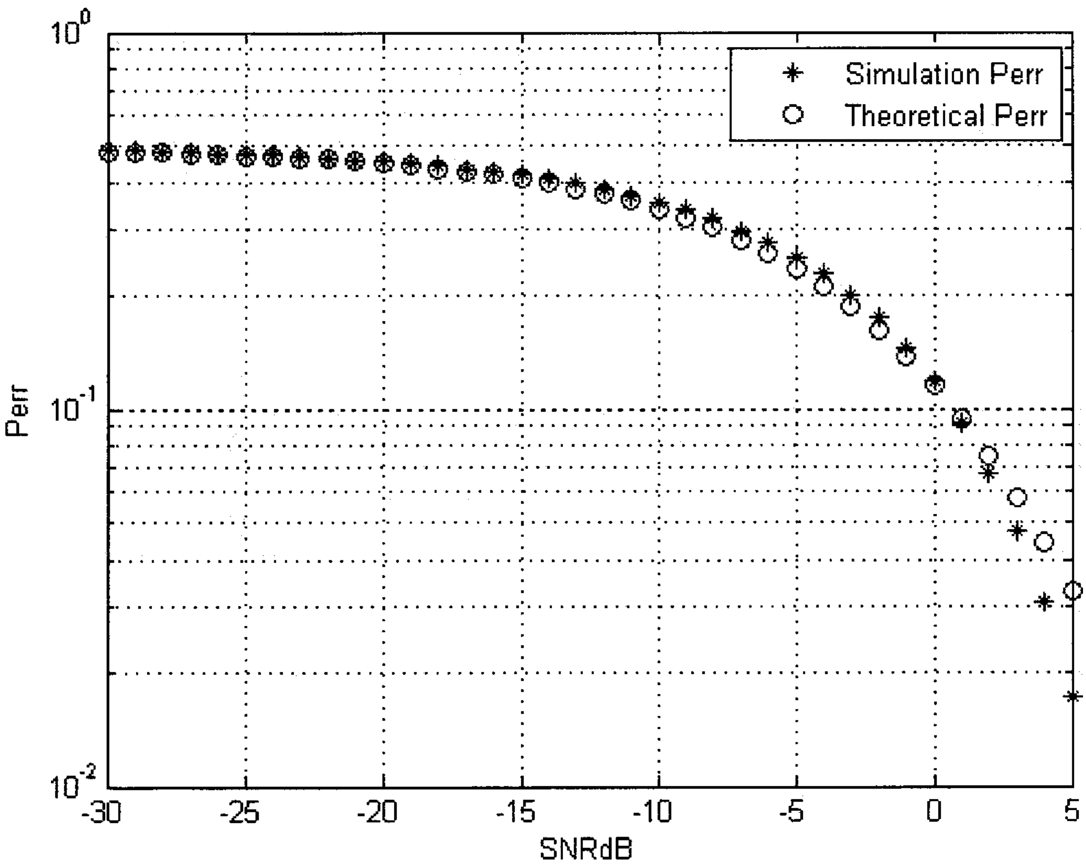

Figure 8.4: Probability of error on Alamouti Scheme using M2M channel.

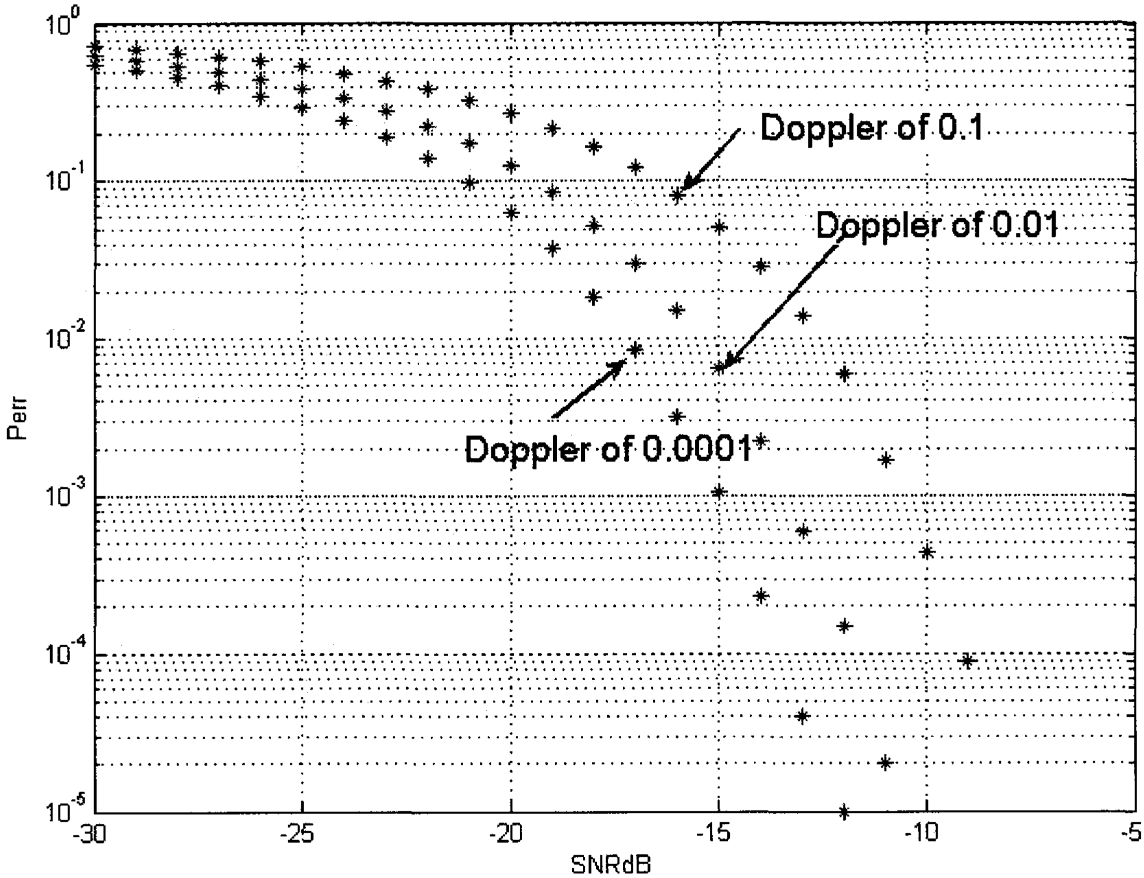

Figure 8.5: Probability of error on Alamouti scheme using M2M channel with different Doppler frequency (speed).

the cars are moving at the same speed causing the same doppler frequency. The effect of Doppler frequency on the probability of error on Alamouti scheme is shown in the figure (8.5). We can see that when the Doppler frequency is 0.0001 we have lower probability of error compare to when the Doppler frequency is 0.1.The results in Figure 8.4 shows that, our simulations results are same as the theoretical simulation results. From the above two figures, we can clearly see that there are less error when the channel is i.i.d then M2M because there is diversity involve in the M2M channel.

8.1.3 Pairwise Probability of Error

This section will explain how the pairwise probability of error is defined and used in our simulations for mobile to mobile case. The results of the theoretical PEP and simulation will be presented at the end of this section. The question that we should ask ourself is, What is pairwise probability of error means? Pairwise probability of error means that the probability that a certain "true" transmitted code matrix $\mathbf{X}_0$ is mistaken for a different matrix $\mathbf{X} \neq \mathbf{X}_0$ at the receiver. We can clearly see that, this error measure depends on which particular matrices $\mathbf{X}$ and $\mathbf{X}_0$ one chooses to study. The pairwise error probability is a meaningful quantity because the system performance is dominated by the error events where $\mathbf{X}$ and $\mathbf{X}_0$ are close.

We can also look at the upper bound on the total error probability of the system. Assuming that al the code matrices X are equally likely to be transmitted, the average error rate is upper bounded by

$$P_{tot} \leq \frac{1}{|X|} \sum_{X_n \in X} \sum_{X_k \in X, k \neq n} P(\mathbf{X}_n \rightarrow \mathbf{X}_k) \tag{8.7}$$

where $P(\mathbf{X}_n \rightarrow \mathbf{X}_k)$ is that pairwise error probability, and the $|X|$ is the number of elements in the matrix constellation X. the following theorem explains more about the Pairwise error probability for MIMO channel.

Theorem: Let study the linear model where X is of dimension r x m and consider the event that the ML detector decides for a matrix $\mathbf{X} \rightarrow \mathbf{X}_0$ in favor of X_0.Then the following results should hold. For a given h, the probability of error is

$$P(\mathbf{X}_0 \rightarrow \mathbf{X}) = Q\left(\sqrt{\frac{||(\mathbf{X}_0 - \mathbf{X})h||^2}{2\sigma^2}}\right)$$

secondly, suppose h is random then

$$\mathbf{h} \sim N_C(\mathbf{0}, \Upsilon)$$

where Υ is an m x m positive semi-definite matrix, therefore the rank can be found as

$$n = \text{rank}(\mathbf{X}_0 - \mathbf{X})\Upsilon(\mathbf{X}_0 - \mathbf{X})^H$$

finally, the probability of an incorrect decision can be bounded as follows:

$$E_h[P(X_0 - X)] \leq \left| I + \frac{1}{4\sigma^2}(X_0 - X)\Upsilon(X_0 - X)^H \right|^{-1} \tag{8.8}$$

$$\leq \left(\frac{1}{4\sigma^2}\right)^{-n} \Pi_{k=1}^{n} \varepsilon_k^{-1} \tag{8.9}$$

We will use the following theorem and compare it with our 4 x 4 Orthogonal space-time block coding pairwise error. Since we have shown the results of alamouti space time coding, we will show 4 transmitter and 4 receiver case. For our case, we will chose the code word matrix as equation 8.1.2.4 and first implement all the possible outcomes. Our matrix has only 3 bits with BPSK modulation, therefore we will have 8 possible matrices as codeword that can be sent. Then we will test this over 2 different type of channels. For better and easy understanding, we chose X_0 in equation 8.1.3 as the first codeword from the 8 codeword matrices. Then we found the pairwise error probability for the codeword that was sent using the above theorem and plotted it on log scale against SNR values and presented in the later section.

8.1.3.1 PPE for different channel conditions

Again in this section, we will test the performance of PPE using two types of channel - i.i.d Gaussian Channel and the M-To-M channel. We will compare the results to show how the performance changes based on different types of channels.

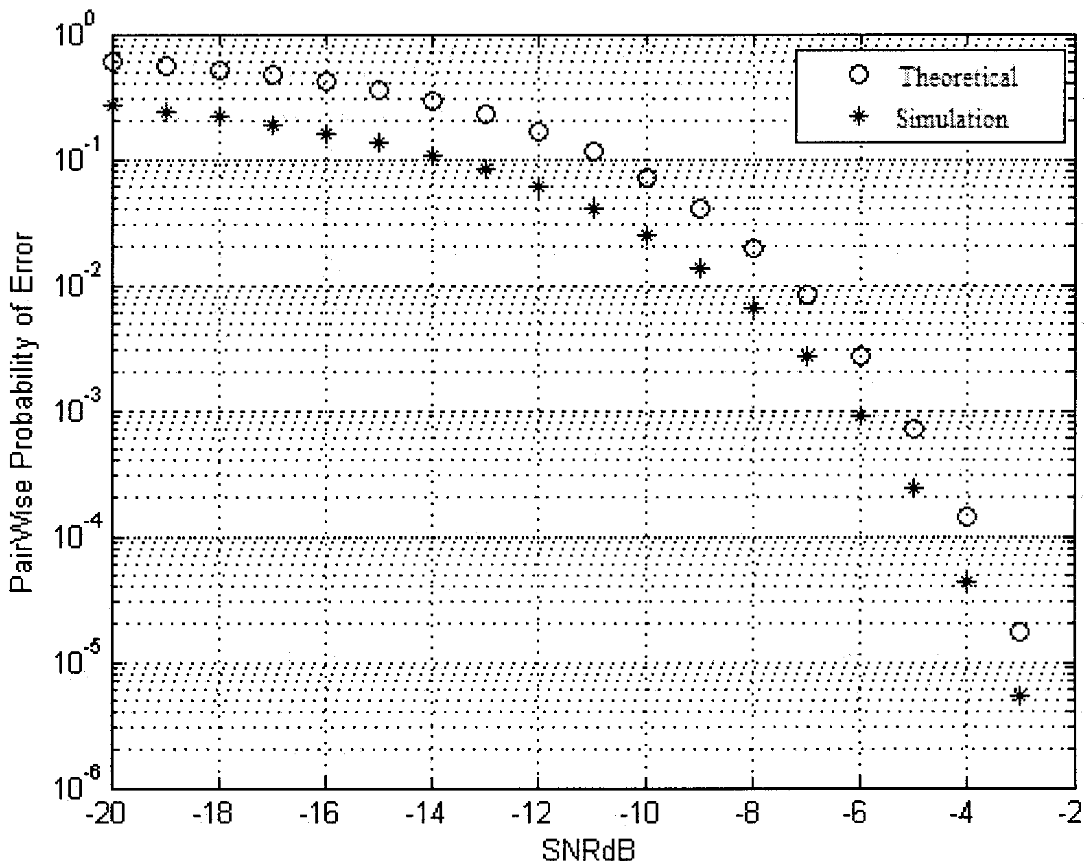

Figure 8.6: Pairwise probability of error for 4 X 4 OSTBC using i.i.d Gaussian channel.

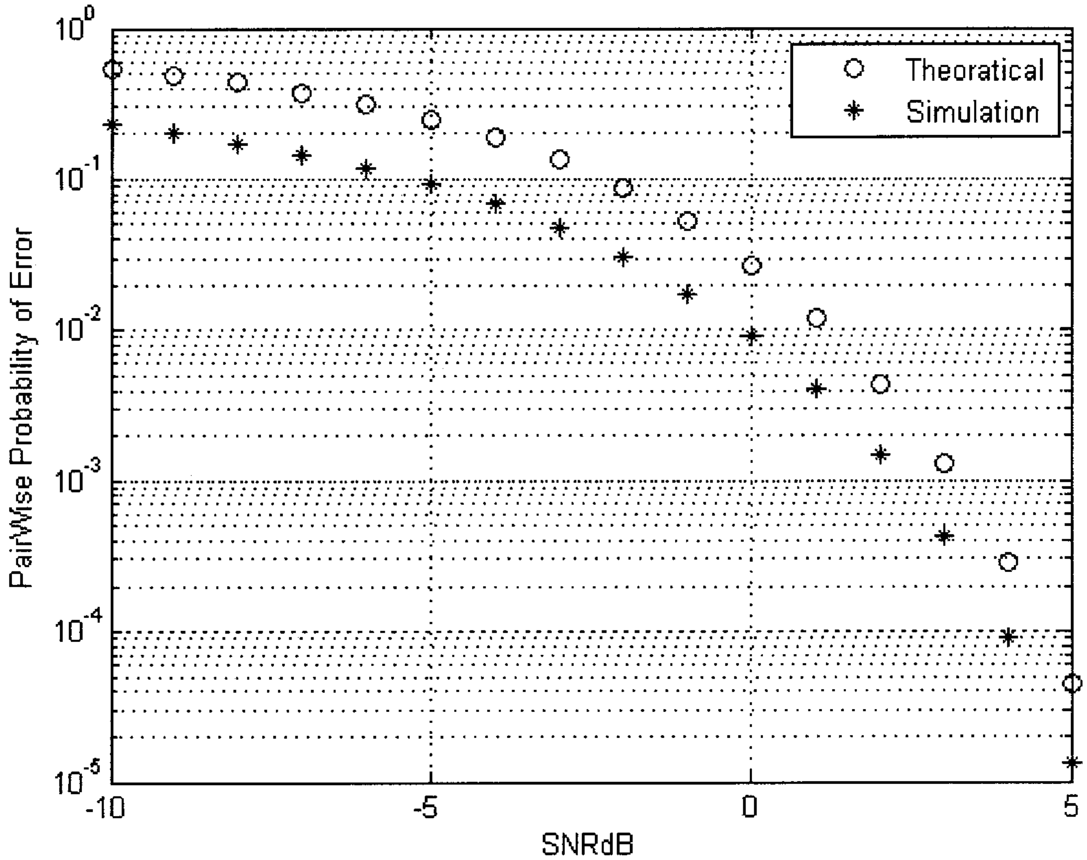

Figure 8.7: Pairwise probability of error for 4 x 4 OSTBC using M2M channel.

The figure 8.6 shows that, both the simulation results and theoretical results have the same shape but the results of our simulation outperformed the theoretical results again in this case.

We can clearly see from figure 8.7 that we have less probability of error in this case due to the trade of in the diversity in Mobile-to-Mobile channel. The results still show that the simulation results out performed the theoretical results.

For the simulation, we chose different codeword matrices over the physical channel. The channel is then effected by the white gaussian noise with zero mean and the variance was calculated from different SNRs. Then we calculate the distance between the codeword matrix that we received and all the possible codeword matrices and chose the minimum distance codeword matrix as the matrix that was sent. This

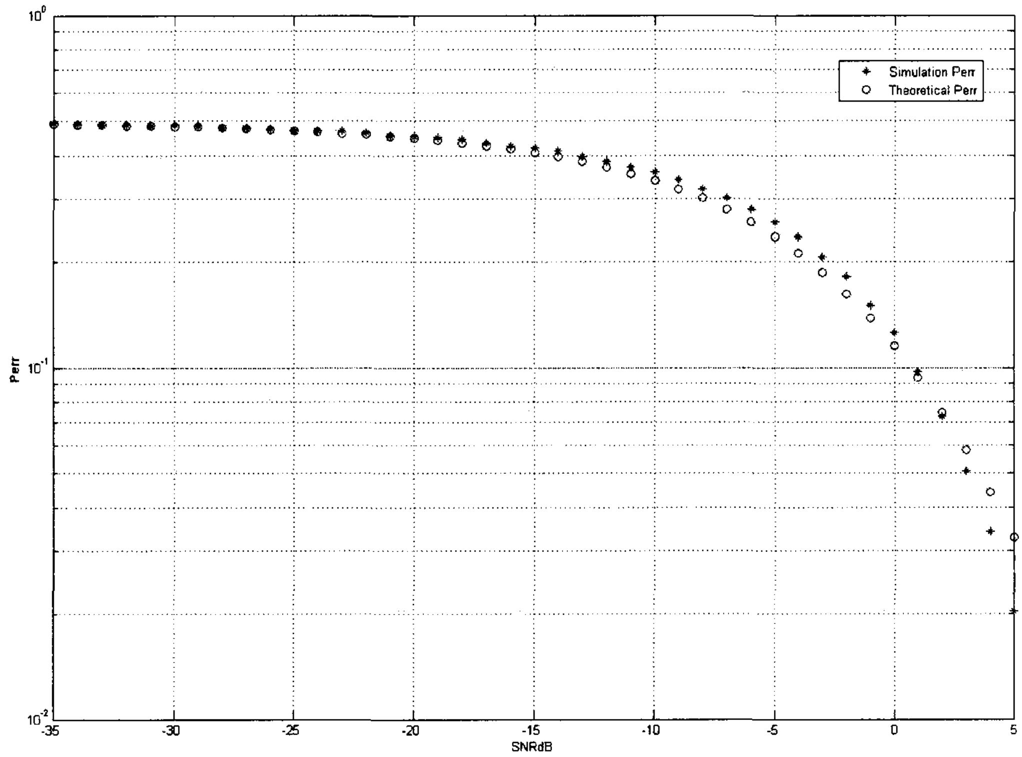

Figure 8.8: Performance of Alamouti on AR(20) channel model.

method is known as the ML decoding. If the $||receivedcodeword - sentcodeword||$ are not equal to zero then we can consider that as an error for Pairwise. After doing serval iterations, we can find out the Pairwise Error probability for given SNR. From the result, we can see that, when the SNR is 20dB there is a difference in results, we have lower P_{error} then theoretical, when the SNR is about -2dB the result became same.

8.2 Results using AR Channel Model

As the last step, we will create an AR model of order 20 and use it to test the performance and alamouti and pair-wise. The result from the Alamouti scheme is as follows

We can see from the figure 8.8, our simulation results and the theoretical results

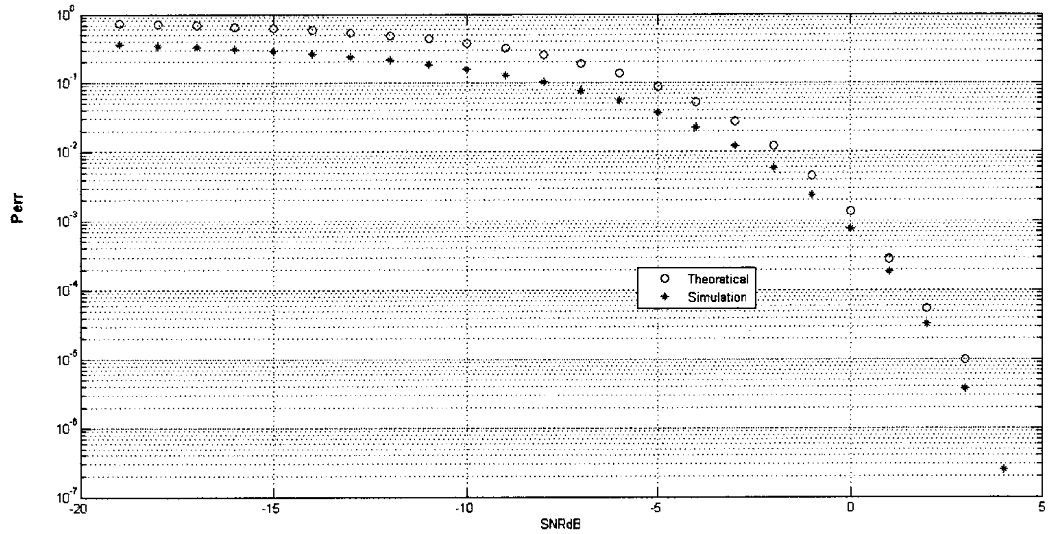

Figure 8.9: Performance of pair wise on AR(20) channel model.

were very close and the system perform very well as we have expected.

In figure 8.9, our simulation results were better for the lower SNR but as SNR increase it got closer and closer to the theoretical values at about 5 SNR. All the results from the above conclude that the modeling of AR model and performance test of the channel was a complete success.

8.3 Conclusion

We have compare the results between Alamouti scheme using i.i.d Gaussian channel and the M2M channels. We can see that we have lower probability of error in M2M performance case due to diversity and Doppler frequency effect. We can also see this effect in pairwise probability of error as well. We also simulated the different effect of Doppler frequency on the probability error and we came to conclusion that, when the Doppler frequency of the car is at 0.0001, the probability of error is lower then when the Doppler frequency is at 0.1.

Chapter 9
Conclusion

In this chapter, the principle results obtained in the thesis are summarized and conclusions are drawn. The recommendations for future related research is also presented.

Chapter 1 and Chapter 2, they are included in the thesis for the better understanding of the reader. It not only explain the background of the MIMO channels but also explain about the introduction to the thesis mainly how the thesis is contributed. In chapter 2, we not only explain how the mobile channels are formed but also explain all different types of channels for the reader to understand. We did get in details in that were out of the scope for us.

In chapter 3, we show how to model a UIU channel model using physical and virtual scattering. All the theoretical mathematical equations are presented in the chapter for the reader to understand the connection between the math and the design. In our simulations, we have the following conditions as the input functions

- Joint AoA/AoD PDF and the net power. The corresponding PAS is then just $P_0 p(\theta_T, \theta_R)$
- Number of transmit N_T and receive N_R antennas as well as the separation between antennas d_T and d_R in λ.
- Maximum Doppler frequency f_D and the sampling frequency F_s
- Number of required samples L

For the channel design, we used Gaussian PDF as the input PDF but for the capacity performance, we used uniform PDF. We did that to show the performance in both cases. The channel modeling results match perfectly with the theoretical results. The performance on this channel, Alamouti scheme and pair-wise, are also simulated and had a good performance as well. For the future case, they can have different input PDF instead of the Gaussian and uniform that we used. They can also have other types of performance scheme not just Alamouti and pairwise scheme. They can also test out the effect of correlation in this case and how not only the channel reacts to it but also how the capacity at that given case performs.

The chapter 4 explains every details on designing M2M channel model. We also explain the reference model, the old sum-of-sinusoids model and the two ring model. We explained how the modeling of this channel is done and showed the simulation results for $f_d T_s = 0.01$ and $N_0 = M = 8$. Our simulation results on autocorrelation of in-phase, quadrature and the main faded envelope of this model matches with the theoretical results in high simulation trials. We can see the miss match results in lower simulation trials in the appendix B. We also presented a good match in cross-correlation between in-phase and quadrature components of the channel.

In chapter 5 we have shown fading channel modeling using AR model. In our performance section,we have showed the effect of the order of the AR model. When we have AR model order of 20, the results did not match with the theoretical results but when the order was 100, the results matched perfectly to the theoretical results. For completeness, we decided to show the autocorrelation of in-phase and cross-correlation of the AR models for isotropic scattering and non-isotropic scattering. Once thing we should note is that, when the scattering is not isotropic, there is cross-correlation. We also show how the ill-conditioning in Yule-Walker equation effects the 1-step prediction MMSE for the AR model. We can see that when the ill-condition is large we have error of 10^{-3}, but when the condition becomes very small the error grows out of control. We also want the readers to understand more on how the isotropic and non-iso effect the auto and cross correlation. We can see those difference in our results in the chapter as well. All our simulation results matched the theoretical cases in either iso or non isotropic scattering.

Chapter 6 deals with different type of MIMO Capacity. Three types of capacity for MIMO that we have tested are listed. All the results we have achieved from this section clearly matched the results as we have expected.

Chapter 7 is to give us the better understanding of error performance on channel estimation. In the chapter, we explain how the transmitter, receiver and channels are design and how Alamouti scheme is used in this design. We also discussed two different decoding scheme - the linear combining scheme and Maximum likelihood scheme. We have also presented the transmission and receiver structure and the estimation filter design. In our design, we deal with a block fading due to its simplicity and easy understanding and implementation. All the auto and cross correlation simulation results clearly matches with the theoretical results. The performance of Alamouti space time code with the LC-STD with 11 tap Wiener filter for different doppler frequency with different channel SNR were presented with very good performance results. We also perform the same test for ML decoder. As the final step for this chapter, we performed both test, Alamouti scheme with the LC-STD and the ML decoder with different antenna spacing to find out the probability of error performance. We should note that, when the channel is not correlated, 0.5λ the error performance is higher than when the channel is correlated 0.1λ or 0.25λ. For future research the same test can be performed with different sets of channels to show the performance difference in other channels. We can also do different size of filter, and also different filters to see any improvements in the results. We can also have bit-by-bit estimation instead of block-by-block estimation.

In the last chapter, chapter 8, we have explained in details on Alamouti error probability scheme and pairwise probability scheme using M2M channel model and run performance test using them. The simulation results are compared against the i.i.d Gaussian performance results. We can clearly see better performance in our case. We also did the same performance using AR channel models and the results were in a good agreement.

References

[1] G. Tsoulos, *MIMO System Technology for Wireless Communications*, A. Poularikas, Ed. Taylor and Francis, 2006.

[2] T. Rappaport, *Wireless Communications: Principles and practice.* Upper Saddle River: Prentice Hall, 2002.

[3] T. M.Duman and A. Ghrayeb, *Coding for MIMO Communication Systems*, Wiley, Ed. John Wiley & Sons, 2007.

[4] D.Gesbert, M.Kountouris, R.W.Heath, Jr.C.B.Chae, and T.Salzer, "Shifting the MIMO paradigm: From Single User to Multiuser Communications," IEEE, Oct 2007.

[5] C. Oestges and B. Clerckx, *MIMO Wireless Communications : From Real-world Propagation to Space-time Code Design*, July.

[6] K. E. Baddour, "Simulation, Estimation and Predictoin of Flat Fading Mobile Wireless Channels," Ph.D. dissertation, Queen's University, Kingston,Ontario,Canada, November 2005.

[7] J.K.Cavers and M.Liao, "A comparison of pilot tones and pilot symbol techniques for digital mobile communication," *IEEE Global Conf on Telecommun*, pp. 915–921, December 1992.

[8] M.L.Loher and J.H.Lodge, "Tcmp- a Modulation and Coding Strategy for Rician Fading Channels," *IEEE J. in Selected Areas in Commun*, vol. 7, pp. 1347–1355, December 1989.

[9] J.K.Cavers, "An analysis of pilot symbol assisted modulation for Rayleigh fading channel," *IEEE Trans on Veh Tech*, no. 40, pp. 686–693, November 1991.

[10] V.Buchoux, O.Cappe, E.Moulines, and A.Gorokhov, "On the Performance of semi-blind subspace-based Channel Estimation," *IEEE Trans on Signal Proc*, vol. 48, pp. 1750–1759, June 2000.

[11] L.Dong, H.Choo, R.W.Heath, and H.Ling, "Simulation of MIMO Channel Capacity With Antenna Polarization Diversity," *IEEE Trans on wireless Commun*, vol. 4, no. 4, pp. 1869–1873, July 2005.

[12] E.A.Jorsweick and H.Boche, "Channel Capacity and Capacity-Range of Beamforming in MIMO Wireless Systems Under Correlated Fading With Covariance Feedback," *IEEE Trans on Wireless Commun*, vol. 3, no. 5, pp. 1543–1553, Sept 2004.

[13] D.-S. Shiu, G.J.Foschini, M.J.Gans, and J.M.Kahn, "Fading Correlation and Its Effect on the Capacity of Multielement Antenna Systems," *IEEE Trans on Commun*, vol. 48, no. 3, pp. 502–513, March 2000.

[14] S.L.Loyka, "Channel Capacity of MIMO Architecture Using the Exponential Correlation Matrix," *IEEE Commun Letters*, vol. 5, no. 9, pp. 369–371, Septemeber 2001.

[15] W. C. Lee, *Mobile Communications Engineering*, 2nd ed. California: McGraw-Hill, 1997.

[16] J. Andersen and N. Blaustaein, *Multipath Phenomena in Cellular Networks.* 2002: Artech House, 2003.

[17] A.Burr, "Capacity bounds and estimates for the finite scatterers MIMO wireless channel," *IEEE J. Selec Areas Commun.*, vol. 21, no. 5, pp. 812–818, June 2003.

[18] M.Debbah and R.Muller, "MIMO channel modeling and the principle of maximum entrophy," *IEEE Trans. on Info. Theo.*, vol. 51, no. 5, May 2005.

[19] A.Sayeed, "Deconstructing multiantenna fading channels," *IEEE Trans. on Sig. Proc.*, vol. 50, no. 10, pp. 2563–2579, Oct 2002.

[20] H. van Trees, *Detection, Estimation and Modulation Theory: Optimal Array Processing*, 1st ed. New York: Wiley-Interscience, 2002.

[21] F. Neeser and J. Massey, "Proper complex random processes with applications to information theory," *IEEE Journel Info Tech*, vol. 39, no. 4, pp. 1293–1302, July 1993.

[22] J. Wallace and B. Maharaj, "The accuracy of tensor and directional methods for MIMO channel modeling," in *Antennas and Propagation, 2007. EuCAP 2007. The Second European Conference on*, 2007, pp. 1–6.

[23] M. Debbah and R. Muller, "MIMO channel modeling and the principle of maximum entropy," *IEEE J Info Tech*, vol. 51, no. 5, pp. 1667– 1690, May 2005.

[24] K.Yu and B.Ottersten, "Models for MIMO propagation channels: A review," *Wireless Communications and Mobile Computing,Special Issue on Adaptive Antennas and MIMO systesms*, vol. 2, no. 7, pp. 653–666, Nov 2002.

[25] J.W.Wallace and M.A.Jensen, "Modeling the indoor MIMO wireless channel," *IEEE Trans. on Antennas and Propagation*, vol. 50, no. 5, pp. 591–599, 2002.

[26] P.Almers, E.Bonek, A.Burr, N.Czink, M.Debbah, and V.Degli-Esposti, "Survey of channel and radio propagation models for wireless MIMO systems," *EURASIP Journal on Wireless Communications and Networking*, vol. 2007, Article ID 19070,19, p. 19, 2007.

[27] D.S.Shiu, G.J.Foschini, M.J.Gans, and J.M.Khan, "Fading correlation and its effect on the capacity of multielement antenna systems," *IEEE Trans. On Commun.*, vol. 48, no. 3, pp. 502–513, March 2000.

[28] J.P.Kermoal, L.Schumacher, K.I.Pedersen, P.E.Mogensen, and F.Frederiksen, "A stochastic MIMO radio channel model with experimental validation," *IEEE J. on Selec. Areas in Commun.*, vol. 20, no. 6, pp. 1211–1226, 2002.

[29] I.Telatar, "Capacity of Multi-antenna Gaussian Channel," *Techanical Memorandum, Bell Laboratoeris, Lucent Technologies*, vol. 10, no. 6, pp. 585–595, 1998.

[30] W.Weichselberger, M.Herdin, H.Ozvelik, and E.Bonek, "A Stochastic MIMO Channel model with joint Correlation of both link ends," *IEEE Trans. on Wireless Commun.*, vol. 5, no. 1, pp. 90–99, 2006.

[31] M.Steinbauer, A.F.Molich, and E.Bonek, "The Double-Directional Radio Channel," *IEEE Mag. in Antenas and Propagation*, vol. 43, no. 4, pp. 51–63, 2001.

[32] C.Balanis, *Advance Engineering Electromagnetic*, N. John Wiley & Sons, Ed. John Wiley & Sons, 1999.

[33] A. Abdi and M. Kaveh, "A space-time correlation model for multielement antenna systems in mobile fading channels," vol. 20, no. 3, pp. 550–560, March 2002.

[34] A.Abdi and M.Kaveh, "Space-Time Correlation Modeling of Multielement Antenna Systems in Mobile Fading Channels," *In Proc. Inter. Conf. on Acoustics, Speech, and Sig. Proc.*, vol. 4, pp. 2505–2508, May 2001.

[35] ——, "A Space-Time Correlation Model for Multielement Antenna Systems in Mobile Fading Channels," *IEEE J. on Selected Areas in Commun.*, vol. 20, no. 3, pp. 550–560, April 2002.

[36] A. F. Molisch, H. Asplund, R. Heddergott, M. Steinbauer, and T. Zwick, "The COST 259 directional channel modelpart i: Overview and methodology," vol. 5, no. 12, pp. 3421–3433, December 2006.

[37] L. Correia, Ed., *Mobile Broadband Multimedia Networks.* UK: Wiley, 2007.

[38] S. Editors, "UMTS: Spatial channel model for MIMO simulations," in *Tech. report 25.996*, June 2006.

[39] A.F.Molisch, H.Asplund, R.Heddergott, M.Steinbauer, and T.Zuick, "The COST 259 directional channel model A-I:Overview and Methodology," *IEEE Trans. on Wireless Commun.*, vol. 5, no. 12, pp. 3421–3433, 2006.

[40] L.M.Correia, "Wireless Flexible Peronalised Communications," John Wiley & Sons, (COST 259 Final Report), 2001.

[41] http://www-ist winner.org/, "IST-WINNER."

[42] P.Karlsson, B.Ottersten, and R.Stridh, "MIMO channel capacity on a measure indoor radio channel at 5.8 GHz," *In Proceedings of the Asilomar Conference on Signals, Systems and Computers*, vol. 1, pp. 733–737, Oct 2000.

[43] A.F.Molisch, M.Steinbauer, M.Toeltsch, E.Bonek, and R.S.Thoma, "Capacity of MIMO systems based on measured wireless channels," *IEEE Journal on Selected Area in Communications*, vol. 20, no. 3, pp. 539–549, April 2002.

[44] T.S.Rapport, S.Y.Seidel, and K.Takamizawa, "Statistical channel impulse response models for factory and open plan building radio communication system design," *IEEE Transactions on Communications*, vol. 39, no. 5, pp. 794–807, May 1991.

[45] H.Hashemi, "Impulse response modeling of indoor radio propagation channels," *IEEE Journal on Selected Areas in Communications*, vol. 11, no. 7, pp. 967–978, Sep 1993.

[46] S.J.Howard and K.Pahlavan, "Autoregressive modeling of wide-band indoor radio propagation," *IEEE Transactions on Communications*, vol. 40, no. 9, pp. 1540–1552, Sep 1992.

[47] R.Genesh and K.Pahlavan, "Statistical modelling and computer simulation of indoor radio channel," *IEEE Proceedings*, vol. 138, no. 3, pp. 153–161, June 1991.

[48] J.Medbo, H.Andersson, P.Schramm, H.Asplund, and J.E.Berg, "Channel models for HIPERLAN/2 in different indoor scenarios," *COST 259 TD(98)70*, April 1998.

[49] K.Pahlavan and A.HLevesque, *Wireless Information Networks.* New York: Wiley & Sons, 1995.

[50] H.Suzuki, "A statistical model for urban radio propagation," *IEEE Transactions on Communications*, vol. COM-25, no. 7, pp. 673–680, July 1977.

[51] H.Iwai and Y.Karasawa, "Wideband propagation model for the analysis of the effect of the multipath fading on the near-far problem in CDMA mobile radio systems," *IEICE Transactions on Communications*, vol. E76-B, no. 2, pp. 103–112, Feb 1993.

[52] T.Zwick, C.Fischer, D.Didascalou, and W.Wiesbeck, "A Stochastic Spatial Channel Model Based on Wave Propagation Modeling," *IEEE J. Sel Areas Commun., YEAR = 2000, volume = 18, pages = 6-15, month = January,*.

[53] D.Gesbert, M.Shafi, D.S.Shium, P.J.Smith, and A.Naguib, "From theory or practice: An overview of MIMO space-time coded wireless systems," *IEEE Journal on Selec. Areas in Commun.*, vol. 21, pp. 281–302, April 2003.

[54] J.P.Kermoal, L.Schumacher, P.E.Mogensen, and K.I.Pedersen, "Experimental investigation of correlation properties of MIMO radio channels for indoor picocell scenarios," *Proceedings IEEE Veh. Tech Conf.*, vol. 1, pp. 14–21, Fall 2000.

[55] K.I.Pedersen, J.B.Andersen, J.P.Kermoa, and P.Ogensen, "A stochastic multiple-input multiple-output radio channel model for evalution of space-time coding algorithms," *Proc. IEEE Veh. Tech. Conf.*, vol. 2, pp. 893–897, Fall 2000.

[56] K.Yu, M.Bengtsson, B.Ottersten, D.McNamara, P.Karlasson, and M.Beach, "A wideband statistical model for NLOS indoor MIMO channels," *IEEE Veh. Tech. Conf.*, vol. 1, pp. 70–374, Spring 2002.

[57] ——, "Measurement analaysis of MLOS indoor MIMO channels," *Proc. IST Mobile Commun. Summit*, pp. 277–282, September 2001.

[58] ——, "Second order statistics of NLOS indoor MIMO channels based on 5.2GHz measurements," *Proc. IEEE Global Telecom. Conf.*, vol. 1, pp. 156–160, November 2001.

[59] J.W.Wallace and M.A.Jensen, "Statistical characteristics of measured MIMO wireless channel data and comparison to conventional models," *Proc. IEEE Veh. Tech. Conf.*, vol. 2, pp. 1078–1082, Fall IEEE VTC 2001.

[60] D.Gesbert, H.Bolcskei, D.Gore, and A.Paulraj, "MIMO wireless channels: Capacity and performnace," *In Proc. Global Telecommun. Conf.*, vol. 2, pp. 1083–1088, November 2000.

[61] E.Telatar, "Capactiy of Multi-Anetenna Gaussian Channels," *AT&T Bell Labs Inter. Tech*, 1995.

[62] G.J.Foschini and M.J.Gans, "On the limits of wireless communications in a fading environment when using multiple antennas," *Wireless Personal Communications*, vol. 6, no. 3, pp. 311–335, March 1998.

[63] A.Goldsmith, S.A.Jafar, N.Jindal, and S.Vishwanath, "Capacity limits of MIMO Channels," *IEEE J. on Selected Areas in Commun.*, vol. 21, no. 5, pp. 684–702, June 2003.

[64] D.S.Shiu, G.J.Foschini, M.J.Gans, and J.M.Kahn, "Fading correlation and its effect on the capacity of multielement antenna systems," *IEEE Trans. Commun.*, vol. 48, no. 3, pp. 502–513, March 2000.

[65] C.N.Chuah, D.N.Tse, J.M.Kahn, and R.A.Valanzuela, "Wireless Indoor Channel Mdeling:Statistical agreement of Ray Tracing Simulations and Channel Sounding Measurement," *IEEE Trans Infrom.*, vol. 48, no. 3, pp. 637–650, March 2002.

[66] A.M.Sayeed, "Deconstructing Multi-Antenna Fading Channels," *IEEE Trans Signal Proc*, vol. 50, no. 10, pp. 2563–2579, Oct 2002.

[67] H.Ozcelik, M.I.Herdin, R.Prestros, and E.Bonek, "How MIMO Capactiy is linked with Multipath Distruction," *Proc Inter. Conf. on Electromagnetics in Advance App*, pp. 775–778, 2003.

[68] Y.R.Zheng and C.Xiao, "Improved Models for The Generation of Multiple Uncorrelated Rayleigh Fading Waveforms," *IEEE commun Lett*, vol. 1, pp. 144–149, March 2002.

[69] C.Xiao and Y.R.Zheng, "A Statistical Simulation Model for Mobile Radio Fading Channels," *Proc. IEEE Wireless Commun. Network Conf*, vol. 1, pp. 144–149, 2002.

[70] A.Akki and F.Haber, "A Statistical Model for Mobile-to-Mobile Land Communication Channel," *IEEE Trans. Veh Tech*, vol. 35, no. 1, pp. 2–7, Feb 1986.

[71] A.S.Akki, "Statistical Properties of Mobile-to-Mmobile Land Communication Channels," *IEEE Trans Veh Technol*, vol. 43, no. 4, pp. 826–831, November 1994.

[72] T.S.J.Maureer and T.Fugen, "A New Inter Vehicle Communiction (IVC) Channel Model," *IEEE veh tech conf(vtc 04)*, Sept 2004.

[73] I.Z.Kovacs, P.C.F.Eggers, K.Olesen, and W.Wiesbeck, "Investigations of Outdoor-to-Indoor Mobile-to-Mobile Radio Communication Channels," *Proc. IEEE Veh. Technol Conf*, vol. 1, pp. 430–434, Sept 2002.

[74] A.Kato, K.Sato, and S.Kawakami, "Propagation characteristics of 60-GHz millimeter waves for its Inter-Vehicle communications," *IEICE Trans Commun*, vol. E84-B, no. 9, pp. 2530–2539, Sept 2001.

[75] C. S.Patel, G. L.Stuber, and T. G.Pratt, "Simulation of Rayleigh Faded Mobile-to-Mobile Communication Channels," *IEEE Trans on Commun*, vol. 53, no. 11, pp. 1876–1884, November 2005.

[76] G.Acosta, K.Tokuda, and M.A.Ingram, "Measured joint Doppler-delay power profiles for Vehicle-to-Vehicle Communications at 2.4GHz," *Proc IEEE GLOBECOM*, vol. 6, pp. 3813–3817, Nov 2004.

[77] R.Wang and D.Cox, "Channel Modeling for Ad hoc Mobile Wirelesss Networks," *IEEE Trnas On Commun*, vol. 1, pp. 21–25, May 2005.

[78] A. G. Jakic.

[79] A.S.Akki and F.Haber, "A Statistical Model of Mobile-to-Mobile Land Communication Channel," *IEEE Trans. Vehic Tech.*, vol. VT-35, no. 1, pp. 2–7, Feb 1986.

[80] D. Matolak, "Channel modeling for vehicle-to-vehicle communications," *IEEE M. COM*, vol. 46, no. 5, pp. 76–83, May 2008.

[81] G. Acosta-Marum and M. Ingram, "Six time- and frequency-selective empirical channel models for vehicular wireless LANs," in *Proc. IEEE 66th VTC 2007 Fall*, Baltimor, MD, September 2007.

[82] G.L.Stuber, *Principle of Mobile Communication.* Kluwer, 2001, vol. 2e.

[83] L.-C. Wang and Y.-H. Cheng, "Modelling and capacity analysis of MIMO Rician Fading Channels for Mobile-to-Mobile," *Veh Tech Conf, 2005. VTC-2005-Fall. 2005 IEEE 62nd*, vol. 2, pp. 1279–1283, Sept., 2005.

[84] D.J.Young and N.C.Beaulieu, "The generation of correlated Rayleigh random variates by inverse Fourier transform," *IEEE Trans Commun*, vol. 48, pp. 1114–1127, July 2000.

[85] C.Loo and N.Secord, "Computer Modles for Fading Channels with Applications to Digital Transmission," *IEEE Trans Veh Technol*, vol. 40, pp. 700–707, Nov 1991.

[86] P.Honer, "A Statistical Discrete-time Model for the WSSUS multipath channel," *IEEE Trans Veh Technol*, vol. 41, pp. 461–468, July 1992.

[87] D.Verdin and T.Tozer, "Generating a fading process for the Simultion of Land-Mobile Radio Communication," *Electron letter*, vol. 29, pp. 2011–2012, Nov 11 1993.

[88] M.Tsatsanis and Z.Xu, "Pilot Symbol Assisted Modulation in Frequency Selective Fading Wireless Channels," *IEEE Trans Signal Proc*, vol. 48, pp. 2353–2365, August 2000.

[89] H.Wu and A.Duel-Hallen, "On the Performance of Coherent and Noncoherent Multiuser Detectors for Mobile Radio CDMA Channels," *In Proc IEEE conf of Universal Personal Comms*, pp. 76–80, 1996.

[90] T.Eyceoz, A.Duel-Hallen, and H.Hallen, "Determiniztic channel modeling and long range prediction of fast fading mobile radio channels," *IEEE Commun Letter*, vol. 2, pp. 254–256, September 1998.

[91] A.Kuchar, E.A.Aparicio, J.P.Rossi, and E.Bonek, "Azimuth, Elevation and Delay of Signals at Mobile Station Site," *Wireless Personal Communication:Emerging Technologies for Enhanced Communications*, pp. 99–110, 1999.

[92] J.P.Rossi, J.P.Barbot, and A.J.Levy, "Theory and Measurement of the Angle of Arrival and Time Delay of UHF Radio Waves Using a Ring Array," *IEEE Trans Antennas Propagat*, vol. 45, pp. 876–884, 1997.

[93] J.Fuhl, J.P.Rossi, and E.Bonek, "High-resolution 3D direction of arrival determination for Urban Mobile Radio," *IEEE Trans Antennas Propgat*, vol. 45, pp. 672–682, 1997.

[94] A.Saleh and R.Valenzuela, "A statistical model for indoor multipath propagation," *IEEE Journal on Selected Areas in Communications*, vol. SAC-5, no. 2, pp. 128–137, Feb 1987.

[95] P.C.Fannin and A.Molina, "Analysis of Mobile Radio Channel Sounding Measurements in Inner City," *Inst Elect Eng Proc Commun*, vol. 143, pp. 311–316, 1996.

[96] J.G.Wang, A.S.Mohan, and T.A.Aubrey, "Angles of Arrival of Multipath Signals in Indoor Environments," *Proc IEEE Veh Tech Conf*, pp. 155–159, 1996.

[97] S.Guerin, "Indoor Wideband and Narrowband Propagation Measurements Around 60.5GHz in an Empty and Furnished Room," *Proc IEEE Veh Tech Conf*, pp. 160–164, 1996.

[98] T.Lo and J.Litva.

[99] D.O.Reudink, "Large-Scale Variations of the Average Signal," *Microwave Mobile Communications*, pp. 79–131, 1974.

[100] W.C.Y.Lee, "Finding the approximate Angular Probability Density Function of Wave Arrival by Using a Directional Antenna," *IEEE Trans Antennas Prop*, vol. AP-21, pp. 328–334, 1973.

[101] P.Petrus, J.H.Reed, and T.S.Rappaport, "Finding the Approximate Angular Probability Density Function of Wave Arrival by Using a Directional Antenna," *IEEE Trans Antennas Prop*, vol. 1, pp. 40–42, 1997.

[102] J.C.Liberti and T.S.Rappaport, "A Geometrically Based Model for line-of-sight Multipath Radio Channels," *Proc IEEE Veh Tech Conf, Alanta, GA*, pp. 844–848, 1996.

[103] W.C.Jakes, *Microwave Mobile Communications*, Ed, Ed. New York: Wiley, 1974.

[104] Y.R.Zheng and C.Xiao, "Simulation Model with Correct Statistical Properties for Rayleigh Fading Channels," *IEEE Trans on Commun*, vol. 51, no. 6, 2003.

[105] K. E. Baddour and N. C. Beaulieu, "Accurate Simulation of Multiple Cross-Correlated Rician Fading Channels," *IEEE Trans on Commun*, vol. 52, no. 11, pp. 1980–1987, November 2004.

[106] A.Abdi, J.A.Barger, and M.Kaveh, "A parametric model for the distribution of the angle of arrival and the associated correlation function and power spectrum at the mobile station," *IEEE Trans on Veh Tech*, vol. 51, no. 3, pp. 425–434, 2002.

[107] S.Primak, V.Kontrovitch, and V.Lyandres, *Stochastic Methods & Their Applications to Communications: Stochastic Differential Equations Approach*, L. John Wiley & Sons Inc., Ed. John Wiley & Sons, 2004.

[108] K.E.Baddour and N.C.Beaulieu, "Autoregressive modeling for fading channel simulation," *IEEE Trans on Wirelss Communications*, vol. 4, no. 4, pp. 1650–1662, July 2005.

[109] I. Telatar, "Capacity on Multi-Antenna Gaussian Channels," *European Trans. on Telecommunications*, vol. 10, no. 6, pp. 585–595, 1999.

[110] I.E.Telatar, "Capacity of Multi-Antenna Gaussian Channels," AT&T bell labs internal report, http://mars.bells-labs.com/cm/ms/what/mars/index.html, Tech. Rep., 1995.

[111] G. Foshini, R. Gitlin, and S. Weinstein, "Optimization of two-dimensional signal constellations in presence of Gaussian noise," *IEEE J Commun*, vol. 22, no. 1, pp. 28–38, January 1974.

[112] A. Paulraj, R. Nabar, and D. Gore, *Introduction to Space-Time Wireless Communications.* Cambridge, UK: Cambridge University Press, 2003.

[113] R.Steele, *Mobile Radio Communication*, Wiley, Ed. Wiley, 1992.

[114] M.Luccini, S.Primak, and A.Shami, "On the Capacity of MIMO Channels and Its Effect on Network Performance," *Info and Commu Techn:From Theory to Applications(ICTTA)*, pp. 1–6, April 2008.

[115] A. Paulraj, R. Nabar, and D. Gore, *Introduction to space-time wireless communications*, Cambridge, Ed. Cambridge University Press, 2003.

[116] M. Jankiraman, *Space-time code and MIMO systesms*, Wiley, Ed. Artech House, 2004.

[117] H. Jafarkhani, *Space-time coding: theory and practice*, Cambridge, Ed. Cambride Universty Press, 2005.

[118] A. B.Gershman and N. D. Sidiropoulos, *Space-time processing for MIMO communications*, J. W. . Sons, Ed. John Wiley & Sons, 2005.

[119] S.M.Alamouti, "A Simple Transmit Diveristy Technique for Wireless Communications," *IEEE J. Selec Areas of Commun*, vol. 16, pp. 1451–1458, October 1998.

[120] J.G.Proakis, J.Jootar, and J.R.Zeidler, "Performance of Alamouti Space-Time Code in Time-Varying Channels wiht Noisy Channel Estimates," *Proc Wireless Commun and Networking Conf*, pp. 498–503, March 2005.

[121] M.Biguesh and A.B.Gershman, "Mimo Channel Estimation: Optimal Training and Tradeoff Between Estimation Techniques," *IEEE Inter Conf Commun*, vol. 5, no. 5, pp. 2658–2662, June 2004.

[122] D.GU and C.Leung, "Performance Analysis of Transmit Diveristy Scheme with Imperfet Channel Estimation," *Electronic Letters*, vol. 39, pp. 402–403, Feb 2003.

[123] W.C.Ang and C.S.Ng, "Analysis of a trasnmit diveristy scheme in fading channels and imperfect channel estimation," *Proc. International Conf. on Commun. Sys.(ICCS 2002)*, pp. 188–192, November 2002.

[124] E.Biglieri, G.Caire, G.Taricco, and J.Ventura-Traveset, "Simple method for evaluating error probabilities," *Electronic Letters*, vol. 32, pp. 191–192, 1996.

[125] J.K.Cavers, "An analysis of pilot symbol assisted modulation for Rayleigh Fading Channels," *IEEE Trans. Veh. Tech.*, vol. 40, pp. 686–693, Nov 1991.

[126] S. Alamouti, "A simple transmit diversity technique for wireless communications," *Selected Areas in Communications, IEEE Journal on*, vol. 16, no. 8, pp. 1451–1458, Oct 1998.

[127] A. Papoulis, *Probability, Random Variables, and Stochastic Processes*, 3rd ed. Boston, MA: McGraw-Hill, 1991.

Appendix A

Appendix A

A.1 Derivation of Bit Error Probability

This section will simply explain the step of substitutions and the assumptions that was taken to derive the bit error probability, which is used in our research as the theoretical simulation.The derivation is as follows:

Given before the assumption:

$$\varepsilon_0 = \mathbf{w}_0^H(\mathbf{D}_0/2 + \bar{\gamma}_p^{-1}\mathbf{I}_{2M+1})^{-1}\mathbf{w}_0 \tag{A.1}$$

$$\varepsilon_1 = \mathbf{w}_1^H(\mathbf{D}_0/2 + \bar{\gamma}_p^{-1}\mathbf{I}_{2M+1})^{-1}\mathbf{w}_0 \tag{A.2}$$

$$\Upsilon = \left(\frac{4(1+\bar{\gamma}_s^{-1})}{\varepsilon_0} - \left(\frac{\varepsilon_1}{\varepsilon_0}\right)^2\right)^{-1/2} \tag{A.3}$$

$$P_b = \frac{1}{4}(2+\Upsilon)(1-\Upsilon)^2 \tag{A.4}$$

For the perfect CSI case, the paper set $\bar{\gamma}_p \to \infty$.Since $\mathbf{D}_0^{-1}\mathbf{D}_0 = \mathbf{I}_{2M+1}$ and $\mathbf{w}_0$ is the $(M+1)^{th}$ column of D_0, we get $\mathbf{D}_0^{-1}\mathbf{w}_0 = [0 \ \dots \ 0 \ 1 \ 0 \ \dots \ 0]^T$ (with one in the $(M+1)^{th}$ row). Therefore, the values of $\varepsilon_0, \varepsilon_1$ and Υ when $\bar{\gamma}_p \to \infty$ are equal to 2,2 and $2R(\tau)$ respectively.We will show the derivation for 2 different types of channel - very fast fading ($R(\tau) = 0$), and static channel ($R(\tau) = 1$).

A.2 Very Fast Fading ($R(\tau) = 0$)

We can rewrite the equation A.3 in the following form due to the derivation we have shown above.

$$\Upsilon = \frac{1}{\sqrt{2 + \frac{2}{\bar{\gamma}_s} - R^2(\tau)}} \tag{A.5}$$

when $R(\tau) = 0$, the equation A.5 can we written as

$$\Upsilon = \frac{1}{\sqrt{2 + \frac{2}{\bar{\gamma}_s}}} = \frac{1}{\sqrt{\frac{2\bar{\gamma}_s + 2}{\bar{\gamma}_s}}} = \sqrt{\frac{\bar{\gamma}_s}{2\bar{\gamma}_s + 2}} \tag{A.6}$$

now we will substitute equation A.6 into A.4 and we write equation A.4 as

$$P_b = \frac{1}{4}(2 + \Upsilon)(1 - \Upsilon)^2 = \frac{1}{4}\left(2 + \sqrt{\frac{\bar{\gamma}_s}{2\bar{\gamma}_s + 2}}\right)\left(1 - \sqrt{\frac{\bar{\gamma}_s}{2\bar{\gamma}_s + 2}}\right)^2 \tag{A.7}$$

We can see that the equation A.7 exactly same as what we have given in the chapter.

A.3 Static Channel ($R(\tau) = 1$)

when $R(\tau) = 1$, the equation A.5 can we written as

$$\Upsilon = \frac{1}{\sqrt{2 + \frac{2}{\bar{\gamma}_s} - 1}} = \frac{1}{\sqrt{\frac{\bar{\gamma}_s + 2}{\bar{\gamma}_s}}} = \sqrt{\frac{\bar{\gamma}_s}{\bar{\gamma}_s + 2}} \tag{A.8}$$

now we will substitute equation A.8 into A.4 and we write equation A.4 as

$$P_b = \frac{1}{4}(2+\Upsilon)(1-\Upsilon)^2 = \frac{1}{4}\left(2+\sqrt{\frac{\bar{\gamma}_s}{\bar{\gamma}_s+2}}\right)\left(1-\sqrt{\frac{\bar{\gamma}_s}{\bar{\gamma}_s+2}}\right)^2 \tag{A.9}$$

The equation A.9, shows that the derivation is same as what is given in the chapter.

Appendix B

Appendix B

B.1 Derivation Of Auto-Correlation Function of the In-phase component

We have our k^{th} complex faded envelope as

$$g_k(t) = \sum_{n=1}^{N}\sum_{m=1}^{M} C\exp\{j[\omega_1 t\cos(\alpha_{nk}) + \omega_2 t\cos(\beta_{mk}) + \phi_{nmk}]\} \quad \text{(B.1)}$$

We can split the above equation into the following

$$\begin{aligned} g_k(t) &= \frac{2}{\sqrt{N_0\, M}}\sum_{n=1}^{N_0}\sum_{m=1}^{M} \cos(\omega_2 t\cos(\beta_{mk}))\cos(\omega_1 t\cos(\alpha_{nk}) + \phi_{nmk}) \quad \text{(B.2)} \\ &+ j\sum_{n=1}^{N}\sum_{m=1}^{M} \sin(\omega_2 t\cos(\beta_{mk}))\sin(\omega_1 t\sin(\alpha_{nk}) + \phi_{nmk}) \end{aligned}$$

Since we are discussing about the In-phase part only in this case, we can ignore the imaginary party from the above equation and we can we write the In-phase part as

$$g_{ik}(t) = \frac{2}{\sqrt{N_0\, M}}\sum_{n=1}^{N_0}\sum_{m=1}^{M} \cos(\omega_2 t\cos(\beta_{mk}))\cos(\omega_1 t\cos(\alpha_{nk}) + \phi_{nmk}) \quad \text{(B.3)}$$

We have to prove that

$$R_{g_i g_I}(\tau) = E[g_i(t+\tau)g_i(t)] = J_0(\omega_1\tau)J_0(\omega_2\tau) \tag{B.4}$$

Proof:

$$R_{g_{ik}g_{ik}}(\tau) = E[g_{ik}(t+\tau)g_{ik}(\tau)] \tag{B.5}$$

we can write $g_{ik}(t+\tau)$ and $g_{ik}(\tau)$ as

$$\begin{aligned} g_{ik}(t) &= \frac{2}{\sqrt{N_0\,M}}\sum_{n=1}^{N_0}\sum_{m=1}^{M}\cos(\omega_2 t\cos(\beta_{mk}))\cos(\omega_1 t\cos(\alpha_{nk})+\phi_{nmk}) \\ g_{ik}(t+\tau) &= \frac{2}{\sqrt{N_0\,M}}\sum_{n=1}^{N_0}\sum_{m=1}^{M}\cos(\omega_2(t+\tau)\cos(\beta_{mk}))\cos(\omega_1(t+\tau)\cos(\alpha_{nk})+\phi_{nmk}) \end{aligned}$$

Then we get:

$$\begin{aligned} E[g_i(t+\tau)g_i(t)] = {} & \frac{4}{N_0M}\sum_{n=1}^{N_0}\sum_{m=1}^{M}\sum_{p=1}^{N_0}\sum_{r=1}^{M}\cos(\omega_2(t+\tau)\cos(\beta_{mk})) \\ & \cos(\omega_1(t+\tau)\cos(\alpha_{nk})+\phi_{nmk})\cos(\omega_2 t\cos(\beta_{pk}))\cos(\omega_1 t\cos(\alpha_{rk})+\phi_{prk}) \end{aligned} \tag{B.6}$$

After multiplying and taking E inside, we only have terms left that are not dependent of time.

$$R_{g_{ik}g_{ik}}(\tau) = \frac{1}{N_0M}\sum_{n=1}^{N_0}\sum_{m=1}^{M}E[\cos(\omega_2\tau\cos(\beta_{mk}))\cos(\omega_1\tau\cos(\alpha_{nk}))]$$

Now we can substitute the α_{nk} and β_{mk} and rewrite the equation as:

$$
\begin{aligned}
R_{g_{ik}g_{ik}}(\tau) &= \frac{1}{N_0 M}\sum_{n=1}^{N_0}\sum_{m=1}^{M} E[\cos\left(\omega_2\tau\cos\left(0.5\left(\frac{2\pi\, m}{M}+\frac{2\pi\, k}{PM}+\frac{\psi-\pi}{M}\right)\right)\right) \\
&\cos\left(\omega_1\tau\cos\left(\frac{2\pi\, n}{4N_0}+\frac{2\pi\, k}{4PN_0}+\frac{\theta-\pi}{4N_0}\right)\right)] \\
&= \frac{1}{M}\sum_{m=1}^{M}\frac{1}{2\pi}\int_{-\pi}^{\pi}\cos\left(\omega_2\tau\cos\left(0.5\left(\frac{2\pi\, m}{M}+\frac{2\pi\, k}{PM}+\frac{\psi-\pi}{M}\right)\right)\right)d\psi \\
&\frac{1}{N_0}\sum_{n=1}^{N}\frac{1}{2\pi}\int_{-\pi}^{\pi}\cos\left(\omega_1\tau\cos\left(\frac{2\pi\, n}{4N_0}+\frac{2\pi\, k}{4PN_0}+\frac{\theta-\pi}{4N_0}\right)\right)d\theta
\end{aligned}
$$

after solving this integral and taking the assumption of $N_0 \to \infty$ and $M \to \infty$ then we can get

$$\lim_{N_0, M\to\infty} R_{g_{ik}g_{ik}}(\tau) = J_0(\omega_1\tau)J_0(\omega_2\tau)$$

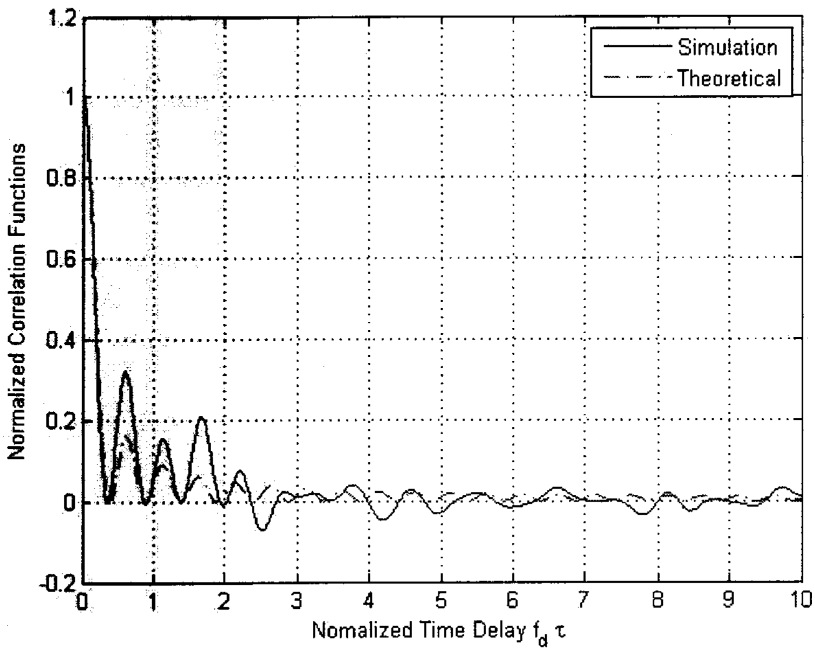

Figure B.1: Theoretical and Simulation (number of simulation of 1)auto-correlation of in-phase components of M-to-M channel

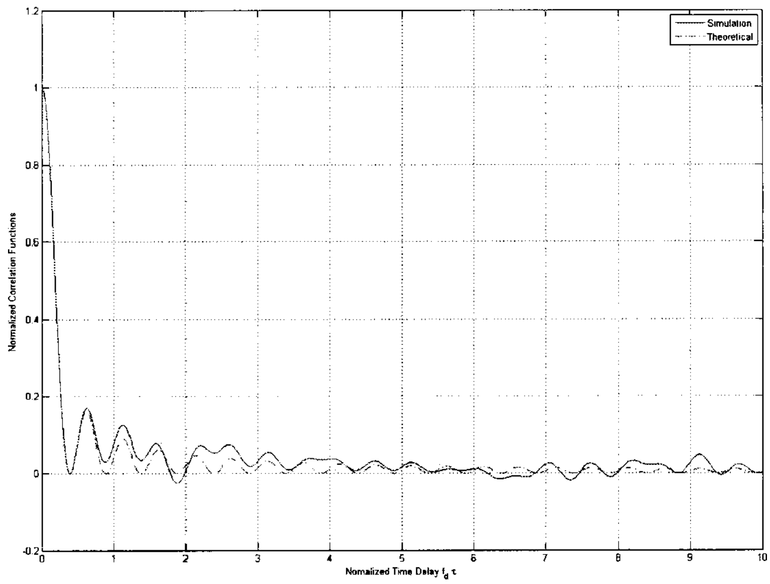

Figure B.2: Theoretical and Simulation (number of simulation of 50) auto-correlation of in-phase components of M-to-M channel

We can clearly see form the Figures B.1 and B.2 that when the number of trials of simulation is small our simulation results have a lot of fluctuations and does not match at some values of $f_S T_S$ with the theoretical values. We can see a better match of our simulation results with the theoretical one in high number of simulation results. We will see the same result for auto-correlation of the quadrature components and the main envelope.

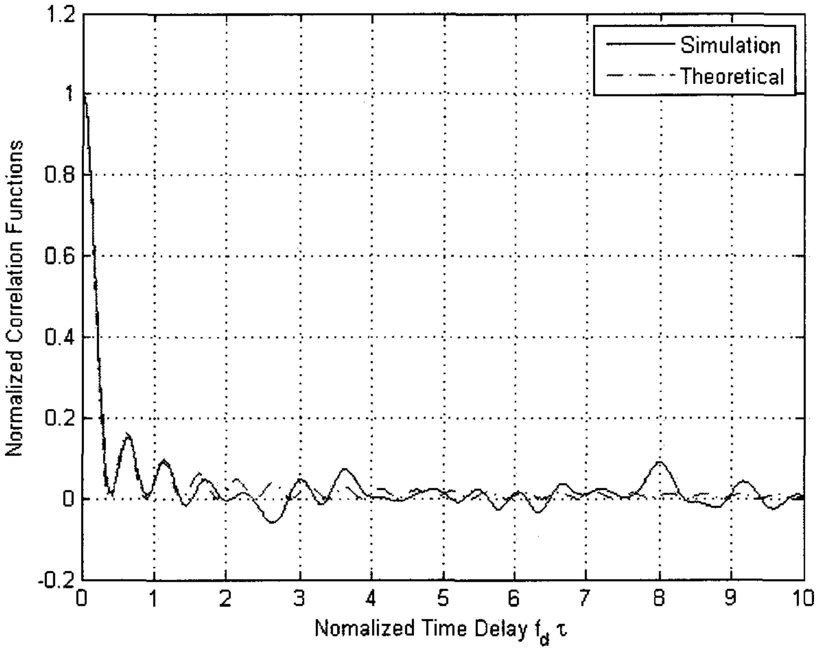

Figure B.3: Theoretical and Simulation (number of simulation of 1) auto-correlation of the main envelope part of M-to-M channel

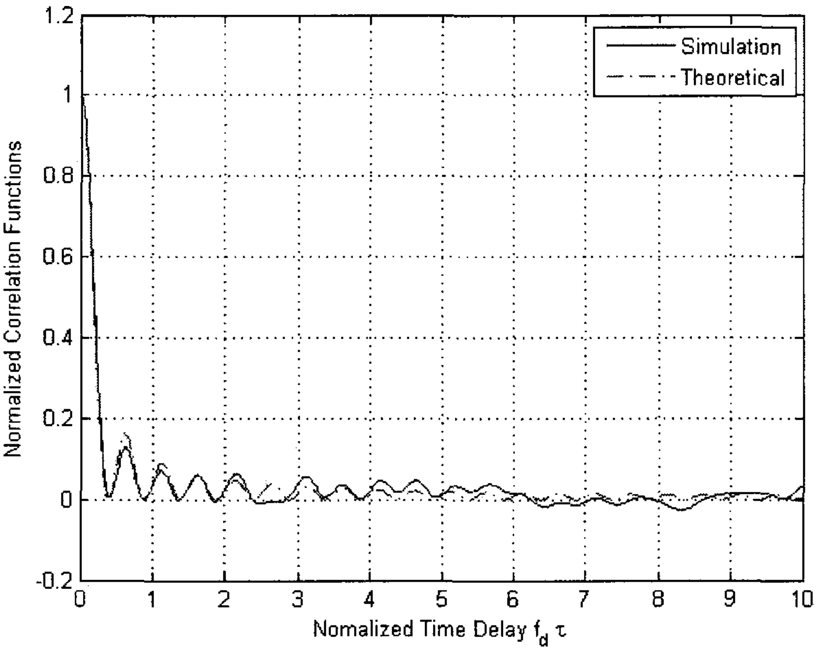

Figure B.4: Theoretical and Simulation (number of simulation of 10) auto-correlation of the main envelope part of M-to-M channel

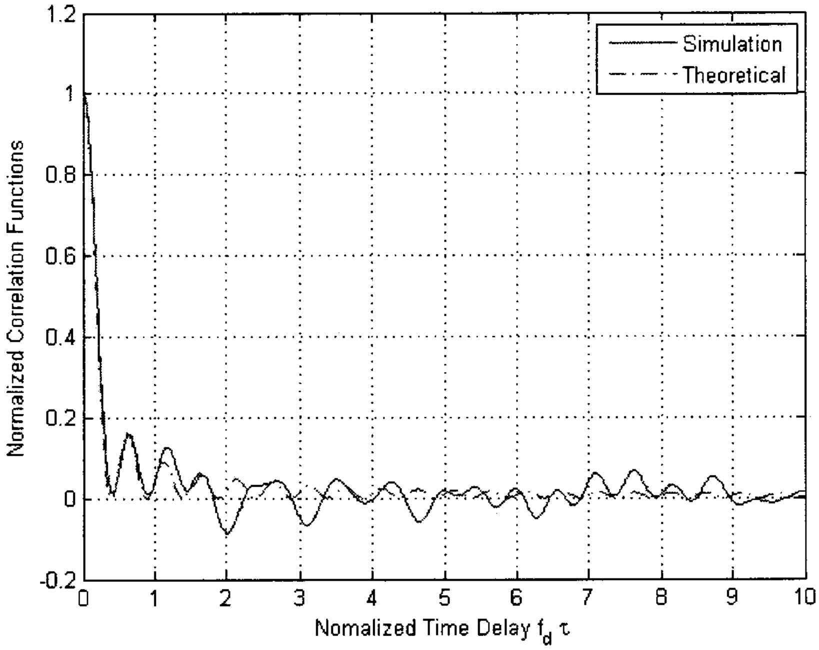

Figure B.5: Theoretical and Simulation (number of simulation of 1) auto-correlation of quadrature component of M-to-M channel

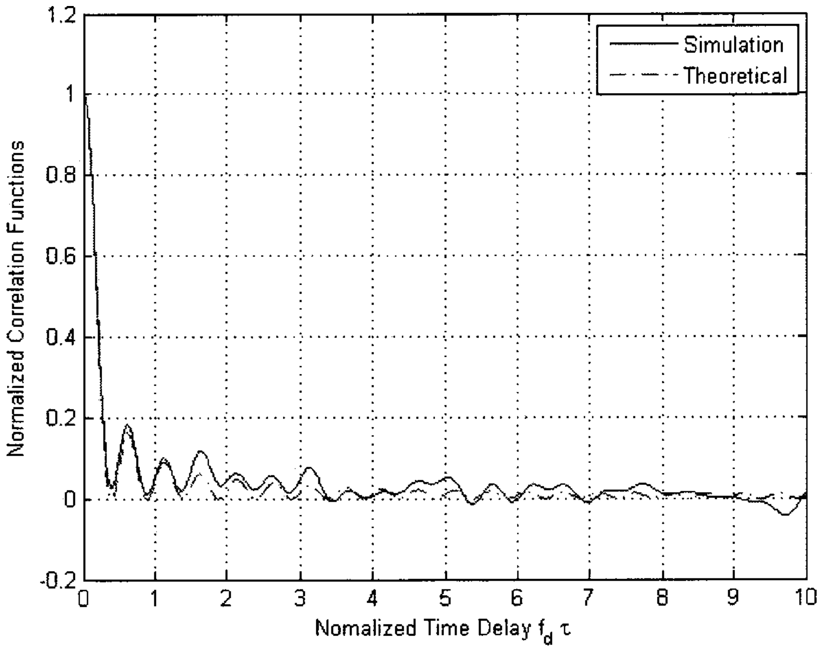

Figure B.6: Theoretical and Simulation (number of simulation of 10) auto-correlation of quadrature component of M-to-M channel